Arctic and Antarctic Research Institute

*Manuscript copyright*

Egorova Elizaveta Stanislavovna

# ICE CONDITIONS IN GREENLAND SEA AND BARENTS SEA UNDER CHANGING CLIMATE

Scientific Specialty 1.6.17. Oceanology

**Dissertation is submitted for the degree**
**of Candidate of Sciences in Geography**
Translation from Russian

**Scientific Supervisor:**
Dr. Sci. in Geography
Mironov Yevgeny U.

Saint-Petersburg — 2024

**CONTENTS**

**INTRODUCTION ..... 4**

**CHAPTER 1. KNOWLEDGE OF ICE CONDITIONS IN THE GREENLAND SEA AND THE BARENTS SEA ..... 19**

1.1. Physical features of the research area ..... 19

1.2. Greenland Sea and Barents Sea hydrometeorological regime ..... 22

1.3. Degree of study of sea ice conditions ..... 26

1.4. Conclusions for Chapter 1 ..... 32

**CHAPTER 2. DATA AND RESEARCH METHODS ..... 34**

2.1. Creation of sea ice parameters electronic archives ..... 34

2.2. Hydrometeorological factors ..... 37

2.3. Research methods ..... 40

2.3.1. Method for determining average-weighted ice thickness in Fram Strait ..... 40

2.3.2. Data for calculating the ice export in Greenland Sea and Barents Sea ..... 44

2.3.3. Statistical methods of analysis ..... 45

2.3.4. Availability and efficiency of forecasting method ..... 48

2.4. Conclusions for Chapter 2 ..... 49

**CHAPTER 3. REGULARITIES OF SPATIO-TEMPORAL VARIATIONS OF ICE REGIME KEY CHARACTERICTISC IN GREENLAND SEA ..... 50**

3.1. Ice coverage ..... 50

3.1.1. Seasonal variations ..... 50

3.1.2. Interannual variations ..... 52

3.2. Drift ice edge position in annual cycle ..... 59

3.3. Ice age composition ..... 61

3.3.1. Seasonal variations ..... 61

3.3.2. Interannual variations ..... 65

3.3.3. Ice age composition in Fram Strait ..... 70

3.4. Boundary of old ice prevalence ..... 71

3.4.1. Seasonal variations ..... 71

3.4.2. Interannual variations ..... 74
3.5. Ice volume export from the Arctic Basin ..... 76
3.5.1. Seasonal variations ..... 77
3.5.2. Interannual variations ..... 81
3.6. Conclusions for Chapter 3 ..... 85

**CHAPTER 4. REGULARITIES OF SPATIO-TEMPORAL VARIATIONS OF ICE REGIME KEY CHARACTERICTISC IN BARENTS SEA ..... 87**
4.1. Ice coverage ..... 87
4.1.1. Seasonal variations ..... 87
4.1.2. Interannual variations ..... 90
4.2. Drift ice edge position in annual cycle ..... 100
4.3. Ice age composition ..... 103
4.3.1. Seasonal variations ..... 103
4.3.2. Interannual variations ..... 107
4.4. Boundaries of old ice and first-year ice prevalence ..... 112
4.4.1. Seasonal variations ..... 112
4.4.2. Interannual variations ..... 117
4.5. Drivers of interannual variations of sea ice age composition in homogeneous sub-areas of Barents Sea ..... 122
4.6. Conclusions for Chapter 4 ..... 131

**CONCLUSIONS ..... 133**

**LIST OF ADOPTED ABBREVIATIONS ..... 137**

**REFERENCES ..... 138**

## INTRODUCTION

*The relevance of the research topic and the degree of its scientific development*. The Greenland Sea and the Barents Sea occupy a special place in the Northern Hemisphere climate system, primarily due to its geographical location. Special hydrometeorological and ice conditions are formed here due to the proximity to the warm Norwegian Sea and the cold Arctic Ocean. The combination of large-scale circulation factors of cold and warm currents, as well as air advection, determines the climate of temperate latitudes (in particular, the European sector).

Currently observed climate changes encompass the entire planet. However, in the high latitudes of the Northern Hemisphere, they are most pronounced: here, the average temperature of the surface layer of the atmosphere is increasing 2.5 times faster than in other latitudinal zones [IPCC Special Report..., 2019]. This phenomenon in the literature is referred to as *Arctic Amplification* (or *Polar Amplification*) [Serreze and Barry, 2011; Previdi et al., 2021]. The reasons for the occurrence of this phenomenon, as well as the oceanic mechanisms of its influence on the "ocean-ice-atmosphere" system are described in [Ivanov, 2022]. The study by [Alekseev et al., 2023] includes a quantitative assessment of the role of atmospheric transports in enhancing the air temperature variability in high latitudes. Authors [Latonin et al., 2020] have identified two main types of mechanisms driving Arctic Amplification. The question of this phenomenon impact of on the Arctic region is currently actively studied through modeling [Graff et al., 2019; Chylek et al., 2022] and satellite monitoring [Esau et al., 2023].

An increase in air temperature is accompanied by a decrease in the sea ice area (extent) and mean thickness all year through [Onarheim et al., 2018; Kwok, 2018]. Climate modeling results [Bonan et al., 2021; Årthun et al., 2021] indicate a continued reduction in the sea ice area, which could lead to seasonal ice-free conditions in the Arctic Ocean by the mid-21st century. However, as noted by [Jahn et al., 2016], the possible outcomes and predicted timelines vary significantly among different numerical sea ice models. Therefore, understanding the causes and consequences of the internal variability in sea ice cover is particularly important for predicting future changes in the climate system.

The current state of the Arctic sea ice cover is the subject of intense scrutiny by scientists and researchers of polar regions worldwide. It is known that since the early 2000s, changes in the Arctic Seas ice regime have been characterized, on the one hand, by a noticeable decrease in sea ice area (extent) during the summer months [Yulin et al., 2019; Cai et al., 2021; Årthun et al., 2021], and on the other hand, by the replacement of old ice with thinner first-year ice [Alexandrov and Johannessen, 2012; Egorov, 2020]. It is noted that the Greenland Sea and the Barents Sea are among the first to respond to fluctuations in the climate system [Barry et al., 1993; Gudkovich et al., 1997; Smedsrud et al., 2013; Rieke et al., 2023], which, given global changes, makes the study of sea ice conditions in this region particularly relevant. This explains the choice of the *research area*. Estimates of sea ice coverage presented in the work [Timokhov et al., 2019] indicate that under average conditions, the seasonal reduction in ice area in the Greenland Sea (for the period 1950–2018) occurs more slowly than in the Barents Sea (for the period 1928–2018).

High rates of sea ice area reduction in the Greenland Sea and the Barents Sea are observed not only during the summer months (typical for the Arctic region as a whole) but also during the period of maximum ice cover. A joint analysis of sea ice concentration data in the Barents Sea, including results from climate modeling and satellite observations, shows that during the period of 2007–2017 from April to November, the sea ice extent decreased by almost half compared to the average value from 1850 to 1978 [Onarheim and Årthun, 2017]. As noted by [Xia et al., 2014], the most noticeable reduction in sea ice cover, characterized by the retreat of the drift ice edge to the north from 1979 to 2012, is observed from January to May in the Greenland Sea and for most months of the year in the Barents Sea. Based on statistical trend analysis by the authors of the latter cited study, it was concluded that in the research area, the sea ice extent in the winter months, from January to April, sharply changed around 2000, with a statistically significant negative trend identified from 2005 onwards (at a 95% confidence level). Interestingly, according to the assessment by [Müller et al., 2022], based on reanalysis data, the seasonal ice coverage of the Greenland Sea decreased on average from 30–60% in the period from 1980 to 2000 to 20–30% specifically after 2005. The work [Bliss et al., 2019] includes assessments of the

trend's statistical significance in the change of ice area in the Greenland Sea and the Barents Sea from 1979 to 2016 specifically for March. As a result, significant negative linear trends were noted (at a 99% confidence level), amounting to $–0.7 \cdot 10^5$ km² (for Greenland Sea) and $–0.6 \cdot 10^5$ km² (for Barents Sea).

Authors [Onarheim and Årthun, 2017] have found that despite the relatively small area of the Barents Sea (about 4% of the Northern Hemisphere's ice-covered area), it accounted for 24% of the total observed reduction in sea ice extent (or $0.4 \cdot 10^6$ km² in absolute values) during the winter months since 1979. Only in March, according to estimates by [Stroeve and Notz, 2018; Onarheim et al., 2018], which were obtained from 1979 to 2018, the Greenland Sea and the Barents Sea contribute the most, each contributing 27%, to the reduction in the total ice extent compared to other ice-covered seas of the Northern Hemisphere.

Furthermore, a consistent shift in the timing of seasonal ice retreat to earlier dates is characteristic of the entire Barents Sea after 2003 [Sumkina et al., 2022]. The authors identified a noticeable influence of Atlantic water influx on the date of complete ice retreat (the maximum correlation coefficient is approximately 0.5). However, this is typical for specific Barents Sea sub-areas with highlighted synchronous dynamics of ice retreat dates in the study. The onset date of ice melting, according to [Bliss et al., 2019], shows a statistically significant linear trend towards earlier dates: for the Greenland Sea, the shift is 2.5 days per decade (at a 95% confidence level), and for the Barents Sea, it is 5.0 days per decade (at a 99% confidence level).

Literature analysis indicates that the majority of Russian and foreign studies are dedicated to changes in ice area (extent) in the Greenland Sea and the Barents Sea. Numerous works on separate parameters of its ice regimes since the 1970s have been summarized in the monograph [Mironov, 2004]. Additionally, the author provided a description of the regional climatic features to identify spatial and temporal patterns of ice cover distribution in these seas. The study identified the main natural factors influencing the formation of ice conditions in the Greenland Sea and the Barents Sea and presented new methods for long-term forecasts of ice coverage up to 6 months in advance. However, unique satellite

data accumulated since the mid-1990s on the state of ice cover in the Greenland Sea and the Barents Sea already allow for *a significant expansion* of existing knowledge about its ice regime and tracking changes in the main parameters of sea ice cover at different stages of Earth's climate fluctuations.

*The study object* is the sea ice cover of the Greenland Sea and the Barents Sea. *The study subject* is seasonal and interannual changes in the main features of the Greenland Sea and the Barents Sea ice regime.

*The purpose and objectives of the research*. The aim of this study is to establish the spatio-temporal patterns of changes in the ice cover main parameters, determining the ice regime features of the Greenland Sea and the Barents Sea, under modern climate change.

In accordance with the aim of the work, the following objectives were formulated:

1. Creation of electronic data archives on the main parameters of the sea ice cover of the Greenland Sea and the Barents Sea.
2. Identification and description of the patterns of seasonal and interannual changes in the *following* main features of the ice regime of the Greenland Sea and the Barents Sea: ice coverage, position of the drift ice edge, ice age composition, boundaries of prevalence of ice of separate age gradations, as well as the ice volume flux through the Fram Strait into the Greenland Sea.
3. Determination of statistically significant factors shaping the interannual changes in the ice area of separate age gradations in the Barents Sea sub-areas, and assessment of its contribution to changes in the ice age structure.

*The research methodology* is based on a comprehensive physical-geographical approach to the study of processes and objects of the environment using the following methods of statistical analysis of hydrometeorological information: identification and analysis of the time series trend components, multi-regression data analysis. The theoretical basis for conducting work on the dissertation topic consists of the results of previous studies on the parameters of the sea ice cover of Arctic Seas.

*The reliability of the obtained results* is ensured by the high quality of the data used in the study. Regional ice charts from the Arctic and Antarctic Research Institute (AARI), actively utilized for a range of scientific and practical purposes [Afanasyeva et al., 2019], were employed in creating electronic data archives on the main parameters of the sea ice regime in the Greenland Sea and the Barents Sea. Modern, verified, and widely used among Russian and foreign scientists hydrometeorological databases were utilized in assessing the ice volume flux and in forming a series of potential predictors determining variations in the ice area of separate age gradations in the Barents Sea. These databases include ERA5 reanalysis data on surface air temperature [Hersbach et al., 2020], NSIDC data on ice drift [Tschudi et al., 2020], and data on *in-situ* observations of water temperature along the oceanographic transect "Kola Meridian" [Karsakov et al., 2022]. Furthermore, the statistical methods analysis is widely accepted for studying its interannual variations. Finally, the dissertation research main conclusions, constituting the statements submitted to the defense, have been published in RSCI, Scopus and WoS scientific journals and presented at both Russian and international conferences.

*The scientific novelty* of the conducted research lies in the following aspects:

For the first time, seasonal and interannual changes in the ice age structure in the Greenland Sea and the Barents Sea during the winter period (October-May) have been described, and the boundaries of the prevalence of ice of separate age gradations have been determined. The volume of ice exported through the Fram Strait into the Greenland Sea has been estimated using an original method for accounting for its thickness based on ice charts from AARI. The obtained estimates are comparable to the results of studies that used instrumental observations of sea ice thickness. Based on multiple regression analysis, statistically significant natural factors that shape the interannual changes in the ice age structure in the Barents Sea sub-areas at its maximum development in April have been identified for the first time, and their contribution has been assessed. A detailed analysis of seasonal and interannual changes in the main parameters of the Greenland Sea and the Barents Sea ice cover during the modern climatic period has been conducted. The results significantly complement the information on their ice regime.

*Practical significance of the work*. The results of this study will be used in the development of new methods and the improvement of existing methods for ice forecasting in the Barents Sea. These methods will take into account the identified patterns of changes in ice coverage, the position of the drift ice edge, age composition (average thickness), and the boundaries of the prevalence of ice of separate age gradations. In ice navigation, knowledge of the sea ice age is of great practical importance for the navigation of both non-ice-class and ice-class vessels, as the physical properties of the ice cover directly depend on its thickness. Information on the spatial distribution of ice also influences the selection of optimal navigation routes. The proposed method for accounting for ice thickness in the Fram Strait to estimate the sea ice volume flux can be applied to other ice export gateways between the Arctic Seas and surrounding basins, where ice export is a key characteristic determining their ice conditions. The presented estimates of the volume of ice exported from the Arctic Basin, a key indicator of observed climate changes, complement a wide range of research results where various data on ice drift and approaches to determining its thickness have been used.

*Author's personal contribution*. The author personally prepared the electronic data archives on sea ice parameters, such as drift ice edge position, ice age composition, and boundaries of prevalence of ice of separate age gradations in the Greenland Sea and the Barents Sea. The author independently conducted the analysis of seasonal and interannual changes in all features of the sea ice regime of the Seas, followed by the description of observed regularities. The calculations of the ice volume flux, including the determination of ice flow width and ice concentration at the Fram Strait site, auxiliary characteristics for assessment, belong to the author. The author also constructed statistical equations and assessed the contributions of statistically significant factors. The text of scientific articles containing the main results of the work, as well as illustrative and tabular materials, was prepared by the author. Discussion and correction of the results at all stages of preparing the dissertation were carried out jointly with the scientific supervisor. The author personally presented the obtained research results at Russian and international conferences.

The main findings of the study were *presented* at **9** Russian and international conferences:

1. **Egorova, E.S**. Drivers of the Interannual Variations of Sea Ice Age Composition in the Barents Sea During Its Maximum Extent / **E.S. Egorova**, N.A. Lis, Ye.U. Mironov // Marine Research and Education: Materials of the XII International Scientific and Practical Conference. Volume II (IV). – Tver: LLC PolyPRESS, 2024. – P. 142-148. (In Russian; in-person, oral presentation).
2. **Egorova, E.S.** Assessment of Seasonal and Interannual Changes in the Age Structure of Ice in the Greenland and Barents Seas / **E.S. Egorova**, Ye.U. Mironov // Comprehensive Studies of the World Ocean: Materials of the VII All-Russian Scientific Conference of Young Scientists. – St. Petersburg: Own publishing house, 2023. – P. 47-48. (In Russian; in-person, oral presentation).
3. **Egorova, E.S.** Seasonal and Interannual Changes in Ice Export between the Greenland and Barents Seas with Adjacent Areas / **E.S. Egorova**, Ye.U. Mironov, I.A. Ilyushenkova // Oceanological Research: Materials of the X Conference of Young Scientists. – Vladivostok: POI FEB RAS, 2023b. – P. 20-21. (In Russian; in-person, oral presentation).
4. **Egorova, E.S.** Formation of the Age Composition of Ice in the Southeastern Part of the Barents Sea in the Winter Period / **E.S. Egorova**, Ye.U. Mironov // Seas of Russia: Challenges of Domestic Science: Abstracts of the All-Russian Scientific Conference. – Sevastopol: FSBSI FRS MHI RAS, 2022. – P. 83-84. (In Russian; online, poster presentation).
5. **Egorova, E.S.** Assessment of the Seasonal and Multi-Year Variability in the Sea Ice Volume Export via the Fram Strait / **E.S. Egorova**, Ye.U. Mironov // Proceedings of the 32nd International Ocean and Polar Engineering Conference. – Shanghai: ISOPE, 2022. – ISOPE-I-22-324 (Online, oral presentation).
6. **Egorova, E.S.** Sea ice coverage in the southeastern sub-area of the Barents Sea and its long-term forecasting method / **E.S. Egorova** // Proceedings of the IV Regional

Scientific and Practical Conference “The Future of the Arctic Begins Here”. – Apatity: MASU, 2022. – PP. 7-10. (In Russian; in-person, oral presentation).

7. **Egorova, E.S.** Main Patterns of Changes in the Age Composition of Ice in the Greenland Sea / **E.S. Egorova** // Comprehensive Studies of the World Ocean: Materials of the VI All-Russian Scientific Conference of Young Scientists. – Moscow: P.P. Shirshov IO RAS, 2021. – P. 65-66. (In Russian; in-person, oral presentation).
8. **Egorova, E.S.** Assessment of Ice Drift through the Fram Strait Based on Various Models / **E.S. Egorova**, E.S. Vinogradnaya // Comprehensive Studies of the World Ocean: Materials of the V All-Russian Scientific Conference of Young Scientists. – Kaliningrad: AB IO RAS, 2020. – P. 60-61. (In Russian; online, oral presentation).
9. **Egorova, E.S.** Interannual variability in the Greenland Sea ice coverage and its causes / **E.S. Egorova**, N.A. Vyazigina // Comprehensive Studies of the World Ocean: Materials of the IV All-Russian Scientific Conference of Young Scientists. – Sevastopol: FSBSI FRS MHI RAS, 2019. – PP. 54-55. (In Russian; in-person, poster presentation).

The dissertation research was carried out with the financial support of the Russian Science Foundation (grant No. 22-27-00443, topic: “Investigation of the Greenland and Barents Seas ice conditions in the context of contemporary climate change”, the 2022–2023). The results of the study are also included in the in reports on Roshydromet projects for the period 2020–2024.

*Publications*. In total, **7** articles based on the research were published in Russian and international scientific journals, of which: **6** — in journals included in the Higher Attestation Commission (*VAK*) list, and **3** — in journals indexed by Scopus.

1. Mironov, Ye.U. Seasonal and Interannual Variations in the Greenland Sea Ice Age Composition in the Winter Period / Ye.U. Mironov, **E.S. Egorova** // Meteorology and Hydrology. – 2024. – No. 3. – P. 54-65. (In Russian; RSCI, WoS, Scopus).

2. **Egorova, E.S.** Drivers of Interannual Variations of Ice Age Composition in Sub-Areas of the Barents Sea / **E.S. Egorova**, N.A. Lis, Ye.U. Mironov // Arctic and Antarctic Research. – 2023. – Vol. 69. – No. 3. – P. 290-309. (In Russian; RSCI).
3. **Egorova, E.S.** Assessment of the Seasonal and Multiyear Variability in the Sea Ice Volume Export via the Fram Strait / **E.S. Egorova**, Ye.U. Mironov // International Journal of Offshore and Polar Engineering. – 2023. – Vol. 33. – P. 18-26. (WoS, Scopus).
4. Lis, N.A. Informativeness (Information-Bearing) of Factors Forming Interannual Variability of the Barents Sea and Its Individual Areas Ice Coveren / N.A. Lis, E.A. Cherniavskaia, Ye.U. Mironov … **E.S. Egorova** // Russian Arctic. – 2023. – Vol. 5. – No. 2. – P. 17-32. (In Russian; RSCI).
5. Lis, N.A. Climate Variability of the Ice Extent in the Barents Sea and Its Individual Areas / N.A. Lis, **E.S. Egorova** // Arctic and Antarctic Research. – 2022. – Vol. 68. – No. 3. – P. 234-247. (In Russian; RSCI).
6. **Egorova, E.S.** Ice Age Composition in the Barents Sea / **E.S. Egorova**, Ye.U. Mironov // Arctic and Antarctic Research. – 2022. – Vol. 68. – No. 3. – P. 216-233. (In Russian; RSCI).
7. Viazigina, N.A. Informativeness (Information-Bearing) of Hydrometeorological and Astrogeophysical Factors in the Problem of Describing Interannual Fluctuations of the Greenland Sea Ice Coverage / N.A. Viazigina, L.A. Timokhova, **E.S. Egorova** [et al.] // Ice and Snow. – 2021. – Vol. 61. – No. 3. – P. 431-444. (In Russian; RSCI, Scopus).

The dissertation corresponds to the *specialization passport* of the Higher Attestation Commission (*VAK*) in the field of Oceanology (1.6.17), covering the following sections:

- Properties and processes of formation of sea ice, their distribution, and movement in the World Ocean.
- Interaction in the lithosphere-hydrosphere-atmosphere system.
- Methods of research, modeling, and forecasting of processes and phenomena in the oceans and seas.

*The structure* of the dissertation includes an introduction, four chapters, conclusion, list of adopted abbreviations, and references. The work has 158 pages in English (171 pages in Russian), including 29 figures and 33 tables. The references consist of 191 items, including 88 in English.

**The Introduction** provides a general overview of the dissertation, including the justification of its relevance, scientific novelty, reliability, and practical significance of the results obtained, as well as the author's personal contribution and the validation of research results.

**Chapter 1** offers a physical characterization of the Greenland Sea and the Barents Sea, describing its hydrometeorological regime. Special attention is given to the description of sea ice conditions, presenting the main results of numerous studies on the key parameters of the ice cover of the Greenland Sea and the Barents Sea analyzed in the dissertation.

**Chapter 2** is dedicated to describing the data used in the study and the methods of analysis.

**Chapter 3** demonstrates the regularities of spatial-temporal changes in the main parameters of the ice cover of the Greenland Sea, which shape its ice regime. Here, the results of the analysis of interannual changes of ice coverage, conducted using the method of their anomalies accumulation curves, are presented. Additionally, the regularities of seasonal changes in the ice coverage and the drift ice edge position in the modern climatic period are refined by comparison with results obtained in a colder period. Based on regional ice charts, the seasonal and interannual changes in the age composition of the Greenland Sea are established, and the seasonal variation of the boundary of predominance of old ice during the winter months is determined. In this chapter, the value of ice volume flux via the Fram Strait during the winter months is estimated using an original method. The method utilizes data on the ice age composition adjusted for ice hummocking. The obtained estimates are validated by comparing them with the results of previous studies using various approaches to determine ice drift and thickness in the strait site.

**Chapter 4** provides a description of the regularities of spatial-temporal changes in the main features of the Barents Sea ice regime. This includes the analysis of seasonal and interannual variations in the ice coverage and the drift ice edge position. The chapter analyzes seasonal and interannual changes in the ice age structure in the Barents Sea sub-areas, as well as the boundaries of predominance of old and first-year ice during the winter months. The contribution of factors shaping the interannual changes in the ice age composition in the Barents Sea sub-areas is determined by constructing statistical equations relating the ice area of separate age gradations to a series of hydrometeorological and ice factors.

**The Conclusion** summarizes the main results and conclusions of the dissertation research.

*Main scientific results:*

1. Investigation of the ice cover structure of the Greenland Sea by *age* gradations. The ice areas for seven standard age gradations during the winter period (October-May) were obtained using the electronic archive of AARI regional ice charts for the period 1997–2022 [Mironov and Egorova, 2024; pp. 55-56]. Seasonal changes of the drift ice age composition in the Greenland Sea were described [Mironov and Egorova, 2024; pp. 56-58]. It was shown that despite the noted decrease in the total ice cover area of the Greenland Sea, the relative areas of young, one-year, and old ice do not exhibit a statistically significant linear trend (at the 99% significance level) over the 25-year observation period [Mironov and Egorova, 2024; pp. 62-63]. Changes in the boundary of old ice predominance under average, maximum, and minimum distribution in the Greenland Sea were recorded [Mironov and Egorova, 2024; pp. 61-62]. A review of literature sources and a comparison of the estimates of the age structure of the Greenland Sea ice cover, obtained in present study, with the results from the late 1980s to early 1990s were conducted [Mironov and Egorova, 2024; p. 63]. Author personal contribution: formation of the electronic data archive, data analysis, review of literature sources on the research topic, preparation of the article manuscript, and preparation of graphical and tabular materials.

2. Investigation of the ice cover structure of the sub-areas of the Barents Sea by *age* gradations. Using the archive of AARI regional ice charts, the areas of ice for seven standard age gradations for all winter months over the period 1997–2021 were obtained [Egorova and Mironov, 2022a; pp. 219-220]. Seasonal changes in the ice cover age composition in the western, north-eastern, and south-eastern sub-areas of the Barents Sea were shown [Egorova and Mironov, 2022a; pp. 222-225]. Common features in the ice structure by age, characteristic of the northern region of the Sea, were identified [Egorova and Mironov, 2022a; p. 224]. For April, the month of maximum ice cover, interannual changes in the ice cover age structure in sub-areas of the Barents Sea were described [Egorova and Mironov, 2022a; pp. 226-227]. The absence of statistically significant linear trends (at the 99% significance level) for the relative area of young and one-year ice in the Barents Sea was demonstrated against the backdrop of a reduction in the total ice cover area of the Sea [Egorova and Mironov, 2022a; p. 228]. The estimates obtained in present study were compared with the results of studies from the 1970s [Egorova and Mironov, 2022a; pp. 228-229]. Author personal contribution: formation of the electronic data archive, data analysis, review of literature sources on the research topic, preparation of the article manuscript, and preparation of graphical and tabular materials.
3. Identification of the *drivers* determining interannual changes in the ice age composition in the sub-areas of the Barents Sea. Based on literature sources, potentially significant predictors were selected and described [Egorova et al., 2023a; pp. 293-295]. Statistical equations with the highest correlation and determination coefficients were obtained, describing interannual changes in the area of young and first-year (thin, medium, and thick) ice [Egorova et al., 2023a; pp. 295, 298]. The contributions of each statistically significant predictor (in %) were determined [Egorova et al., 2023a; pp. 297-299], and dominant factors for the sub-areas of the Sea were shown [Egorova et al., 2023a; p. 304]. Possible schemes of the impact of various natural factors on changes in the ice cover age structure in the Barents Sea were presented [Egorova et al., 2023a; pp. 300-301]. The possibility of using the obtained statistical equations for long-term forecasting of the ice area of various

age gradations was demonstrated based on the assessment of their availability and efficiency [Egorova et al., 2023a; pp. 301-302]. Author personal contribution: analysis of literature sources for factor selection, calculation of ice area flux in the Barents Sea with surrounding basins, construction of statistical equations, analysis of results, preparation of the article manuscript, and preparation of graphical and tabular materials.

4. Estimates of the *ice volume flux* from the Arctic Basin through the Fram Strait in the winter period. A method for estimating the ice cover thickness at the Fram Strait site based on age composition data with an additional correction for deformed ice was proposed [Egorova and Mironov, 2023; pp. 19-21]. For the period 1997–2022, the age structure and partial ice concentration for separate ice zones, as well as the total ice flow width in the Fram Strait, were determined [Egorova and Mironov, 2023; p. 19]. The ice cover structure of the Fram Strait by age gradations was described [Egorova and Mironov, 2023; pp. 21-22]. Seasonal changes in the ice volume export, highlighting the months of maximum and minimum values, were shown [Egorova and Mironov, 2023; pp. 22-23]. Interannual changes in the ice volume flux via the Fram Strait were presented [Egorova and Mironov, 2023; pp. 23-24]. An analysis of literature sources on the topic (primarily English-language) was conducted; the ice volume flux estimates published in other studies were compared with the results obtained in present study [Egorova and Mironov, 2023; p. 25]. Author personal contribution: formation of the electronic data archive, selection of open-access databases on ice drift, calculations of the ice volume exported through the Fram Strait, analysis of results, review of literature sources on the research topic, preparation of the article manuscript, and preparation of graphical and tabular materials.

5. Analyzed intra- and inter-annual *changes* in the *ice coverage* of the Barents Sea and its sub-areas. A description of the data used and the methods of statistical analysis was prepared [Lis and Egorova, 2022; pp. 236-237]. Seasonal changes in the ice coverage of the western, north-eastern, and south-eastern parts were examined: in the annual cycle, multi-year average values were calculated, periods of maximum

and minimum ice coverage were identified, and the recurrence of these periods for different months of the year was determined [Lis and Egorova, 2022; pp. 237-239]. It was shown that the seasonal reduction of ice coverage in the Barents Sea occurs faster than its increase, leading to a decrease in the ice cover area [Lis and Egorova, 2022; p. 239]. For the winter (December-April) and summer (July-September) months, two periods of climatic changes in the ice coverage of the Barents Sea were identified [Lis and Egorova, 2022; pp. 239-240]. The first period, from 1928 to 1985, is characterized by relative stability in ice coverage changes, with linear trends being statistically insignificant for both seasons. The second period, from 1986 to 2021, is marked by active melting of the Barents Sea ice cover: statistically significant linear trends in ice coverage were presented, along with a description of the proposed schemes of various natural factors influencing its reduction [Lis and Egorova, 2022; pp. 240-242]. The inertia of ice coverage changes in the Barents Sea sub-areas was demonstrated [Lis and Egorova, 2022; pp. 243-244]. Author personal contribution in obtaining the results included the preparation of the initial data and their description, analysis of seasonal changes in ice coverage, as well as partial preparation of the manuscript and graphical materials.

6. The *drivers* determining the interannual variations in the Greenland Sea and the Barents Sea ice coverage were considered. When presenting the initial data, the authors paid particular attention to describing the hydrometeorological indices and parameters [Viazigina et al., 2021; pp. 433-434; Lis et al., 2023; pp. 19-20]. Periods of cyclical fluctuations in ice coverage and the main natural factors forming them were identified [Viazigina et al., 2021; pp. 434-435; Lis et al., 2023; pp. 21-23]. The association of various factors with the ice coverage of the Greenland Sea and the Barents Sea was studied through the analysis of paired correlation coefficients [Viazigina et al., 2021; pp. 435-437; Lis et al., 2023; pp. 21-22]. Statistical equations describing the interannual changes in the ice coverage of the Greenland Sea were developed for the summer (July-September), autumn (October-November), winter (December-April), and spring (May-June) periods [Viazigina et al., 2021; pp. 438-440]. For the ice coverage of the western, north-eastern, and south-eastern

sub-areas of the Barents Sea, statistical equations were obtained for the winter and summer periods [Lis et al., 2023; pp. 23-24]. A comparison of the actual and calculated values of the ice coverage was presented [Viazigina et al., 2021; pp. 441-442; Lis et al., 2023; pp. 25-26]. The contribution of statistically significant predictors to the interannual changes in the ice coverage of the Barents Sea sub-areas was determined [Lis et al., 2023; p. 24]. Author personal contribution included the analysis of literary sources, hydrometeorological and ice factors selection, the analysis of the multiregression analysis results of the ice coverage of the Greenland Sea and the Barents Sea, and the partial preparation of article manuscripts.

*The statements submitted to the defense*:

1. New data on the ice age composition and the boundaries of the prevalence of ice of separate age gradations in the Greenland Sea and the Barents Seas for the period 1997–2022.
2. The sea ice volume flux through the Fram Strait for the period 1997–2022, where the average-weighted ice thickness is obtained based on data on its age structure, adjusted for ridged formations. The average sea ice export during the winter period is 2141 $km^3$. During that time period the average-weighted ice thickness decreased by 3.8 cm per ice season, however interannual changes in the ice volume export do not have a statistically significant linear trend.
3. Quantitative assessments of the contribution of hydrometeorological and ice factors to the interannual variations in the area of young and first-year ice in the Barents Sea sub-areas, explaining from 52% to 79% of their total variance.

# CHAPTER 1. KNOWLEDGE OF ICE CONDITIONS IN THE GREENLAND SEA AND THE BARENTS SEA

## 1.1. Physical features of the research area

*The Greenland Sea* is a marginal sea of the Arctic Ocean, situated between the islands of Greenland, Iceland, Jan Mayen, Bear, and the Svalbard Archipelago. According to commonly accepted maritime boundaries [Atlas..., 1980; Boundaries..., 2000], maritime boundaries of the Greenland Sea are delimited by land and the following imaginary lines (see Figure 1.1). The western boundary of the Sea is delineated by the eastern coast of Greenland Island, extending from Cape Brewster in the north to Cape Bridgman in the south. In the southern part, where the Greenland Sea freely communicates with the Norwegian Sea and the northern part of the Atlantic Ocean, the boundary from Cape Brewster extends to Cape Reykjaness (Iceland Island) and further from Cape Hjerpe (Iceland Island) to Jan Mayen Island. To the east, the Greenland Sea is connected with the Barents Sea along a line from Jan Mayen Island through Bear Island to Cape Zuidkaap (West Spitsbergen Island, Svalbard Archipelago). Finally, in the north, the boundary of the Greenland Sea with the Arctic Basin is conventionally drawn along a line from Cape Bridgman (Greenland Island) to Cape Westerly Point (located on the same island of the Svalbard Archipelago).

*The Barents Sea* is located in the shelf zone of the Arctic Ocean between the northern coast of Europe, the islands of Vaygach and Bear, and three major archipelagos: Svalbard, Franz Josef Land, and Novaya Zemlya. According to [Atlas..., 1980; Boundaries..., 2000], its maritime boundaries run along the following imaginary lines (see Figure 1.1). In the west, where the Barents Sea borders the Greenland Sea and the Norwegian Sea, the boundary extends from Cape Zuidkaap through Bear Island to Cape Nordkapp (located on the northern coast of the Scandinavian Peninsula). The southern boundary stretches along the continent from Cape Nordkapp to Yugorsky Shar Strait; at the point of Saint Nose (Kola Peninsula) — Cape Kanin (Kanin Peninsula), the Barents Sea borders the White Sea. To the east, the Barents Sea communicates with the Kara Sea, and its eastern

boundary runs from Yugorsky Shar and Kara Gates Straits along the western coast of Novaya Zemlya to Cape Desires and then to Cape Koltsovat (Graham Bell Island, Franz Josef Land Archipelago). The northern boundary of the Barents Sea with the Arctic Basin from Cape Koltsovat encircles from the north the Franz Josef Land Archipelago to Cape Mary Harmsworth (Alexandra Land, Franz Josef Land Archipelago), passes through the northern islands of Victoria and White to Cape Lee Smith (Severo-Vostochnaya Zemlya Island of the same archipelago) and from Lamgroundudde Cape to Cape Verlegenhuken (located on the same island of the Franz Josef Land Archipelago).

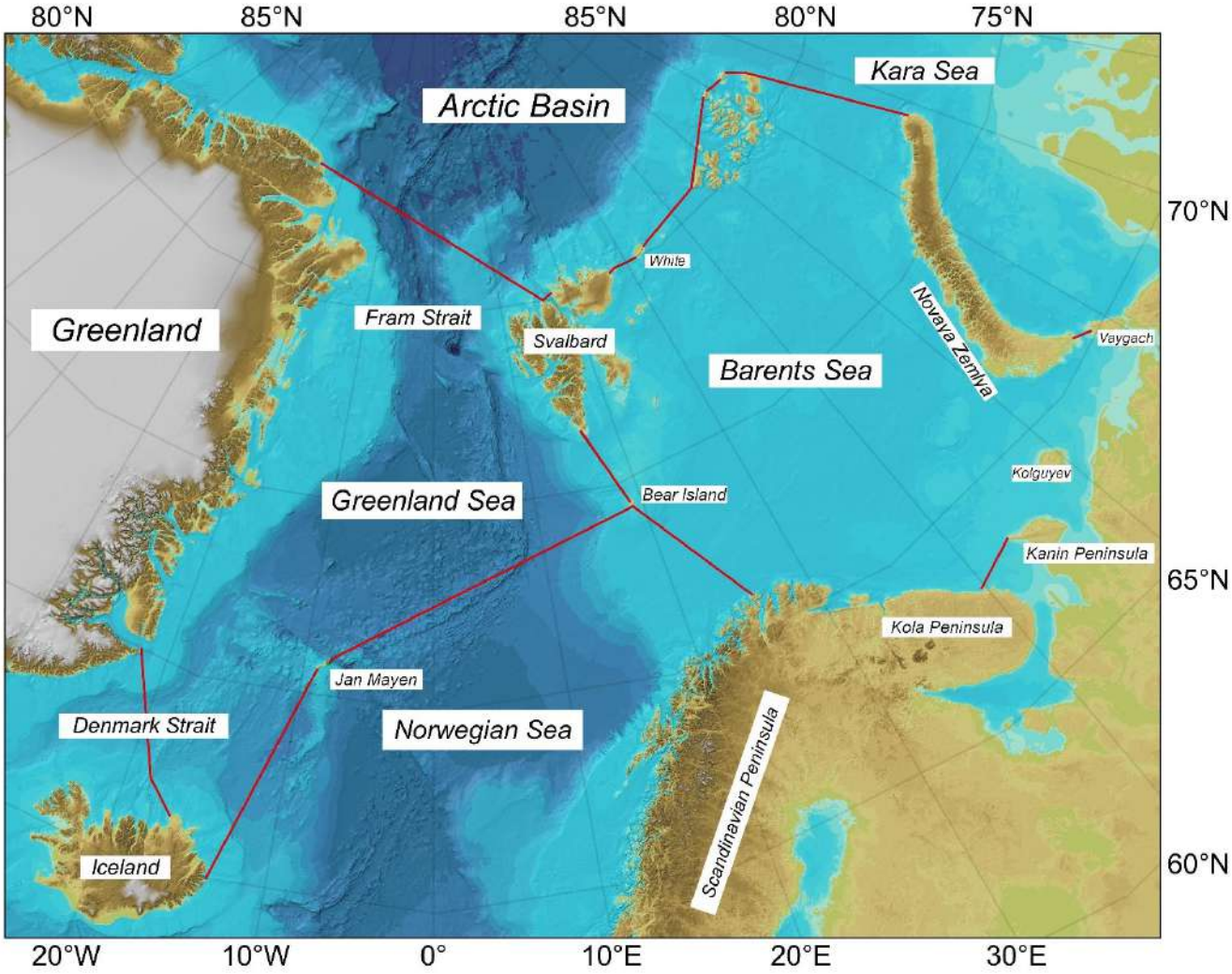


Figure 1.1. Boundaries of the Greenland and Barents Seas, drawn according to [Atlas..., 1980; Boundaries..., 2000], are indicated by red lines. The seafloor relief is depicted based on data from [Jakobsson et al., 2012].

In accordance with the Nomenclature of Seafloor Relief [Treshnikov et al., 1967], the Greenland Sea and the Barents Sea belong to the North European Basin. The morphometric

characteristics (area, water volume, as well as maximum and mean depths) of the Greenland Sea and the Barents Sea are presented in Table 1.1. The Greenland Sea and the Barents Sea are the main water bodies of the North European Basin and the largest seas in terms of area: they occupy 30% and 35% of the total area of the basin, respectively. The main difference in their morphometric characteristics lies in the depths, which affects the volume of water. Despite both seas constituting approximately 50% of the total volume of the North European Basin, the volume of water in the Greenland Sea represents 43% of the total volume, while the Barents Sea accounts for only 7%. Moreover, the volume of water in the Greenland Sea exceeds the volume of water in the Barents Sea by six times [Mironov, 2004].

Table 1.1. Key morphometrical characteristics of the Greenland Sea and the Barents Sea [Atlas…, 1980]

| *Morphometrical characteristic* | *Greenland Sea* | *Barents Sea* |
|---|---|---|
| Sea area, $10^3$ km$^2$ | 1195 | 1424 |
| Water volume, $10^3$ km$^3$ | 1961 | 316 |
| Average depth, m | 1641 | 222 |
| Maximum depth, m | 5527 | 600 |

The seabed of the *Greenland Sea* is characterized by complex intersecting relief features. The largest part of the seabed is occupied by the Greenland Basin (maximum depth 5527 m), which is separated from the shallower Icelandic Basin (2793 m) to the south by the underwater Greenland-Iceland Ridge. To the east, the basins are bounded by mid-oceanic ridges, including the Mohn, Knipovich, and Iceland-Jan Mayen Ridges (minimum depth 549 m). The bottom of the Greenland Basin initially rises slowly in a westward direction, but towards the edge of the continental slope, closer to the coastal strip of Greenland, the ascent sharply increases. The shelf near Greenland Island ranges in width from 90 km in the south to 340 km in the north; near Iceland, the shelf extends for 90–100 km, while near West Spitsbergen Island, it ranges from 30 to 60 km, and near the coasts of Bear Island, the shelf forms an extensive plateau called the Bear Bank [Atlas..., 1980].

Despite the location of the *Barents Sea* within continental shelves, the majority of its area have depths of up to 400 m, making it the deepest among the shelf seas of the Arctic Ocean. On small-scale maps, the seabed relief of the Sea appears smoothed, but in reality, it is highly rugged. The bottom of the Barents Sea consists of an underwater plain called the Central Plateau, with alternating depressions, troughs, and underwater elevations, including the Central (minimum depth 64 m), and Persey (51 m) Elevation; Bear, Goose, North Kanin, and Murmansk Banks (up to 200 m); Central Depression (maximum depth 386 m), as well as the Franz-Victoria, Saint Anna, and Western Troughs (ranging from 400 m to 600 m), and others. Near major archipelagos, depths are less than 100 m [Atlas..., 1980].

### 1.2. Greenland Sea and Barents Sea hydrometeorological regime

The main characteristics of the climate in the Greenland Sea and the Barents Sea are primarily determined by: (1) their polar geographical location, (2) the pattern of atmospheric circulation, (3) the interaction of water masses with various thermophysical characteristics here, and (4) the state of underlying surfaces of the Seas. Despite their high latitudinal position beyond the Arctic Circle, which predisposes them to the formation and development of ice cover similar to the seas of the Siberian shelf in the Russian sector of the Arctic, in reality, both the Greenland and Barents Seas are never completely covered with ice [Dobrovolskiy and Zalogin, 1982; Mironov, 2004]. The peculiarities of ice processes development are determined by a complex set of climate-forming factors. The unique ice conditions in the Greenland Sea are primarily due to the interaction of warm Atlantic-origin waters and cold Arctic waters [Rudels, 1995; Martin and Wadhams, 1999; Beszczynska-Möller et al., 2012]. In the Barents Sea, the characteristics of its ice regime are primarily shaped by the large-scale interaction of atmospheric transports from the North Atlantic and warm ocean currents [Loeng et al., 1997; Mironov, 2004; Rikiishi et al., 2005].

*Water dynamics*. An important physical feature of the Barents Sea and the Greenland Sea is the presence of a stable system of warm and cold ocean currents [Nikiforov and Shpaiher, 1980; Rudels, 1987]. The pattern of currents in the research area is quite complex

and variable, primarily due to the influence of large-scale atmospheric circulation, the relief of the seabed, and the inflow of waters from surrounding basins. Figure 1.2 shows a schematic representation of the main ocean currents in the North European Basin (in accordance with the works of [Nikiforov and Shpaiher, 1980; Loeng, 1991; Rudels et al., 1994; Ozhigin et al., 2000]).

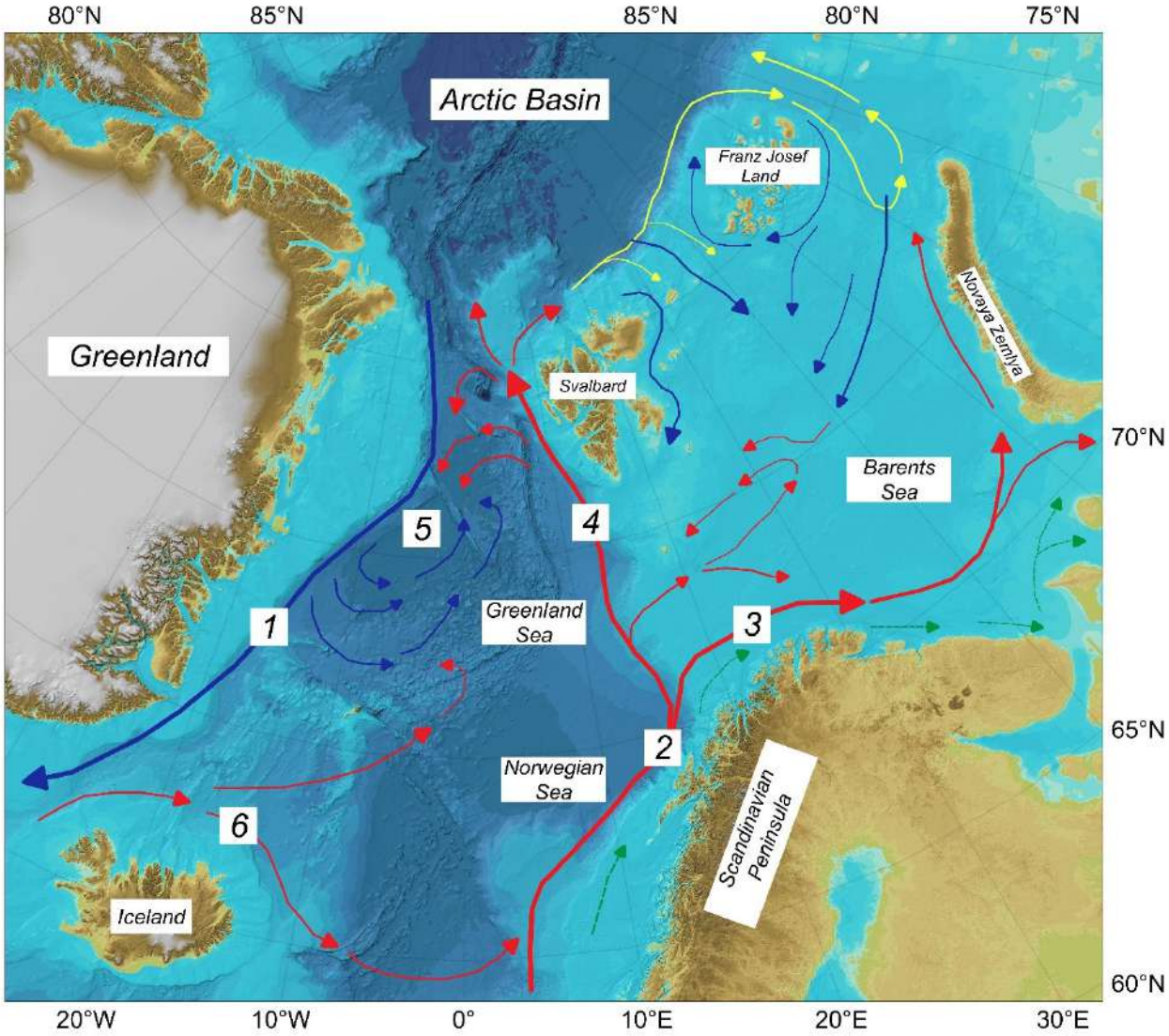


Figure 1.2. Simplified circulation scheme of water in the seas of the North European Basin. The numbers denote: *1* — East Greenland Current, *2* — Norwegian Current, *3* — North Cape Current, *4* — Spitsbergen Current, *5* — system of cyclonic currents, *6* — West Icelandic and East Icelandic currents. Warm currents are indicated by red arrows, cold ones by blue arrows, surface currents by yellow, and nearshore currents by green dashed arrows. The scheme is adapted in accordance with [Nikiforov and Shpaiher, 1980; Loeng, 1991; Rudels et al., 1994; Ozhigin et al., 2000]

Warm and saline waters of Atlantic origin penetrate into the North European Basin seas through the Iceland-Faroe-Scotland Ridge [Hansen and Østerhus, 2000; Hakkinen and Rhines, 2009]. Along the continental slope of the Scandinavian Peninsula, they move northward in a broad stream known as the Norwegian Current, which then divides into two main branches [Furevik et al., 2007; Beszczynska-Möller, 2011; Lundesgaard et al., 2022]. The *first* branch is the North Cape Current, through which Atlantic waters enter the Barents Sea from the southeast and split into two branches [Schauer et al., 2002]. The northern branch flows northeastward along the Hope Island Trench, partially turning east between the Perseus Ridge and the Central Bank at the 76° N, and continues as subsurface waters [Loeng, 1991]. The southern branch, much larger in volume compared to the northern branch, transports the majority of Atlantic waters as the Murmansk Current, spreading eastward towards the Novaya Zemlya Archipelago. In the area of the Kanin Banks, Goose Bank, and Novaya Zemlya, the movement changes to a northeastward direction. Eventually, mixing with local water masses in the Barents Sea, the transformed Atlantic waters enter the Arctic Basin through the St. Anna Trough [Barents Sea System, 2021]. However, their quantity, as shown by numerical modeling results for the northeastern Barents Sea, is extremely small [Makhotin and Ivanov, 2016]. The estimation of the volume and pathways of Atlantic waters spreading into the Barents Sea from the Arctic Basin remains a subject of discussion [Lind and Ingvaldsen, 2012; Ivanov et al., 2020; Lundesgaard et al., 2022]. The presence of ice cover in the northern regions of the sea significantly complicates any field measurements [Barents Sea System, 2021].

The *second* branch of the Norwegian Current, the Spitsbergen Current, carries Atlantic waters along the Spitsbergen Archipelago towards the Fram Strait in the north of the Greenland Sea [Beszczynska-Möller et al., 2012]. North of the archipelago, the current divides into two branches, the Yermak and Spitsbergen branches [von Appen et al., 2015; Koenig et al., 2017]. During the winter period, the advection of warm water masses by the main currents, namely the Spitsbergen and North Cape currents, compensates for the radiative cooling of the ocean's underlying surface to a significant extent. This not only affects air temperature but also inhibits ice formation over a large area of the Seas,

resulting in the displacement of the drift ice edge to the east in the Greenland Sea and to the north in the Barents Sea [Mironov, 2004].

Additionally, along the coast of Greenland Island from the Fram Strait to the south of the Greenland Sea, the East Greenland Current carries cold, freshened waters and old ice from Arctic Basin [Aagaard and Coachman, 1968; Martin and Wadhams, 1999; Haine et al., 2015], which define the ice conditions in the Greenland Sea on a seasonal cycle. Arctic waters flow broadly, narrowing at the Danish Strait and further spreading along the western coast of Greenland Island in a narrow band [Mironov, 2004]. The current has two major branches in the central part of the Greenland Sea, the Jan Mayen and Icelandic currents, which constitute a system of cyclonic currents in the North European Basin. The East Greenland Current transports a portion of Atlantic-origin waters (they come from the Yermak and Spitsbergen branches), which recirculate from the southern part of the Fram Strait further southward due to the strong cyclonic Greenland Sea Gyre [Håvik et al., 2017; Chatterjee et al., 2021]. Authors [Liu et al., 2022] note that the surface layer of water in the western part of the sea thus represents a mixture of Atlantic and Arctic waters.

*Atmospheric circulation*. Descriptions of synoptic processes over the Greenland Sea and the Barents Sea are provided in [Atlas…, 1980], while the atmospheric conditions shaping the climate are presented in [Dobrovolskiy and Zalogin, 1982; Hydrometeorology and…, 1990; Mironov, 2004]. The Greenland Sea and the Barents Sea are under the influence of a large-scale baric system known as the Icelandic Low. It represents an extensive area of low pressure extending over the northern part of the Atlantic Ocean, between the islands of Greenland and Iceland, at 60°–65° N [Trewartha and Horn, 1980; Serreze et al., 1997; Smirnov et al., 1998]. It is worth noting that the Icelandic Low is a major component of the North Atlantic Oscillation. It describes periodic fluctuations in the redistribution of atmospheric pressure between the minimum over Iceland and the maximum acting over the Azores, which in turn influence the weather in Europe [Hordon, 2005].

Atmospheric processes occurring over the Greenland Sea and the Barents Sea are determined by the location and intensity of the Icelandic Low. In the winter months,

during low solar activity (typical for the northern hemisphere), the zone of activity of the Icelandic depression expands as the sea surface temperature exceeds the air temperature over the continent [Hordon, 2005]. Strong storms and winds (typical wind speeds ranging from 88 to 121 km/h) predominantly from the northeast (over the entire Greenland Sea and the northern part of the Barents Sea), as well as from the southwest and south (in the southern parts of the Seas), are generated due to the stable pressure gradient. In the summer months, cyclonic activity weakens as the air temperature increases relative to the sea surface temperature, resulting in the establishment of a uniform area of high pressure over the Seas, and the influence of the Icelandic Low diminishes. At this time, the air transport system becomes unstable, and the winds become weak and variable in direction [Mironov, 2004].

The magnitude of annual air temperature fluctuations over the Greenland Sea and the Barents Sea is determined by the established system of seasonal air transport, thus significantly varying from region to region. The smallest temperature differences throughout the year, ranging from +10°C to +15°C, are typical for the southern parts of the Seas in the absence of sea ice and with prevailing southwest air transport. In the northern regions of the seas, the largest air temperature changes, ranging from +25°C to +30°C, are observed throughout the year, as the presence of sea ice here promotes radiational cooling of the lower atmosphere layers in winter months, and northeast air transport contributes to the advection of cold air masses from the Arctic Basin [Mironov, 2004].

### 1.3. Degree of study of sea ice conditions

Research on the ice cover conditions of the Greenland Sea and the Barents Sea began in the 1920s with the works of V.Yu. Vize. In the [Vize, 1940; 1944], significant attention was paid by the author to the ice regime of the Seas, although monographies were primarily dedicated to studying the causes of anomalous ice conditions. In the 1950s and 1960s, the main focus shifted towards studying the formation of sea ice under the influence of various factors and seeking quantitative relationships between them. During this time, the first methods for long-term ice forecasts for the Greenland Sea and the Barents Sea were developed by [Karakash, 1950; 1958; Uralov, 1960; Lebedev, 1964; 1981; 1994]. Research

by [Lebedev and Uralov, 1976a; 1976b; 1977a; 1977b] made a significant contribution to understanding the spatio-temporal changes in the ice regime of the study region and the mechanisms behind the formation of anomalous ice processes. In particular, original methodologies for long-term ice forecasts were developed based on data on the ice balance of the Greenland Sea and the Barents Sea and its analysis. Subsequently, in the 1970s and 1980s, extensive fieldwork was conducted to study sea ice from the research icebreaker "Otto Schmidt" using aerial photography and side-looking airborne radar. Generalization of these studies was performed by [Zubakin, 1987a], which provided insights into the synoptic variability of ice conditions in this region. Norwegian scientists also actively conducted research on the ice cover of the Greenland Sea and the Barents Sea: [Vinje, 1975; 1985] provides a description of its ice conditions based on synthesized field data.

The systematic use of man-made Earth satellites for monitoring sea ice began in the late 1970s. The accumulated unique information about the state of the ice cover is now widely applied to analyze seasonal changes and to study the processes of formation and continuity of anomalous ice conditions for separate autumn-winter and spring-summer months. The main regularities of seasonal and interannual changes in the ice regime features in the Greenland Sea and the Barents Sea, identified through the joint analysis of data from ice aerial reconnaissance and satellite data, have been summarized [Mironov, 2004]. These parameters *include*: sea ice area, drift sea ice edge position, sea ice concentration, sea ice thickness, sea ice floe size distribution, and several others. Additionally, large-scale processes determining the formation of the ice condition type in the research area have been identified. The work by [Buzin, 2006] describes the ice conditions key features in a northeastern sub-area of the Barents Sea, as several major hydrocarbon deposits are concentrated here. Comparison and analysis of long-term ice coverage series and various hydrometeorological and ice characteristics of the Barents Sea (air temperature, precipitation amount, extent and recurrence of flaw polynyas) allowed the author of the study [Buzin, 2009] to hypothesize about the reasons for the various directions of the century-long trend in sea ice area changes.

*Ice coverage*. Ice coverage is the most studied ice regime feature in the Greenland Sea and the Barents Sea. It is a generalizing characteristic that sufficiently defines conditions of ice navigation, shows the regional climate changes, and characterizes the extreme ice distribution [Hydrometeorology and…, 1990]. As shown in [Zakharov, 1996], ice coverage, as the most objective indicator, reflects both hydrodynamic and thermal processes in the "atmosphere-ocean-ice" system.

Authors [Tregubova et al., 2015] recorded a reduction in the Greenland Sea ice coverage starting from 1997 (anomaly analysis conducted for the period 1979–2008). In the works of [Matishov et al., 2013; Zhichkin, 2015; Krasheninnikova and Krasheninnikova, 2019], low-frequency changes in sea ice area and separate thermohaline characteristics of the Barents Sea were analyzed, and their connection with changes in the North Atlantic Oscillation (NAO) and the Atlantic Multidecadal Oscillation (AMO) climate indices was established. Additionally, contributions of hydrometeorological factors, astrogeophysical processes, and the preceding state of the ice cover to interannual changes in ice coverage in the Greenland Sea and the Barents Sea were assessed by [Timokhov et al., 2018; 2019].

Currently, significant reductions in sea ice extent throughout the Arctic region are observed year-round, as demonstrated in seminal works [Kwok, 2018; Stroeve and Notz, 2018], due to the identification of a significant linear trend since 1979. Results from [Vinje, 2001a; Frolov et al., 2007a] indicate a slowdown in the rate of ice coverage reduction in the sub-Atlantic seas (including the Greenland Sea and the Barents Sea) by the end of the 20th century. However, significant linear trends in ice coverage in April and September were obtained for the Greenland Sea and in April for the Barents Sea [Frolov et al., 2007a], calculated for the period from 1900 to 2003. According to [Timokhov et al., 2018], ice coverage changes in the Greenland Sea during both summer and winter months from 1950 to 2016 are characterized by a significant negative linear trend. Ice cover decreased by 41% (22.000 $km^2$) in February-March and by 47% (13.000 $km^2$) in August-September. Moreover, the rate of sea ice area reduction in the Greenland Sea is higher in winter than in summer. According to [Krasheninnikova and Krasheninnikova, 2019] results, based on instrumental observations from 1900–2014, ice coverage in the Barents Sea decreased by

20%, which is consistent with results from a global climate model (in this case, the GFDL-CM3 model of the Coupled Model Intercomparison Project Phase 5 was used), which also reflects a trend towards decreasing sea ice area. In the work by [Buzin and Gudkovich, 2011], Barents Sea ice coverage data series from 1928 to 2007 was divided into two seasons: a positive trend of +0.8% per decade was observed for the months from November to January, while a negative trend of –0.9% per decade was observed for the months from February to October. The authors do not specify whether the identified linear trends in ice coverage are significant, only noting the presence of opposite trends within the year.

In the study by [Lis and Egorova, 2022], the series of ice coverage (1928–2021) in the Barents Sea sub-areas were divided into two periods: 1928–1985 and 1986–2021. The rationale for this division by the authors was based on visual analysis, supplemented by a series of studies on temperature, salinity, and mixed layer thickness with similar periods of change before and after the 1980s. Analyzing anomalies in ice coverage in the Barents Sea over extended time periods allowed for the identification of characteristic periods of cooling and warming. According to the analysis starting from 1928 [Timokhov et al., 2019], a significant decrease in ice coverage in the Barents Sea occurred during the 1930s–1950s and the 2000s–2010s, while a considerable increase was observed during the 1960s–1980s and the 1990s. On a shorter timescale, from 1960 to 2014, the work by [Zhichkin, 2015] identified periods of anomalous cooling during the 1962–1970 and 1977–1982, as well as a period of anomalous warming during the 2000–2014. Furthermore, based on changes in the annual mean values of ice coverage in the Barents Sea from 1960 to 2011, authors [Matishov et al., 2013] determined two major intervals of its variation: heavier ice conditions were observed in the Sea until the early 1990s, followed by lighter conditions since the early 1990s.

*Drift ice edge position*. Only several studies have focused on the retrospective (with preliminary data reconstruction) statistical analysis of long-term observations on the edge position of drift ice in the Greenland Sea and the Barents Sea, particularly during the spring-summer season. For instance, the work by [Divine et al., 2006] covers the period from 1750 to 2002, and [Shapiro et al., 2006] covers the period from 1850 to 2001. These studies

identified cycles of anomalies in the drift ice edge position with periodicities of 20–30 years and 60–80 years. The Greenland Sea exhibits lower-frequency fluctuations, while the Barents Sea shows higher-frequency oscillations. Moreover, in the Barents Sea, a retreat of the average position of the ice edge northeastward in April was observed during the 1850–1899 and 1900–1949, indicating the greatest displacement.

*Area (volume) of ice exported to the Greenland Sea via the Fram Strait*. In recent decades, scientists have focused on the Fram Strait, which is the primary gateway for the export of old ice from the Arctic Basin into the Greenland Sea [Kwok, 2009]. According to estimates [Haine et al., 2015; Smedsrud et al., 2017; Zamani et al., 2019], approximately $900 \cdot 10^3$ km$^2$ of ice is transported to the Sea throughout the year, equivalent to 10% of its total area in the entire Arctic Basin. Ice outflow through the Fram Strait is one of the most important components of the ice balance in the region and a key factor in observed climate changes in the Arctic.

Due to limited data on the thickness of the ice cover in the Fram Strait, much of the research has focused on estimating the ice area export, which depends on ice drift and ice concentration [Kwok and Rothrock, 1999; Vinje, 2001b; Kwok, 2009; Cox et al., 2010; Smedsrud et al., 2011; Bi et al., 2016; Smedsrud et al., 2017]. A comparison of ice export estimates based on various model and satellite data is provided in [Zamani et al., 2019; Min et al., 2019]. Ice volume export, which also depends on the distribution of ice thickness, is a more indicative parameter for assessing the sea ice balance in the Arctic region, yet it is more challenging to estimate [Kwok et al., 2004; Krumpen et al., 2016; Zhang et al., 2017; Ricker et al., 2018; Spreen et al., 2020].

For the first time, data on ice thickness based on measurements of its draft using upward-looking sonars were utilized in the work of [Vinje et al., 1998]. To estimate the ice volume exported via the Fram Strait, authors in [Kwok et al., 2004] also used thickness data obtained from upward-looking sonars for the period 1991–1998. Estimates of volume flux for the 2003–2008 presented in [Spreen et al., 2009] are based on observations of ice thickness from the ICESat satellite. Authors [Krumpen et al., 2016] used electromagnetic measurements of sea ice thickness conducted from an aircraft for the period 2001–2012.

In the study by [Zhang et al., 2017], the assessment of ice volume export for the period 1979–2012 was carried out using ice thickness data from the Pan-Arctic Ice Ocean Modeling and Assimilation System (PIOMAS). Studies [Ricker et al., 2018; Bi et al., 2018] include estimates of volume flux obtained respectively for the periods 2010–2017 and 2011–2015 based on ice thickness data from the CryoSat-2 satellite. Finally, authors in [Spreen et al., 2020] used ice thickness data from side-looking sonars and profiling sonars to estimate ice volume export for the period 1992–2014.

Additionally, the influence of large-scale atmospheric circulation factors expressed by the NAO and the Arctic Oscillation (AO) on ice drift and ice area export through the Fram Strait is shown in [Ricker et al., 2018]. A high correlation was also found between ice outflow values and the NAO index positively from December to March [Kwok and Rothrock, 1999]. The role of atmospheric circulation on ice area export via the Fram Strait during the period 1979–2006 is addressed in the work of [Tsukernik et al., 2010].

*Ice age composition*. It is known that ice thickness serves as a highly sensitive and illustrative indicator of modern climate changes [Repina and Ivanov, 2012; Alekseeva et al., 2021]. In the absence of reliable thickness data, ice charts indicating observed age gradations of sea ice (corresponding to values of their mean thickness) can be used for indirect assessment. Being one of the most important feature of the ice regime in the winter season, the ice age structure in the Greenland Sea and the Barents Sea is also indicative and crucial in the study of climate change. Currently, information on the ice age composition in research area is limited in the literature, despite the well-studied ice regime of the Seas in general [Mironov, 2004].

The first estimates of the ice age structure in the Greenland Sea are provided in the work of [Wittmann and Schule, 1966]. Based on ice airborne reconnaissance data from 1960 and 1962, the authors calculated the proportions of young, first-year-old, and old ice in the ice cover of the Sea for the following months: January-May, June-July, August-October, and November-December. Average monthly values of the areas of prevalence of old ice in the Greenland Sea for the period 1988–1992, as well as ice areas of separate age gradations (young, first-year-old, and old ice), are presented in the monograph [Mironov,

2004]. The results are based on regional ice charts from the AARI and are provided for those pairs of months during which the Greenland Sea experiences seasonal maximum and minimum ice cover, for March-April and September-October, respectively.

The first estimates of the ice area of separate age gradations in the Barents Sea were made in the 1950s–1970s. Using monthly surface pressure charts and considering the timing of ice formation, as well as the distribution of the boundaries of residual ice and landfast ice, authors [Gudkovich et al., 1972] calculated the average ice areas of key age gradations (including young, first-year-old, and old ice) by the end of May. Using a similar method, calculations of the ice area of separate age gradations for the Barents Sea sub-areas during periods of seasonal maximum and minimum ice cover in April and September, respectively, with the division of first-year-old ice by the gradations of their mean thickness (thin, medium, and thick fist-year-old ice) were performed in [Mironov, 2004]. The issue of the distribution of old ice in the Barents Sea south of 78° N, which poses a hazard during the development of hydrocarbon deposits on its shelf zone, was addressed in the study by [Buzin, 2009].

### 1.4. Conclusions for Chapter 1

In addition to the physical characteristics and hydrometeorological conditions, this chapter presents a review of the current state of research on the Greenland Sea and the Barents Sea ice regime (separate features thereof). Based on the proposed review, the following conclusions have been drawn:

- There are no descriptions of the regularities of seasonal changes in the drift ice edge position in the Greenland Sea and the Barents Sea in the modern period of climate change (after the 2000s) in the literature sources.
- Authors of various studies propose a large number of estimates of the sea ice volume flux through the Fram Strait, which differ in the method of accounting for ice thickness and drift on the strait site. Quantitatively obtained values of ice export vary significantly (by 2-3 times, specific values are not provided in the review), primarily due to the choice of data for estimation.

- Also lacking are assessments of the spatio-temporal distribution of the ice age in the Greenland Sea and the Barents Sea. This includes the ice area of separate age gradations and the boundaries of their predominance; interannual changes in characteristics are not addressed in the literature at all.

# CHAPTER 2. DATA AND RESEARCH METHODS

## 2.1. Creation of sea ice parameters electronic archives

In the present study, the *following* features of the ice regime in the Greenland Sea and the Barents Sea in the modern climate period were analyzed: sea ice coverage and their anomalies; drift ice edge position in the annual cycle; sea ice age composition; boundaries of predominance of first-year and/or old ice; sea ice volume flux through the Fram Strait from the Arctic Basin.

To create electronic data archives, ice charts of the Greenland Sea and the Barents Sea were utilized. These charts have been compiled by ice experts at AARI starting from October 1997 with weekly resolution. They are based on satellite data from the visible, infrared, and microwave electromagnetic spectrum, augmented with data from ships and polar stations. A detailed description of the methodology for compiling ice charts by AARI is provided in [Afanasyeva et al., 2019]. Access to ice charts is provided through the electronic catalog of the World Data Center for Sea Ice [see http://wdc.aari.ru/datasets/d0004/].

For raw data processing on the studied characteristics, the author utilized the freely available QGIS version 3.14 [see https://qgis.org/ru/site/index.html]. This software allows working with ice charts presented in electronic format and in hard copy. The GIS toolkit *enables* digitizing ice charts in hard copy from the AARI archives and further spatial georeferencing; working with electronic ice charts in .shp format; determining spatial characteristics of homogeneous ice zones (coordinates of their boundaries, area, and width) delineated on ice charts to obtain information about the necessary parameters of the ice cover; presenting the obtained information in tabular and graphical formats.

*Ice age composition* was assessed by calculating the area of drift and landfast ice in standard age gradations of the ice cover in the Greenland Sea and the Barents Sea: old, first-year (thick, medium, and thin), young (grey-white and grey), and initial types, according to the International Sea Ice Nomenclature [JCOMM, 2014]. Data were obtained with monthly resolution during the winter months, covering the period from the onset of ice formation in October to its termination in May, for the years 1997–2022. The

electronic archive includes area values expressed in thousands of square kilometers, as a percentage of the total area of the Sea (or it sub-area), and as a percentage of the total ice cover area of the Sea (sub-area). The analysis of the ice age composition in the Greenland Sea was conducted for the entire sea area, while for the Barents Sea, it was performed according to the traditional division into three homogeneous sub-areas: western, north-eastern, and south-eastern [Gudkovich et al., 1972; Mironov, 2004]. Their boundaries are shown in Figure 2.1.

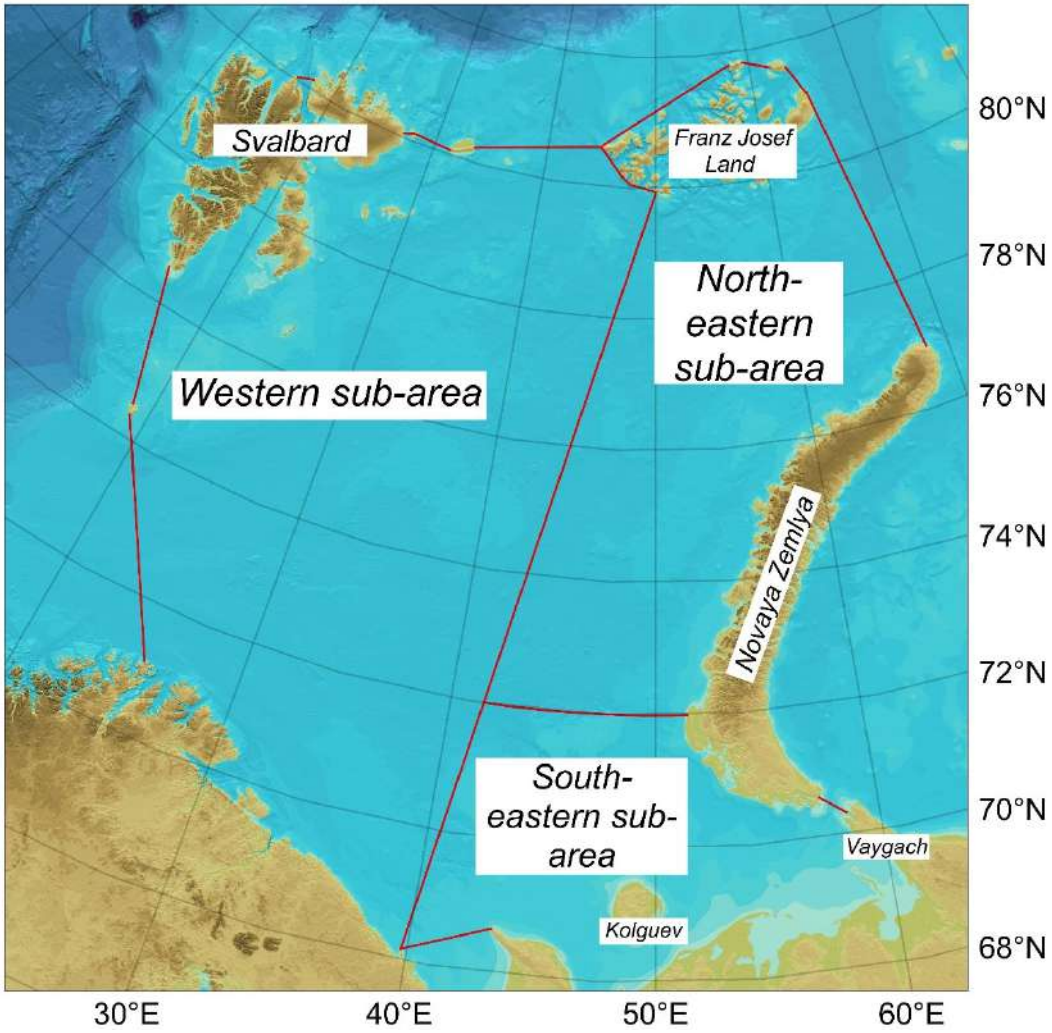


Figure 2.1. Boundaries of delineated homogeneous sub-areas of the Barents Sea (highlighted by red lines) [Gudkovich et al., 1972; Mironov, 2004]

*Boundaries of ice predominance of separate age gradations*. The coordinates of the boundaries of old ice predominance in the Greenland Sea, as well as old and first-year ice (without differentiation into gradations) in the Barents Sea, were determined.

Longitudes in the Greenland Sea were recorded at 1.0° intervals on parallels from 69.0° N to 80.0° N. In the western and northeastern regions of the Barents Sea, latitudes were described by longitude intersections from 20.0° E to 65.0° E at 2.5° intervals, while in the southeastern sub-area of the Sea, it ranged from 69.0° N to 75.0° N at 1.0° intervals. According to the ice age composition, the coordinates of the boundaries of the ice predominance of separate age gradations were obtained with monthly resolution only during the winter period for the years 1997–2022.

The electronic archives described below include both ice reconnaissance data from the period 1950–1978 and satellite data from 1979 to the present. Studies by [Smirnov et al., 2010, 2011] have shown that these data can be merged and treated as a single series for studying the state of the ice cover in the Arctic seas. Joint analysis of NOAA-1 and ECCA-8 satellite images and ice reconnaissance data from 1970–1971 indicates an average discrepancy in the position of the drift ice edge of no more than 7 km, and in the position of the boundaries of ice zones of different concentration and age of no more than 10 km. At the same time, data from Meteor-18 and ice charts compiled based on visual ice observations from an aircraft in July-August 1974 show discrepancies in determining the position of the ice drift edge and boundaries of ice zones of different concentration and age, averaging 1.7 km and a maximum of 8.0 km.

Furthermore, the authors note that the error in determining ice cover parameters obtained for the period 1950–1970, i.e., before the introduction of the first satellites, is approximately ±11.0 km and ±12.8 km respectively for clearly defined and indistinct ice edges and boundaries of zones (in the presence of dense cloud cover). Assuming that this error is systematic and that the edges and boundaries are indistinct, the potential error in determining ice coverage ranges from ±3.2% to ±8.2% of the ice area. It is noted here that the influence of an error of this magnitude on the estimation of ice coverage may only be significant for local areas. For extensive water areas, including entire sea, the impact of random errors in determining the position of the ice drift edge and other ice boundaries will not exceed errors in computational procedures. Additionally, with the introduction of side-looking airborne radar stations (SLAR) into the equipment of ice

reconnaissance aircraft (SLAR systems “Nit” and “Toros”) since 1971, the error in determining these elements of the ice regime has been reduced to ±2.5 km and ±3.5 km respectively for clearly defined and indistinct edges and boundaries.

*Drift ice edge position*. Coordinates of the drift ice edge position in the Greenland Sea and the Barents Sea were obtained at fixed sections, as listed above. The electronic data archive covers the entire ice season, i.e., the period of ice cover existence, from October of the previous year to September of the subsequent year, with monthly resolution. However, the inclusion of ice charts from AARI, stored in hard copy, significantly expands the analysis of the ice cover observation period. For the Greenland Sea, approximately 500 ice charts were digitized and analyzed, while for the Barents Sea, over 6000 ice charts were processed. Therefore, data on the drift ice edge position in the Greenland Sea are available from the 1980/1981 ice season onwards, and in the Barents Sea, from 1933/1934 ice season onwards for specific months. However, continuous monthly data, which will be used in this study to assess changes in the annual cycle, start in the Greenland Sea only from the 1998/1999, and in the Barents Sea, from the 1982/1983.

*Ice coverage*. Finally, the available electronic archives of monthly mean ice coverage values for the Greenland Sea and the Barents Sea (data for the latter are presented for three sub-areas) were supplemented with the latest data provided by the Ice Regime and Forecasting Department of AARI. So, the ready electronic data archives cover the period from 1950 to 2022. Ice coverage is measured in percentage (%) terms because the term “ice coverage” in the literature refers to the percentage of the area covered by ice of any concentration compared to the total area of the Sea or it sub-area [Borodachev et al., 1994]. Do not confuse ice coverage with ice extent, as when determining the latter based on concentration, the area of open water between individual ice floes is taken into account.

### 2.2. Hydrometeorological factors

*Data for determining the factors shaping changes in the ice age composition.* For quantitative assessment of atmospheric circulation intensity, the following atmospheric

(climatic) indices have been selected, the time series of which underlie the establishment of statistical relationships between various hydrometeorological variables and the nature of large-scale processes occurring in the atmosphere [Litvinova, 2018]:

1. *Arctic Oscillation* (AO):

Introduced to modeling the anomalies in the atmospheric circulation of the Northern Hemisphere, the AO represents the first mode of the decomposition of pressure field at the 1000 hPa level from 20° S to 90° N using empirical orthogonal functions [Thompson and Wallace, 1998; 2000]. It indicates redistribution of zones of enhanced (reduced) atmospheric pressure in the Arctic region, leading to strengthening (weakening) of the zonal component of air mass transport [Zhou et al., 2001]. It has positive and negative phases: when vortices of relatively high pressure are observed over the North Pole and low pressure over mid-latitudes, a negative phase of Oscillation is noted; the opposite pressure distribution is observed in the positive phase.

2. *Arctic Dipole* (AD):

Represents the second mode of decomposition of the atmospheric pressure field, calculated using natural orthogonal functions at the 700 hPa level from 70° S to 90° N. A characteristic feature of the baric structure is the shift of the high-pressure center to the Barents Sea and the formation of a deep depression over eastern Siberia. Its formation, as noted by [Wu et al., 2006; Overland et al., 2008; Wang et al., 2009], is a consequence of the reorganization of the circulation system in the Arctic.

3. *North Atlantic Oscillation* (NAO):

Being a regional mode of the Arctic Oscillation, the NAO represents anomalies of atmospheric pressure between two large centers of atmospheric action, the Icelandic Low and the Azores High, thus reflecting the zonal transport of air masses from the North Atlantic [Goldenberg et al., 2001; Nesterov, 2013]. It is calculated as the main component of the decomposition using natural orthogonal functions of pressure at the 500 hPa level over the Northern Hemisphere [Popova and Shmakin, 2010]. It exhibits activity throughout the year: the positive phase reflects negative anomalies of atmospheric pressure in the

high latitudes of the northern part of the Atlantic Ocean and positive anomalies in its central part; the negative phase is characterized by the opposite pressure distribution.

Monthly mean values of the AO and NAO indices, starting from 1950, are published by the National Oceanic and Atmospheric Administration (NOAA) [see https://www.ncei.noaa.gov/climate-monitoring/#all]. Additionally, values of the AD index were provided by Markus Janout, a researcher at the Alfred Wegener Institute for Polar and Marine Research, Germany (AWI).

For accounting for the influence of warm Atlantic waters entering the Barents Sea, the following was utilized:

4. *Sea water temperature along the oceanographic section "Kola Meridian"*:

Represents a unique series of natural observations of sea water temperature in the western region of the Barents Sea. Its distinctive features include the duration of observations, the amount of data, and spatial coverage [Karsakov et al., 2018; 2022]. Monthly mean values of sea water temperature at depths up to 200 m at stations covering the coastal (stations 1–3) and main (3–7) branches of the Murman Current, as well as the central branch (8–10) of the North Cape Current from 1950 to 2020, are provided on the website of the Polar Branch of the All-Russian Scientific Research Institute of Fisheries and Oceanography (PINRO named after N.M. Knipovich) [see http://www.pinro.vniro.ru/en/kola-meridian-section/observation-series]. Data up to 2023 were kindly provided by Antsiferov M.Y., the Head of the Laboratory of commercial oceanography. Temperature data in the 0–50 m layer along the entire section were used in the study.

Finally, a predictor potentially determining interannual changes in the state of the ice cover of the Barents Sea is:

5. *Surface air temperature*:

Data from the ERA5 atmospheric reanalysis by the European Centre for Medium-Range Weather Forecasts (ECMWF) with a spatial resolution of 0.25° × 0.25° and a temporal resolution of one month [Hersbach et al., 2020] were utilized. The temporal

coverage spans from January 1940 to present. Various sources were involved in forming the database, including meteorological station data, radiosonde data, and satellite data. ERA5 data is widely used in climate research, meteorology, and environmental monitoring as it provides a comprehensive and detailed picture of global weather conditions. Access to this data is available through the Climate Data Store system of the Copernicus Earth Observation Program [see http://cds.climate.copernicus.eu].

*Data for calculating sea ice export with surrounding basins.* To calculate the magnitude and direction of the total monthly mean sea ice drift vector at specified gateways of sea ice export between the Greenland Sea and the Barents Seas and surrounding waters, the author utilized data on ice drift from the National Snow and Ice Data Center (NSIDC). These include Polar Pathfinder data (1979–2019) and Quicklook Arctic data (from 2020 to present) [see https://nsidc.org/data/nsidc-0116/versions/4 and https://nsidc.org/data/nsidc-0748/versions/1 respectively]. These products combine satellite (primarily passive microwave radiation) observations, buoy station data, and atmospheric reanalysis. The data include information on the *u*- and *v*-components of the sea ice drift velocity vector, which are projected onto a grid with a resolution of 25 km × 25 km [Tschudi et al., 2020].

### 2.3. Research methods

#### 2.3.1. Method for determining average-weighted ice thickness in Fram Strait

*Level ice thickness*. According to the International Nomenclature for Sea Ice [JCOMM, 2014], the sea ice age structure in the Fram Strait is represented by seven standard gradations (ranges of its mean thickness): nilas and initial types of ice (less than 10 cm); grey (10–15 cm) and grey-white (15–30 cm) young ice; thin (30–70 cm), medium (70–120 cm), and thick (more than 120 cm) first-year ice; old ice (more than 250 cm). It's evident that age gradations from initial ice types to first-year medium ice have clearly defined average thickness ranges. Therefore, when estimating the thickness of level ice in the Fram Strait ice flow, the following reference values are used: initial ice types and nilas ice — **5.0** cm; grey and grey-white ice — **12.5** cm and **22.5** cm respectively; young

ice (in cases where it is not possible to identify grey and grey-white ice separately when compiling an ice chart) — **30.0** cm; thin and medium first-year ice — **50.0** cm and **95.0** cm respectively. Estimating the thickness of thick first-year and old ice, whose thickness ranges have no upper limit (more than 120 cm and more than 250 cm respectively), is a more complex task. For this purpose, certain assumptions are introduced.

The author [Mironov, 2004] notes that the main fraction of the ice cover in the Fram Strait consists not of locally formed ice, but of ice brought from the northern regions of the Siberian shelf seas (Kara, Laptev, and East Siberian) by the Transpolar Drift system and distributed into the Greenland Sea by the East Greenland Current. The Transpolar Drift System is one of the main elements of ice circulation in the Arctic Basin and influences Arctic seas ice conditions [Volkov et al., 2016]. In the study [Timofeeva and Sharatunova, 2021] shown that maximum ice thicknesses in the Laptev Sea for the period 2005–2020 decreased by 6% compared to observations before 2004. Furthermore, the author suggests that over this 15-year period, the thickness of drift ice at the Fram Strait site, due to the relatively greater influence of warm Atlantic waters, decreased by 8%.

Therefore, for a quantitative assessment of changes in the average thickness of first-year thick ice in the Fram Strait, data on the thickness of landfast ice at the polar stations Kotelnny (Laptev Sea) and Chelyuskin (Kara Sea) from the Roshydromet network, available in the form of weather bulletins, were utilized [see http://193.227.232.57/meteo/default/bulluten]. The observation series was divided into two periods, 1997–2004 and 2005–2022, in accordance with the assessments in [Timofeeva and Sharatunova, 2021]. Thus, the author obtained the values of the increase in first-year thick ice thickness for each month of observation, averaged based on data from the two polar stations, and calculated the average thickness of level ice, starting from the accepted lower boundary thickness of first-year thick ice of **120.0** cm in December to their maximum values of **193.0** cm and **178.0** cm observed at the stations in 1997–2004 and 2005–2022 respectively.

The average thickness of old ice carried through the Fram Strait was approximately 320.0 cm during the period 1981–1984, according to the results of [Mironov, 2004].

However, data from visual ship observations, which were aggregated for the period 1991–2021 in the studies [Alekseeva et al., 2018; Egorova et al., 2021], indicate a noticeable reduction in the thickness of old ice in the Arctic Basin in certain summer months (June-August) after 2005. Considering the previously introduced division into periods, it is assumed in the study that the average thickness of level old ice cover was **320.0** cm in 1997–2004, and in 2005–2022 it was already **260.0** cm, considering its ablation of 60.0 cm.

*Nominal ice thickness*. Spatial-temporal changes in ice thickness are formed as a result of the influence of a number of factors, grouped into thermal and dynamic categories. The first category includes climatic features of hydrometeorological processes, which affect the natural growth and melting of sea ice (total radiation, precipitation amount, heat flux from the ocean, etc.). The second group of factors includes ice drift and ice hummocking [Smirnov, 2007]. Variations in drift velocity and direction lead to deformations of the ice cover in the form of ridging and rafting, which significantly affect the distribution of ice thicknesses of separate age gradations [Mironov, 2004].

Under real observing conditions, the level ice cover always alternate with various forms of pressure ridges. Therefore, estimating the average ice thickness is associated with the necessity to account for hummocking nature. In this study, an original methodology [Mironov, 2004] is applied for estimating the ice thickness deformed by pressure ridges. Thus, the author distinguishes between the level ice thickness ($H_{lev}$), effective ice thickness ($H_{ef}$), and nominal ice thickness ($H_{nom}$). Effective ice thickness refers to the adjustment introduced to account for pressure ridge formations, while conditional ice thickness characterizes the total thickness of level and deformed ice (see formula 2.1):

$$H_{nom} = H_{lev} + \mathrm{H}_{ef} \tag{2.1}$$

Accordingly, to calculate the effective ice thickness in the study, the *following* empirical equations are proposed (see Table 2.1), where it depends on the age gradation (thin/medium/thick), type of pressure ridge (fresh/old), the height of ridge freeboard ($h_i$), and the number of pressure ridge per 1 km ($n$). The methodology [Mironov, 2004] also

includes empirical values of *n*, the number of pressure ridge per 1 km: its 4.0 in October-December; 4.8 in January-March, and 5.5 in April-May.

Table 2.1. Empirical equations for calculating effective ice thickness [Mironov, 2004]

| *Ice age gradation (mean thickness, m)* | *Type of ridge* | $h_i$, *m* | *Formula* |
|---|---|---|---|
| Thin ($h_1$=0.3) | Fresh | 0.3 | $25 \cdot n \cdot h_1^{\,2}$ |
| Medium ($h_2$=1.0) | Fresh | | $19 \cdot n \cdot h_2^{\,2}$ |
| | Old | | $34 \cdot n \cdot h_2^{\,2}$ |
| Thick ($h_3$=3.0) | Fresh | 1.0 | $16 \cdot n \cdot h_3^{\,2}$ |
| | Old | | $41 \cdot n \cdot h_3^{\,2}$ |

When determining the thickness of ice in the Fram Strait site, relying on data regarding the age structure, it is necessary and correct to appeal to the concept of "weighted-average thickness". This is because within one ice zone on the chart, there is a certain ratio (in points) of two or three prevailing age gradations of different thicknesses. Therefore, according to [Pishchalnik et al., 2020], the weighted-average ice thickness ($H_{wei}$) was calculated proportionally to their partial concentration (in points) based on the average conditional thickness of ice of each age encountered at the gateway (see formula 2.2):

$$H_{wei} = \frac{\sum_{i=1}^{n}\left(H_{av_i} \cdot C_i\right)}{\sum_{i=1}^{n} C_i} \qquad (2.2)$$

where $H_{avi}$ is the average ice thickness of the i-th age gradation,

$C_i$ is the partial ice concentration of the i-th age gradation,

$n$ is the number of distinguished age gradations within one ice zone.

Similarly to the results of [Pishchalnik et al., 2020] for the Sea of Okhotsk, an assessment of errors in calculating the weighted-average ice thickness in the zone dominated by ice of separate age gradations was carried out for the Fram Strait gateway. The number of combinations of ice cover characteristics within the ice zone is limited, so the values of the weighted-average thickness were calculated for all possible cases. According to [Instruction on..., 1981], an ice expert can determine the partial concentration of ice cover of a certain age gradation with an accuracy of 1 point. Thus, the error in

determining the weighted-average thickness in the zone dominated by young ice can be ±1–3 cm, thin first-year ice ±3–6 cm, medium first-year ice ±5–9 cm, thick first-year ice ±6–15 cm, and finally, old ice ±14–20 cm. If the error in calculations in the Fram Strait ice flow reaches a *maximum* of 20 cm, then the error in determining the weighted average thickness using the proposed methodology is 6% with an average characteristic value along the entire strait of 340 cm.

### 2.3.2. Data for calculating the ice export in Greenland Sea and Barents Sea

In the Greenland Sea, ice export with surrounding waters to the north occurs through the Fram Strait, while to the south, it occurs through the Danish Strait (which is not considered in this study). Ice outflow from the Barents Sea occurs through the Shilling Strait (between the archipelagos of Svalbard and Franz Josef Land), Makarov Strait (between Franz Josef Land and Novaya Zemlya), and the Kara Gates. The locations of these sections are indicated in Figure 2.2.

In this study, it is assumed that the area of ice transported through the gateway per unit of time (expressed in $km^2$ per month) depends on the average drift velocity (in km per month) and the ice flow width (in km), taking into account the concentration of the prevailing ice cover in the ice flow. When calculating the volume of ice transport per unit of time (in $km^3$ per month), the weighted-average thickness on the corresponding gateway is added to the parameters mentioned above. Monthly average values of sea ice drift velocity are determined using the Polar Pathfinder and Quicklook Arctic databases (see subsection 2.2). This approach will be briefly referred to as NSIDC throughout the text. To calculate the magnitude and direction of the total monthly mean sea ice drift vector, points closest to the calculated gateways were selected (marked on Figure 2.2 with orange dots). Thus, the area of ice exported at the calculated gateway is calculated by multiplying the sea ice drift velocity from the NSIDC data by the ice flow width. To calculate the volume of ice transport, a term of the weighted-average ice thickness with a correction for hummocky formations is added.

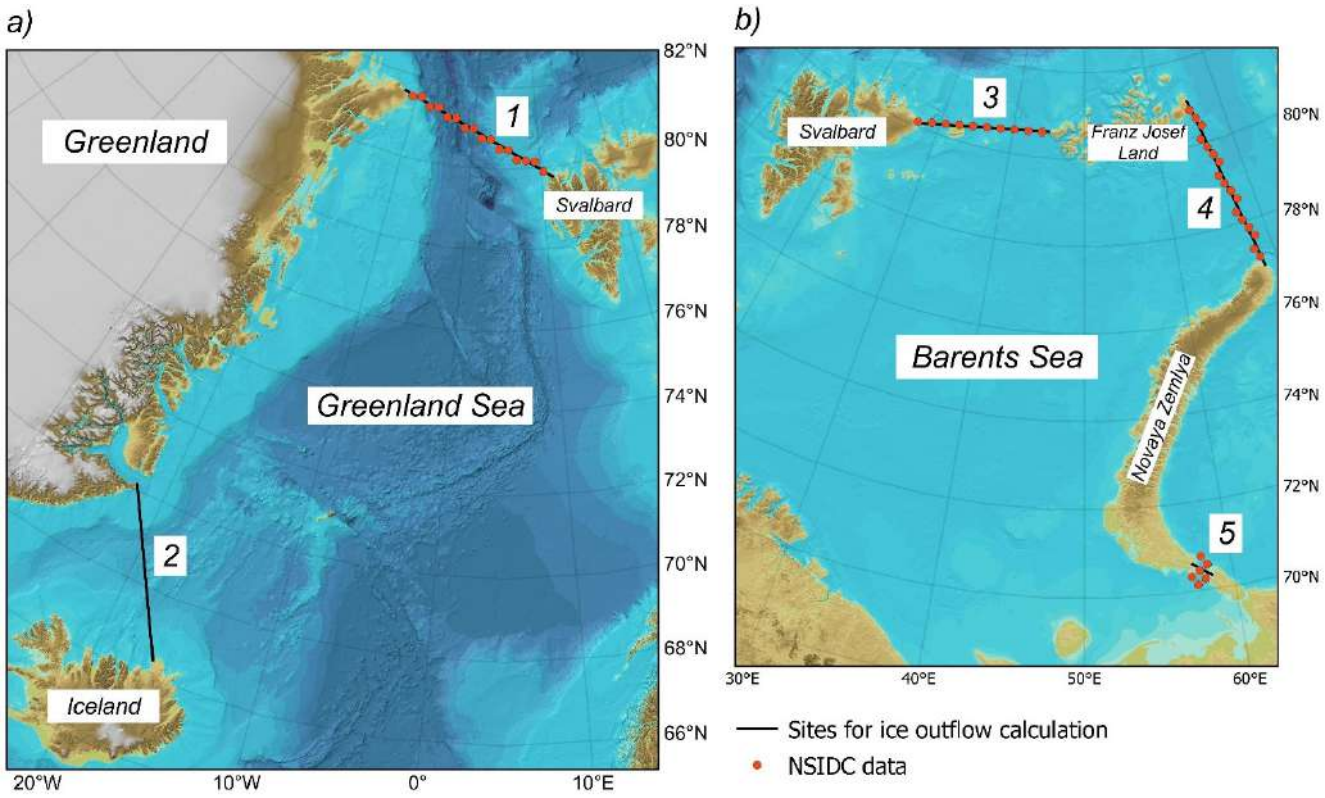


*1* — Fram Strait, *2* — Danish Strait, *3* — Shilling Strait, *4* — Makarov Strait, *5* — Kara Gates

Figure 2.2. Position of ice export strait sites in: *a)* the Greenland Sea and *b)* the Barents Sea (black lines). Drift vectors, which were utilized to calculate the mean ice drift velocity vector based on NSIDC data, are shown as orange dots.

### 2.3.3. Statistical methods of analysis

For the analysis of time series of hydrometeorological and ice data in the present study, the following statistical methods were utilized:

*1. Trend extraction and analysis:*

In statistics, a trend refers to the slow variation of a characteristic without the formation of cycles with a period significantly exceeding the length of the original sample [Malinin, 2020b]. The presence or absence of a trend, its intensity, and form always depend on the length of the series selected from the population. Two types of trends are distinguished: *linear*, which describes the dependency of the parameter of interest on time by a linear equation, and *nonlinear*, which defines the same dependency but by a nonlinear

equation. The behavior of the trend is characterized by its magnitude and contribution to the overall variance of the studied series, established based on the significance testing of the correlation coefficient. As noted by the author [Malinin, 2020b], only for a significant trend is it valid to determine the trend magnitude, understood as the change in the studied characteristic over a certain period of time.

The assessment of the statistical significance of the trend is based on the null hypothesis of the correlation coefficient being equal to zero. To test the hypothesis, the Student's t-test is computed, which depends on both the correlation coefficient itself and the magnitude of its standard deviation in the population. Thus, a trend is statistically significant if the obtained Student's t-test statistic exceeds the critical value at a given level of significance and known length of the analyzed sample; conversely, if the obtained statistic is below the critical value, the trend is considered statistically insignificant [Malinin, 2020b]. In cases where the sample contains both significant linear and nonlinear trends, preference is given to removing the nonlinear trend if it contributes more than 5% to the overall variance of the studied time series, and vice versa for the linear trend [Gordeeva, 2010].

*2. Multiregression analysis:*

With the purpose of identifying statistically significant hydrometeorological and ice factors influencing interannual changes in the ice area of various age gradations in the Barents Sea sub-areas, the author conducted a multivariate analysis of the statistical relationships of the investigated time series. The multiregression analysis toolkit from the statistical analysis software “Statistics” version 7 was employed, allowing for the derivation of statistical relationship equations through the built-in “Multiple Regression” function [Malinin and Gordeeva, 2003; Malinin, 2020a].

The general aim of the multiple regression algorithm is to jointly analyze statistically significant relationships between independent and dependent variables (predictor and predictand, respectively). The main computational task executed by this tool is to maximize the fit between the regression line and a set of data points [Vaynovsky and Malinin, 1992].

However, in the case of studying processes occurring in the natural environment, it is often observed that the relationship between variables is multifactorial. Thus, the regression line cannot be represented in a two-dimensional space, necessitating its expression through a multiple linear regression equation.

For constructing statistical equations with no more than five significant predictors, a procedure of sequential variable elimination was chosen. As a result, statistical equations with the highest correlation ($R$) and determination ($R^2$) coefficients were obtained, which are among the main criteria for assessing their statistical significance. Based on their values, the quality of reproducing the actual distribution of the studied characteristic by these equations was evaluated [Malinin, 2020a].

The multiple linear correlation coefficient $R$ (hereinafter referred to as the correlation coefficient) reflects the degree of linear relationship between the actual and calculated values of the predictand [Malinin, 2020a]. It takes non-negative values from 0, in cases where the variance of the dependent variable is determined by the variance of residuals, to 1, when the factors included in the final equation fully describe the variance of the predictand. The linear coefficient of determination $R^2$ (hereinafter referred to as the determination coefficient) indicates the explained proportion of the predictor's variance, i.e., the proportion described by the selected predictors in the statistical equation. It is in turn related to the standardized regression coefficients $\beta_j$ by the following formula (see formula 2.3):

$$R^2 = \sum \beta_j r_{yj} \tag{2.3}$$

where $r_{yj}$ is the pairwise correlation coefficient between the predictand and the j-th predictor.

Hence, the product $\beta_j$ and $r_{yj}$ represents the contribution of each predictor to the variance of the response function. In this study, the contribution is expressed as a percentage of the explained portion of the variance of the studied quantity, so the total sum of contributions equals 100%, rather than the determination coefficient. As a result, the contribution indicates the degree of influence of significant hydrometeorological and ice parameters on the interannual changes in the ice area of various age gradations. A similar

statistical approach to describing the factors forming interannual changes in ice coverage in the Arctic Seas has already been applied in the works of [Viazigina et al., 2021; Lis et al., 2023].

### 2.3.4. Availability and efficiency of forecasting method

The search for significant factors that determine the interannual changes in the ice area of various age gradations in the Barents Sea sub-areas is a preparatory step necessary for developing a forecasting method. The availability and efficiency of the method reflect the feasibility of using the obtained statistical equations in practice for forecasting (in this case, long-term forecasting with a lead time of one month). The characteristics were calculated according to the methodology outlined in the guiding document [Instruction on…, 2011].

*Availability P* indicates the percentage of successful forecasts relative to their total number (thus expressed as a percentage). To determine it, Table 2 from [Instruction on…, 2011] is used, which shows the dependence of this criterion on various allowable errors from the forecast success rate $S/\sigma_x$. This rate represents the ratio of the root mean square error of the verification forecasts $S$ to the root mean square deviation of the predicted phenomenon from the norm $\sigma_x$ (see formulas 2.4 and 2.5 respectively):

$$S = \sqrt{\frac{\sum_{i=1}^{n}\left(x_{act} - x_{forecast}\right)^2}{n - m}} \tag{2.4}$$

$$\sigma_x = \sqrt{\frac{\sum_{i=1}^{n}(x_i - x_{av})^2}{n}} \tag{2.5}$$

where $x_i$ is the given value of the phenomenon in the long-term observation series,

$x_{av}$ is the long-term average value of the phenomenon,

$x_{act}$ and $x_{forecast}$ are the actual and forecasted values, respectively,

$n$ is the number of members in the series,

*m* is the number of degrees of freedom, characterizing the type of regression equation and equal to the number of constants in it.

The *efficiency* of the forecasting method (expressed as a percentage) indicates the gain in its availability *P* compared to the climatic availability $P_{clim}$ (for a long-term forecast) — the latter is subtracted from the former. Climatic availability is determined by the formula (2.6):

$$P_{clim} = \frac{m}{n} * 100 \quad (2.6)$$

where *m* is the number of cases where the deviation of the climatic value (norm) from the actual values does not exceed the accepted allowable error,

*n* is the number of members in the series.

The allowable error, established for long-term forecasting, is taken as $0{,}8\sigma_x$, based on recommendations in the guiding document. The studied dataset was divided into dependent and independent subsets. The average value of the dependent subset, i.e., for the period from 1997/1998 to 2019/2020 ($n = 23$), was taken in this study as the climatic norm. The independent subset, used to verify the forecast quality, includes three ice seasons, from 2020/2021 to 2022/2023. According to the [Instruction on…, 2011], the application of the long-term forecasting method for practical purposes is considered feasible if its efficiency is more than 10%.

### 2.4. Conclusions for Chapter 2

The chapter provides a description of the data and methods used in the present dissertation work. Their selection is based on the analysis of literature sources related to the research topic. Electronic data archives were first created for the main parameters of the Greenland and Barents Seas ice cover in the contemporary climatic period, utilizing unique regional ice charts. In addition to widely known statistical analysis methods, the author describes an original methodology for estimating the volume of ice export through the Fram Strait based on actual data on the ice age structure (average thickness) in the winter months, with a correction for hummocky formations.

# CHAPTER 3. REGULARITIES OF SPATIO-TEMPORAL VARIATIONS OF ICE REGIME KEY CHARACTERICTISC IN GREENLAND SEA

## 3.1. Ice coverage

### 3.1.1. Seasonal variations

The ice coverage of the Greenland Sea is characterized by the seasonal ratio of ice cover and open water areas, the presence of which throughout the year is a distinctive feature of the Sea's ice conditions. The seasonal variation in ice coverage in the Greenland Sea, averaged over the period from 1950 to 2022, is presented in Table 3.1.

Table 3.1. Seasonal variation of ice coverage in the Greenland Sea (expressed in %) throughout the annual cycle, averaged over the period from 1950 to 2022

| Ice coverage, % / Month | X | XI | XII | I | II | III | IV | V | VI | VII | VIII | IX |
|---|---|---|---|---|---|---|---|---|---|---|---|---|
| Mean | 32 | 37 | 43 | 48 | 52 | 52 | 52 | 47 | 43 | 36 | 28 | 26 |
| Maximum | 45 | 57 | 72 | 80 | 88 | 85 | 89 | 75 | 68 | 62 | 53 | 49 |
| Minimum | 17 | 23 | 28 | 23 | 22 | 27 | 23 | 27 | 29 | 17 | 3 | 7 |
| SD, % | ±6 | ±7 | ±10 | ±13 | ±15 | ±14 | ±13 | ±11 | ±9 | ±8 | ±8 | ±9 |
| Seasonal range, % | 28 | 34 | 44 | 57 | 66 | 58 | 66 | 48 | 39 | 45 | 50 | 42 |

*Note.* Standard deviation (SD) refers to the root mean square deviation. Seasonal range denotes the difference between the maximum and minimum ice coverage values within the seasonal cycle.

The seasonal maximum of ice coverage in the Greenland Sea is observed from February to April: during these months, the ice cover occupies an average of 52% of its area. This is consistent with results from previous studies, where the greatest ice area in the Greenland Sea was recorded in February-March (1958–1996) [Mironov, 2004] or only in March (1950–2016) [Timokhov et al., 2018]. It is known that in the Russian Arctic seas of the Siberian shelf, the maximum development of ice cover under average conditions occurs in April-May [Russian Arctic Seas…, 2021]. This shift is primarily explained by the influence of warm Atlantic waters on the ice cover of the Greenland Sea [Mironov, 2004]. The seasonal minimum of ice cover is characteristic of September, when the ice

cover in the Greenland Sea is at 26%, which matches the estimates in the aforementioned studies to within a month.

Further analysis of ice coverage extremes is conducted based on *ice seasons*. As shown in Table 3.1, during periods of maximum ice development, the ice cover can occupy up to 89% of the Greenland Sea's area, as seen in the ice season of 1953/1954. Among other extremely high ice area values, notable ice seasons include 1967/1968 (with 88% ice cover in February), 1968/1969 (81% in March), as well as 1950/1951 and 1952/1953 (both with 79% ice coverage in February). While within the annual cycle, the timing of ice coverage maximum varies over three months under average conditions from 1950 to 2022, extremely high values are observed in March in 32% of cases, more frequently than in other months, followed by February in 27% of cases and April in 22% of cases. The remaining 8%, 7%, and 4% of cases are distributed across other months, including May, December, and January, respectively. It's worth noting that in the most recent analyzed years, starting from the ice season of 2016/2017, the largest ice cover area in the Greenland Sea is recorded in April.

According to Table 3.1, during mild winters, the ice coverage of the Greenland Sea can decrease to as low as 3%, as observed in August of the ice season of 1997/1998 (although it sharply increased to 23% by September). Another characteristic ice season is 2012/2013 when the Greenland Sea's ice cover occupied no more than 8% of its area in August-September, coinciding with the period of its minimal development in the Arctic Ocean [Ivanov et al., 2013]. Additionally, in the ice seasons of 2001/2002 and 2003/2004, ice cover of around 8% was also observed in September. In 66% of cases (i.e., in the vast majority), the seasonal minimum ice coverage of the Greenland Sea is typically established in September, as expected under average conditions. However, in 29% of ice seasons, its onset occurs in August, while in 4% and 1%, it occurs in October and July, respectively.

The rates of change were calculated by computing the difference between the ice coverage values for adjacent months within the ice season. The maximum rates of ice growth in the Greenland Sea are observed from October to December, as this period corresponds

to active ice formation (with an average increase in ice coverage of approximately +6% per month). In January-February, the rate of ice cover change gradually slows down, ranging from +4% to +5% per month. Ice area reaches its maximum seasonal values from February to April. Although the melting of sea ice in the Greenland Sea begins in May, the maximum rates of its reduction are observed during the period from July to August, reaching approximately –7% to –8% per month. Additionally, the rate of ice coverage decrease during the period from May to June is approximately –4% per month.

### 3.1.2. Interannual variations

In the interannual variations of Greenland Sea ice cover, a statistically significant linear trend indicating a decrease in ice extent has been identified [Viazigina et al., 2021]. These results are consistent with the observed trend towards decreasing sea ice coverage of the Arctic Ocean [Serreze and Stroeve, 2015; Stroeve and Notz, 2018; Yulin et al., 2019]. Against the backdrop of this trend, large interannual fluctuations in ice coverage are observed, as demonstrated by the standard deviation (SD) values for each month within the ice season (see Table 3.1). Maximum SD values, ±13–15%, are characteristic for months with the greatest ice extent within the annual cycle, from February to April. Minimum SD values, ±6–7%, are noted in the months from October to November, during the period of active ice formation in the Greenland Sea. At the same time, during periods of minimum seasonal ice cover in August-September, the SD values amount to ±8–9%.

Typically, statistically significant linear trends have been identified by researchers [Vinje, 2001a; Frolov et al., 2007a; Timokhov et al., 2018] across the entire analyzed dataset. However, when a long time series of observations on Greenland Sea ice coverage (from 1950 to 2022, spanning 73 years) is available, covering various periods of cooling and warming in the Arctic region [Frolov et al., 2007a; Matishov et al., 2011; Diansky et al., 2019], it is advisable to analyze trends over specific time intervals. For the Greenland Sea, a region experiencing the most intense climatic changes [Barry et al., 1993; Gudkovich et al., 1997; Borzenkova, 2016], determining the onset and duration of these “cold” and “warm” periods are an important research task.

For the analysis of the long-term Greenland Sea ice cover dataset in this study, the method of anomalies cumulative curves is utilized, allowing for the determination of characteristic periods of interannual anomaly changes in ice coverage over specific time intervals. The cumulative curves are computed by sequentially algebraically summing the values of ice coverage anomalies according to the methodology proposed by the authors for meteorological characteristics [Girs and Kondratovich, 1978]. A similar approach to analyzing ice parameters has previously been applied in studies of ice coverage anomalies in the Sea of Okhotsk and the Tatar Strait [Pishchalnik et al., 2016; 2019].

In accordance with the identified periods [Zakharov, 1996; Alekseev et al., 2009] within the ice season, the main periods of changes in the ice cover of the Arctic Seas, for the analysis of ice anomalies in the Greenland Sea, the following months were selected: *November*, corresponding to the month of active ice formation; *February*, a period of stable ice formation; as well as *April* and *September*, months of maximum and minimum ice area respectively. The cumulative curves of ice anomalies in the Greenland Sea for the selected months, calculated relative to the multi-year mean values for the period 1950–2022, are presented in Figure 3.1. The cumulative curves distinguish between two to three periods of anomaly changes: the stage of increasing ice coverage is marked on the figure with a red curve, decreasing — with a blue curve, and stationary periods — with a green curve. The duration of these stages can be interpreted differently.

The duration of cooling and warming periods in the Arctic, as identified by authors of various studies, varies. This largely depends on the analyzed parameter of the environment (which can include individual hydro-meteorological and ice characteristics), the sources of data used, and the length of the study period. According to the analysis of changes in ice conditions in the Arctic Seas [Frolov et al., 2007b], three periods of ice coverage variations are identified. The periods of 1933–1961 and 1984–2005 are characterized by reduced, while the period of 1962–1983 is characterized by increased ice coverage, which is associated with changes in atmospheric pressure fields and air temperature. The instrumental observation data on North Atlantic surface water temperature obtained since 1897, analyzed in the study by [Polyakov et al., 2004], allowed the authors to identify

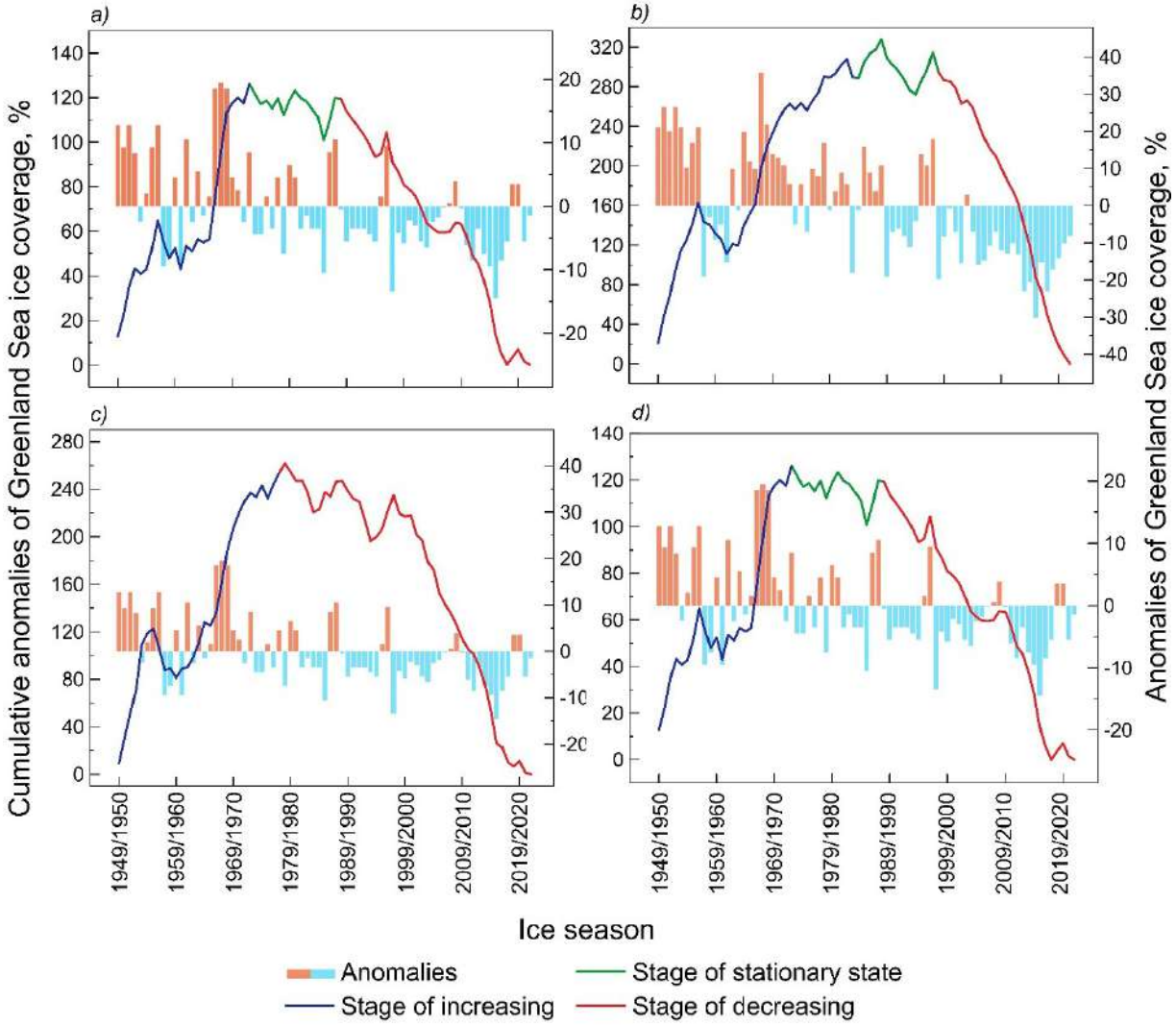


Figure 3.1. Cumulative curves of ice anomalies in the Greenland Sea, computed relative to the multi-year mean values for the period 1950–2022, in *a)* November, *b)* February, *c)* April, and *d)* September.

two warm periods, in the 1930s–1940s and since the 1980s, and two cold periods, in the early 20th century and in the 1960s–1970s. According to the mean annual anomalies of surface air temperature over land for 1880–2014, which were smoothed by a nine-year moving average in the work by [Diansky et al., 2019], two warming periods were observed in the Arctic during 1915–1949 and 1971–2019, and one cooling period occurred in 1950–1970.

In the Greenland Sea, the transitions from the “cold” to the “warm” period within the annual cycle, as indicated by the cumulative curves of ice coverage anomalies, vary. For instance, in the ice seasons of 1973/1974 and 1978/1979, the phases of increasing ice

coverage end in November and April, respectively, while in the subsequent ice season of 1983/1984, they end in February and September. Only in April, no stationary phase is identified on the cumulative curve; thus, the period of ice extent decrease begins from the ice season of 1979/1980 onwards. For the remaining months, stages of relative constancy in ice coverage change of various durations are characteristic. The period of ice coverage decrease then commences from the ice season of 1989/1990 in November, 1999/2000 in February, and 2000/2001 in September. Table 3.2 presents the values of ice coverage anomalies in the Greenland Sea during the identified stages of change.

Table 3.2. Average magnitude and predominant sign of anomalies of absolute values of Greenland Sea ice cover (%) during the stages of its change for the period 1950–2022, identified by integral curves of anomalies

| *Stage of change* | Period | Ice coverage anomaly (%) | | |
|---|---|---|---|---|
| | | Mean | Positive | Negative |
| **November** | | | | |
| *Increasing* | 1950/1951–1973/1974 | +5% | +2%...+20% (19) | –9%...–1% (5) |
| *Stationary state* | 1974/1975–1988/1989 | 0% | +2%...+11% (7) | –10%...–1% (8) |
| *Decreasing* | 1989/1990–2022/2023 | –4% | +1%...+10% (9) | –14%...–1% (25) |
| **February** | | | | |
| *Increasing* | 1949/1950–1983/1984 | +8% | +4%...+26% (25) | –19%...–1% (10) |
| *Stationary state* | 1984/1985–1998/1999 | 0% | +4%...+18% (7) | –20%...–1% (8) |
| *Decreasing* | 1999/2000–2021/2022 | –13% | +3% (1) | –30%...–1% (22) |
| **April** | | | | |
| *Increasing* | 1949/1950–1978/1979 | +9% | +1%... +38% (25) | –18%...–2% (5) |
| *Decreasing* | 1979/1980–2021/2022 | –6% | +1%...+13% (6) | –27%...–1% (37) |
| **September** | | | | |
| *Increasing* | 1949/1950–1983/1984 | +5% | +1%...+23% (31) | –5%...–1% (4) |
| *Stationary state* | 1984/1985–1999/2000 | 0% | +1%...+9% (16) | –11%...–3% (6) |
| *Decreasing* | 2000/2001–2021/2022 | –9% | +1%...+6% (3) | –19%... –3% (19) |

*Note.* The number of ice seasons characterized by predominance of anomalies of a certain sign is given in parentheses.

The contribution of specific months to interannual changes in ice coverage can be assessed by constructing a similar cumulative curve for the average ice season (see Figure 3.2). Thus, three characteristic stages are distinguished: an increase in ice coverage in the Greenland Sea from 1949/1950 to 1981/1982 (blue color in the figure) is followed by a

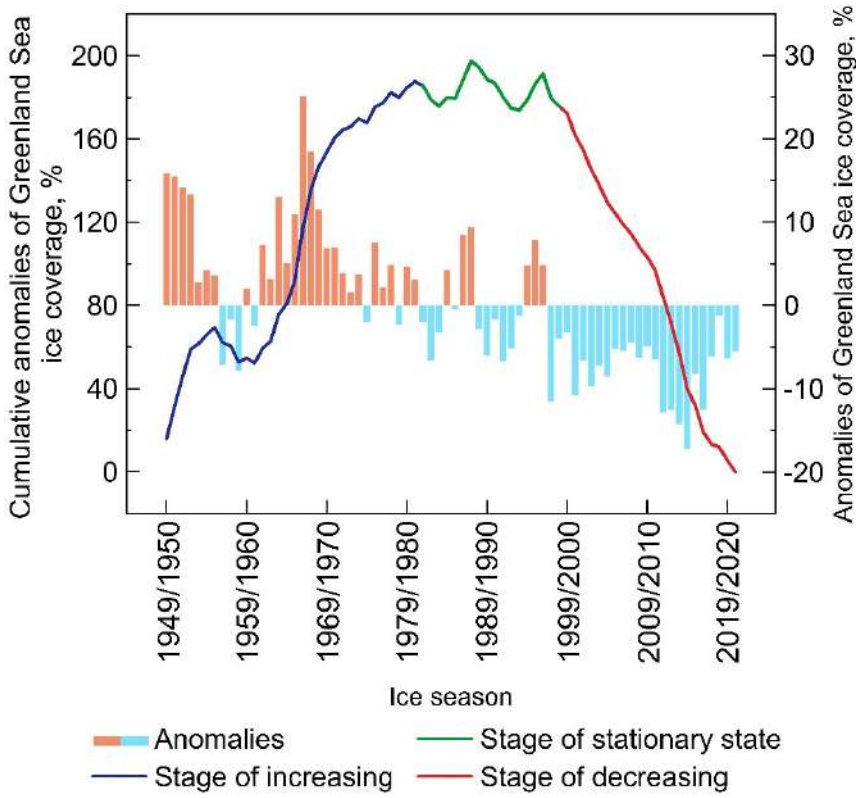


Figure 3.2. Cumulative curve of ice coverage anomalies in the Greenland Sea averaged over the ice season, computed relative to the multi-year mean values for the period 1950–2022

stationary period from 1982/1983 to 1998/1999 (green color), and then by a decrease in ice coverage from 1999/2000 to 2021/2022 (red color). The average magnitude of ice coverage anomalies for each stage is +6%, 0%, and –6%, respectively. During the first stage, out of a total of 32 ice seasons, positive anomalies (+2%...+25%) are observed in 26 cases, while negative anomalies (–8%...–2%) are observed in 6 cases. In the second stage, 7 out of 17 ice seasons are characterized by positive anomalies (+1%...+9%), while 10 seasons exhibit negative anomalies (–11%...–1%). In the third stage, all 30 ice seasons are characterized by negative anomalies in ice extent in the Greenland Sea (–17%...–1%). Similar durations of “cold” and “warm” stages are also identified in the cumulative curve of ice coverage anomalies for February (see Figure 3.1b). This suggests that the main contribution to changes in ice coverage in the Greenland Sea during the ice season comes from the period of stable ice formation when the ice area is close to its maximum seasonal value. Additionally, April makes a smaller contribution to interannual changes in ice

coverage anomalies in the Greenland Sea: the period of ice coverage decrease occurs much earlier than in February, specifically in the early 1980s (see Figure 3.1c).

Next, let's consider the absolute values of ice coverage in the Greenland Sea. Table 3.3 presents its main statistical characteristics for the identified stages, calculated for individual months as well as averaged over the season. A lesser reduction in average ice coverage is noted in November (by 9%), while a greater reduction is observed in April (by 16%); on average for the ice season, the characteristic decreased by 14%. As ice coverage decreases, SD and seasonal range values also decrease. Accordingly, during the stage of increase, relatively large interannual changes in the characteristic are recorded compared to the stages of stability or decrease. For all identified stages, maximum SD values (up to ±13%) and seasonal range (up to 57%) are typically observed in February and April, the months with the greatest ice cover area in the Greenland Sea within the seasonal cycle, while minimum values are observed in November and September (up to ±8% and up to 29%, respectively). However, it is noted that during the stage of ice coverage decrease, the SD value in February has decreased to the level of September. All estimates are presented in absolute values of ice coverage, %.

Table 3.3. Statistical characteristics of ice coverage in the Greenland Sea (in %), during stages of its changes for the period 1950–2022, identified by cumulative curves of anomalies

| *Stage of change* | Period | Ice coverage, % | | |
|---|---|---|---|---|
| | | Mean, % | SD, % | Seasonal range, % |
| **November** | | | | |
| *Increasing* | 1950/1951–1973/1974 | 43 | ±8 | 29 |
| *Stationary state* | 1974/1975–1988/1989 | 37 | ±6 | 24 |
| *Decreasing* | 1989/1990–2022/2023 | 34 | ±5 | 21 |
| **February** | | | | |
| *Increasing* | 1949/1950–1983/1984 | 60 | ±13 | 55 |
| *Stationary state* | 1984/1985–1998/1999 | 52 | ±12 | 38 |
| *Decreasing* | 1999/2000–2021/2022 | 39 | ±7 | 33 |
| **April** | | | | |
| *Increasing* | 1949/1950–1978/1979 | 60 | ±13 | 57 |
| *Decreasing* | 1979/1980–2021/2022 | 44 | ±10 | 43 |
| **September** | | | | |
| *Increasing* | 1949/1950–1983/1984 | 31 | ±6 | 28 |

| | | | | |
|---|---|---|---|---|
| *Stationary state* | 1984/1985–1999/2000 | 26 | ±6 | 20 |
| *Decreasing* | 2000/2001–2021/2022 | 17 | ±7 | 25 |
| **Ice season** | | | | |
| *Increasing* | 1949/1950–1981/1982 | 47 | ±7 | 33 |
| *Stationary state* | 1982/1983–1998/1999 | 41 | ±6 | 21 |
| *Decreasing* | 1999/2000–2021/2022 | 33 | ±4 | 16 |

*Note.* SD stands for standard deviation. Seasonal range refers to the difference between the maximum and minimum values of ice coverage within one stage (increase, stability or decrease).

Additionally, the linear trends of interannual changes in ice coverage in the Greenland Sea were assessed for statistical significance (see Table 3.4, which presents the values of statistically significant linear trends). The t-test was used as the primary criterion for assessing the statistical significance of trends at a significance level of 99% [Malinin, 2020a]. As a result, significant linear trends are identified throughout all analyzed stages for the entire observational series (from 1950 to 2022), with the maximum reduction in the Greenland Sea ice coverage observed in February, amounting to –0.46% per ice season. Moreover, statistically significant linear trends in ice coverage are observed only during the "warm" period in February, amounting to –0.53% per ice season. This aligns with the hypothesis that interannual changes in ice coverage in the Greenland Sea occurring in February drive its fluctuations on average for the ice season.

Table 3.4. Magnitudes of statistically significant linear trends in absolute ice extent values of the Greenland Sea (as % per ice season) for different stages of its anomaly changes

| Stage of changes / *Month* | *November* | *February* | *April* | *September* | *Ice season* |
|---|---|---|---|---|---|
| Increasing | Insignificant | | | | Insignificant |
| Stationary state | Insignificant | | | | |
| Decreasing | Insignificant | –0.53 | Insignificant | | |
| Entire observational series | –0.17 | –0.46 | –0.35 | –0.26 | –0.28 |

According to the results of the analysis of cumulative curves of ice coverage anomalies, the warming stage in the Greenland Sea begins from the ice season of 1999/2000. During this time, for other Arctic Seas (in particular, the Kara, Laptev, East Siberian, and Chukchi Seas), the pivotal point is the ice season of 2004/2005, as indicated by ice coverage data [Timofeeva et al., 2024], age composition [Egorov, 2020], and landfast ice thickness

at the polar stations [Timofeeva and Sharatunova, 2021]. This implies that the response to ongoing climate changes occurred in the Greenland Sea on average five years earlier than in the Russian Arctic seas, which is reflected in its ice coverage in particular.

### 3.2. Drift ice edge position in annual cycle

Due to the significant spatial heterogeneity of the ice cover in the Greenland Sea, interannual variations in ice coverage can be indicative only of major anomalies. In reality, the sea ice in this area is predominantly concentrated in the western part, while large areas of open water are found in the eastern part. The coordinates of the drift ice edge position along fixed transects adequately describe the ice conditions of the Greenland Sea, as it is predominantly elongated in a north-south direction.

Seasonal changes in the drift ice edge position in the Greenland Sea are shown in Figure 3.3. The seasonal minimum occurs in September (at all fixed transects), which is consistent with ice coverage data. However, the period of the seasonal maximum, as in the case of ice coverage, spans from February to April and is established in one of these months for individual transects in the Greenland Sea. A detailed analysis of the spatial distribution of the ice cover in the winter months is provided in Table 3.5, which will allow for a more detailed understanding of the main patterns of its changes.

The period of maximum ice cover development in the Greenland Sea occurs in April for 75% of the cases (i.e., on most calculated transects) at latitudes from 80° N to 77° N and from 73° N to 69° N. There is no clear tendency towards small or large changes in the drift ice edge position, as the SD values range from the maximum to the minimum observed in the dataset, from ±3.2° at 73° N to ±1.3° at 78° N and 79° N. In the remaining 25% of cases, at latitudes from 74° N to 76° N, the seasonal maximum occurs in March (February-March), with an SD of about ±2.3°. Thus, the Greenland Sea exhibits spatial uniformity in periods of maximum and minimum ice coverage establishment. However, seasonal changes in the drift ice edge position in its waters over the annual cycle are characterized by significant seasonal range. During the study period, its position varies

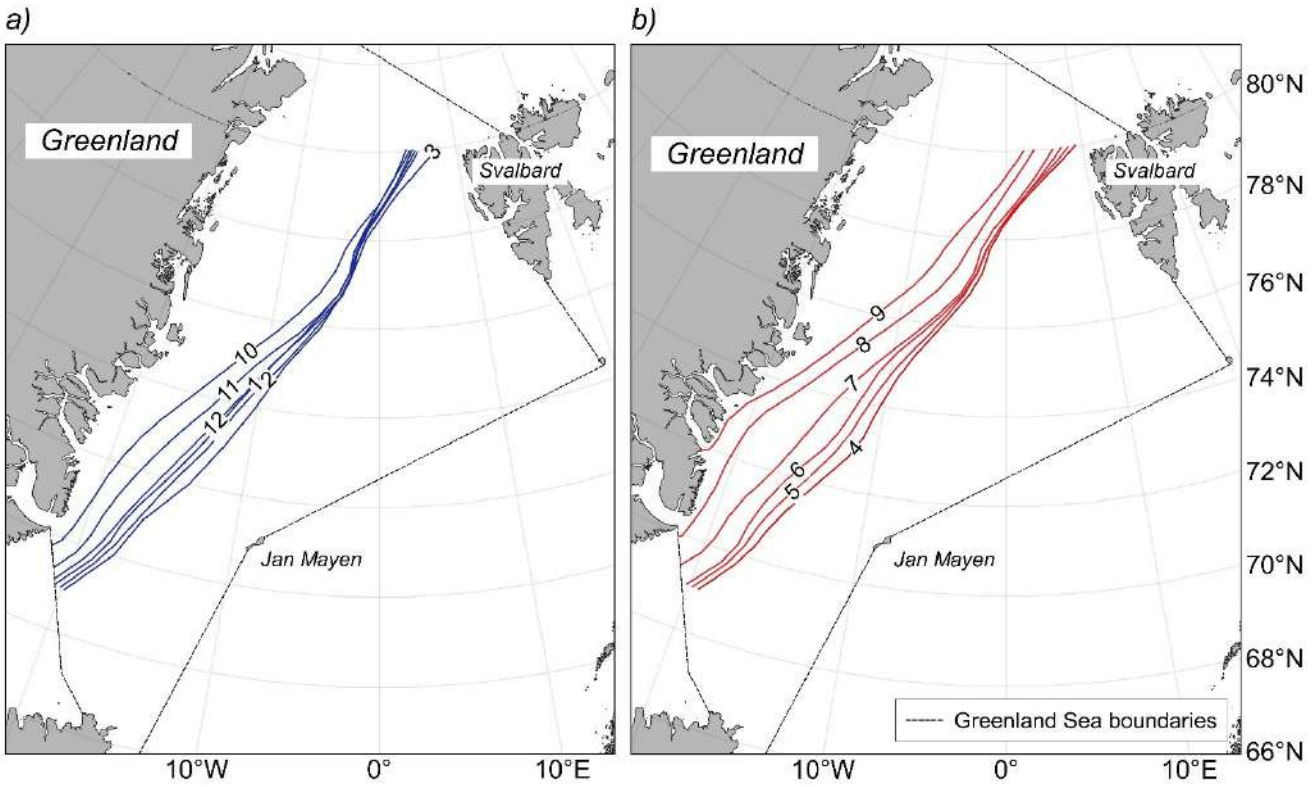


Figure 3.3. Seasonal variations in the drift ice edge position in the Greenland Sea (in ° longitude) along fixed parallels averaged over the ice seasons 1997/1998–2021/2022 for the months: *a)* October to March, *b)* April to September. The numbers along the curves indicate the months

from 4.7° longitude (78° N and 79° N) to 9.8° longitude (73° N). The greatest seasonal amplitude is observed at latitudes from 72° N to 75° N, exceeding 7.1° longitude.

Table 3.5. Characteristics demonstrating the changes in the timing and magnitude of the seasonal maximum of the drift ice edge position in the Greenland Sea averaged over the ice seasons 1997/1998–2021/2022

| *Fixed parallels, ° N* | *Seasonal maximum* | *SD, ° longitude* | *Seasonal range, ° longitude* |
|---|---|---|---|
| 80.0 | April | ±2.1 | 6.6 |
| 79.0 | April | ±1.3 | 4.7 |
| 78.0 | April | ±1.3 | 4.7 |
| 77.0 | April | ±1.7 | 5.7 |
| 76.0 | February- March | ±2.0 | 6.5 |
| 75.0 | March | ±2.2 | 7.1 |
| 74.0 | March | ±2.6 | 8.4 |
| 73.0 | April | ±3.2 | 9.8 |
| 72.0 | April | ±2.6 | 7.9 |
| 71.0 | April | ±1.8 | 5.4 |

| | | | |
|---|---|---|---|
| 70.0 | April | ±1.7 | 4.7 |
| 69.0 | April | ±2.1 | 5.9 |

*Note.* SD stands for the standard deviation. The seasonal range is the difference between the maximum and minimum values of the drift ice edge position coordinates in the seasonal cycle

In the monograph [Mironov, 2004], based on the analysis of the drift ice edge position for the period 1958–1992, the Greenland Sea were divided into three regions. The northern region (80°–76° N) was characterized by the early occurrence of the seasonal maximum and minimum (in February and August, respectively), large interannual variations (SD at the level of ±5.0°), and a small seasonal range (5°–8° longitude). The central region (75°–71° N) was characterized by average timing of both peaks (in February and September), as well as the largest interannual variations (SD around ±6.0°) and the seasonal range (10°–14° longitude). The southern region (70°–69° N) was characterized by later occurrences of the seasonal maximum (in March-April) and minimum (in September), as well as smaller interannual changes in the ice edge position (SD of about ±3.0°) with an average seasonal range (7°–8° longitude).

Comparing the classification of ice cover distribution in the Greenland Sea provided by [Mironov, 2004] for a relatively cold climatic period (1958–1992) with the results of this study indicates: (1) a *spatial smoothing* of the period of the seasonal maximum of the drift ice edge position to a single month, namely April; (2) the *maintenance of the seasonal range* at an average level, despite the absolute ice extent (area) minima observed after the 2000s; (3) significantly *smaller interannual changes* in the drift ice edge position (which may be related to the use of a relatively shorter observation series for the ice conditions of the Greenland Sea in this study).

### 3.3. Ice age composition

#### 3.3.1. Seasonal variations

The average ratio of the relative amount of ice of different age gradations, identified in the ice cover structure in the Greenland Sea during its growth period from October to May, is shown in Table 3.6. Here and further, the relative amount is understood as the

*percentage of the area occupied by ice of one age gradation relative to the total area of the sea ice cover*. Although changes in the landfast ice area are not considered in this study, their share is included in the total ice area and is taken into account when calculating the ratios of ice of different age gradations. Under average conditions, the following features of the Greenland Sea ice age composition in the seasonal cycle are distinguished.

Table 3.6. Average ratio of ice areas of different age gradations in the Greenland Sea ice cover (expressed as % of the total ice area) during the winter period for the ice seasons from 1997/1998 to 2021/2022

| Month / *Age gradation* | X | XI | XII | I | II | III | IV | V |
|---|---|---|---|---|---|---|---|---|
| **Amount of drift ice of different age gradations, % of the total ice area** | | | | | | | | |
| *Initial types and nilas* | 8 | 4 | 4 | 4 | 5 | 4 | 3 | 2 |
| *Young grey* | 8 | 4 | 2 | 5 | 4 | 3 | 2 | 2 |
| *Young grey-white* | 30 | 25 | 21 | 19 | 19 | 19 | 19 | 18 |
| *First-year thin* | 3 | 17 | 14 | 5 | 4 | 3 | 3 | 3 |
| *First-year medium* | 0 | 2 | 10 | 20 | 19 | 17 | 17 | 19 |
| *First-year thick* | 0 | 0 | 0 | 1 | 4 | 7 | 9 | 9 |
| *Old* | 44 | 36 | 35 | 32 | 30 | 30 | 30 | 30 |
| **Amount of landfast ice, % of the total ice area** | | | | | | | | |
| *All ice age gradations* | 8 | 12 | 14 | 14 | 15 | 16 | 16 | 16 |

*Old ice.* The presence of old ice in the Greenland Sea ice cover, which is continuously transported from the Arctic Basin through the Fram Strait, is a distinctive feature of its ice regime [Martin and Wadhams, 1999; Mironov, 2004; Zamani et al., 2019]. Throughout the winter period, old ice occupies no less than 30% of the total sea ice area and constitutes the predominant age gradation in the age structure of the Greenland Sea ice cover. There is a gradual decrease in the proportion of old ice as the relative amount of ice from other age gradations changes, from 44% in October to 30% in February-May, which is particularly noticeable during its active growth period. From October to December, along with the decrease in the young ice area and the increase in the first-year thin and medium ice area, the relative amount of old ice decreases on average by 9%, from 44% to 35%. Conversely, in January-May, its values vary within 2% of the total area of the ice cover, from 32% to 30%. In addition, seasonal maxima of *absolute* values of the old ice area are observed in December and April, amounting to 155 thousand km$^2$ and 153 thousand km$^2$, respectively.

They correspond to two peaks in the seasonal ice export through the Fram Strait [Zhang et al., 2017; Egorova and Vinogradnaya, 2019; Spreen et al., 2020], which determines the amount of old ice in the Greenland Sea.

Estimates of the relative amount of old ice averaged over the period 1989–1992 are provided in the work [Mironov, 2004]. At that time, old ice covered from 50% to 65% of the total ice cover of the Greenland Sea, also predominating in sea ice structure. The proportion of old ice decreased from 61–62% in October-November to 50–51% in January-February as the seasonal ice cover grew, and then increased, reaching a maximum of 65% in May. Comparing these estimates with the results obtained in the present study for the period 1997/1998–2021/2022 (see Table 3.7) indicates that the relative amount of old ice in the Greenland Sea ice cover has significantly decreased since the beginning of the 21st century, from 16% to 35% for individual months. The greatest reduction in the proportion of old ice occurs in April-May (from 63–65% to 30%, i.e., by 33–35%), while the smallest reduction occurs from October to January (from 50–62% to 32–44%, i.e., by 16–18%).

Table 3.7. Estimates of seasonal changes in the relative amount of old ice in the Greenland Sea ice cover (expressed as a % of its total area)

| Period / **Month** | **X** | **XI** | **XII** | **I** | **II** | **III** | **IV** | **V** |
|---|---|---|---|---|---|---|---|---|
| 1989–1992 [Mironov, 2004] | 61 | 62 | 51 | 50 | 51 | 57 | 63 | 65 |
| 1997–2022 (present study) | 44 | 37 | 35 | 32 | 30 | 30 | 30 | 30 |

*Initial ice types and young ice.* The ice formation process in the Greenland Sea continues throughout the entire winter period, thus initial ice types, grey and grey-white young ice, are observed in the ice structure during all considered winter months (October-May). At the onset of ice formation in the Greenland Sea in October, the ice cover consists predominantly of locally formed ice, initial ice types, and young ice (46% of its total area), among which grey-white ice predominates (30% of its total area). The relative amount of initial ice types and grey ice decreases steadily during the winter period from 8% in October to 2% in May, which holds true for both age gradations.

Among the ice age gradations up to 30 cm thick, grey-white ice predominates. Their proportion of the total ice area also gradually decreases, from 25% in November to 18%

in May. Some young grey-white ice naturally transitions into the next gradation of first-year thin ice. Additionally, initial ice types and young ice are formed throughout the entire winter period in disruptions to the continuity of the sea ice cover (e.g., cracks, leads, and rifts) that occur as a result of sea ice divergence.

*First-year thin ice.* In October, only 3% of the total ice area of the Greenland Sea is occupied by first-year ice, including thin and medium gradations; presumably, these ice types were transported through the Fram Strait from the Arctic Basin, where they were formed. The formation of first-year thin ice directly within the sea basin begins in November, as their proportion of the total sea ice area sharply increases to 17% in this month. November marks the peak of the relative amount of first-year thin ice in the seasonal cycle. Subsequently, there is a decrease, from 14% in December to 2% in April-May, with the most significant reduction occurring in December-January (from 14% to 4% of the total area of the ice cover), which is associated with the transition to another age gradation.

*First-year medium ice*. Already in December, some of the first-year thin ice transitions to the gradation of first-year medium ice. It is precisely from December to January that a sharp increase in their relative quantity is observed, from 10% to 21% of the total ice area in the Greenland Sea. Then, their proportion slightly fluctuates within 18–20% up until May. It is noted that among the first-year ice gradation, first-year medium ice predominates during the seasonal cycle (except for October-December, when first-year thin ice prevails in the Greenland Sea).

*First-year thick ice*. They begin to form within the sea basin as early as January, although their share does not exceed 1% of the total ice area at that time. In January, thick ice is not yet observed in the Fram Strait, so these thick ice formations are solely locally formed ice. The relative amount of first-year thick ice in the Greenland Sea ice cover increases from 5% in February to 9% in April-May, reaching its maximum value at the end of the growth period.

Thus, for the majority of the winter period, namely from November to March, old ice predominates in the Greenland Sea, occupying from 30% to 44% of its ice cover. The

combined amount of initial ice types, nilas, and young grey and grey-white ice predominates only in October, during active ice formation, comprising 45% of the total ice area that month. Starting from April, the main part of the ice cover of the Greenland Sea consists of first-year ice: in April, their proportion of the total ice area equals 30%, and in May, it's 31%. Among only first-year ice gradation, thin ice predominates from October to December (up to 17%), while medium ice predominates from January to May (up to 20% of the total ice area). First-year thick ice averages up to 9% of the total ice area in the Greenland Sea.

### 3.3.2. Interannual variations

The author conducted an analysis of interannual changes in the age structure of the Greenland Sea ice for April, the month of maximum ice cover development. As a result, the following distribution of the relative ice area of different age gradations in the Greenland Sea was obtained, as shown in Figure 3.4.

The relative areas of ice of all considered age classifications in the Greenland Sea basin are subject to significant interannual fluctuations. The amount of initial ice types and young ice under average conditions varies from 14% to 36% of the total ice area, first-year ice from 20% to 40%, and old ice from 16% to 44%. Moreover, first-year thin ice occupies up to 10%, medium ice up to 28%, and thick ice up to 30% of the ice area in the Greenland Sea.

Among the first-year ice in the Greenland Sea basin, the predominant age gradation in April is the first-year medium ice (with thickness ranging from 70 cm to 120 cm). An assessment of their recurrence was conducted (see Figure 3.5a). Most frequently, in 25% of cases, first-year medium ice occupies from 20% to 25% of the total Greenland Sea ice area. In 21% of cases, this age classification forms from 25% to 30% of the sea ice cover. First-year medium ice with equal recurrence, in 17% of cases, constitutes 5–10% and 10–15% of the total ice area. It is noted that throughout the entire observation period, first year medium ice never occupies more than a third of the total ice cover of the Greenland Sea.

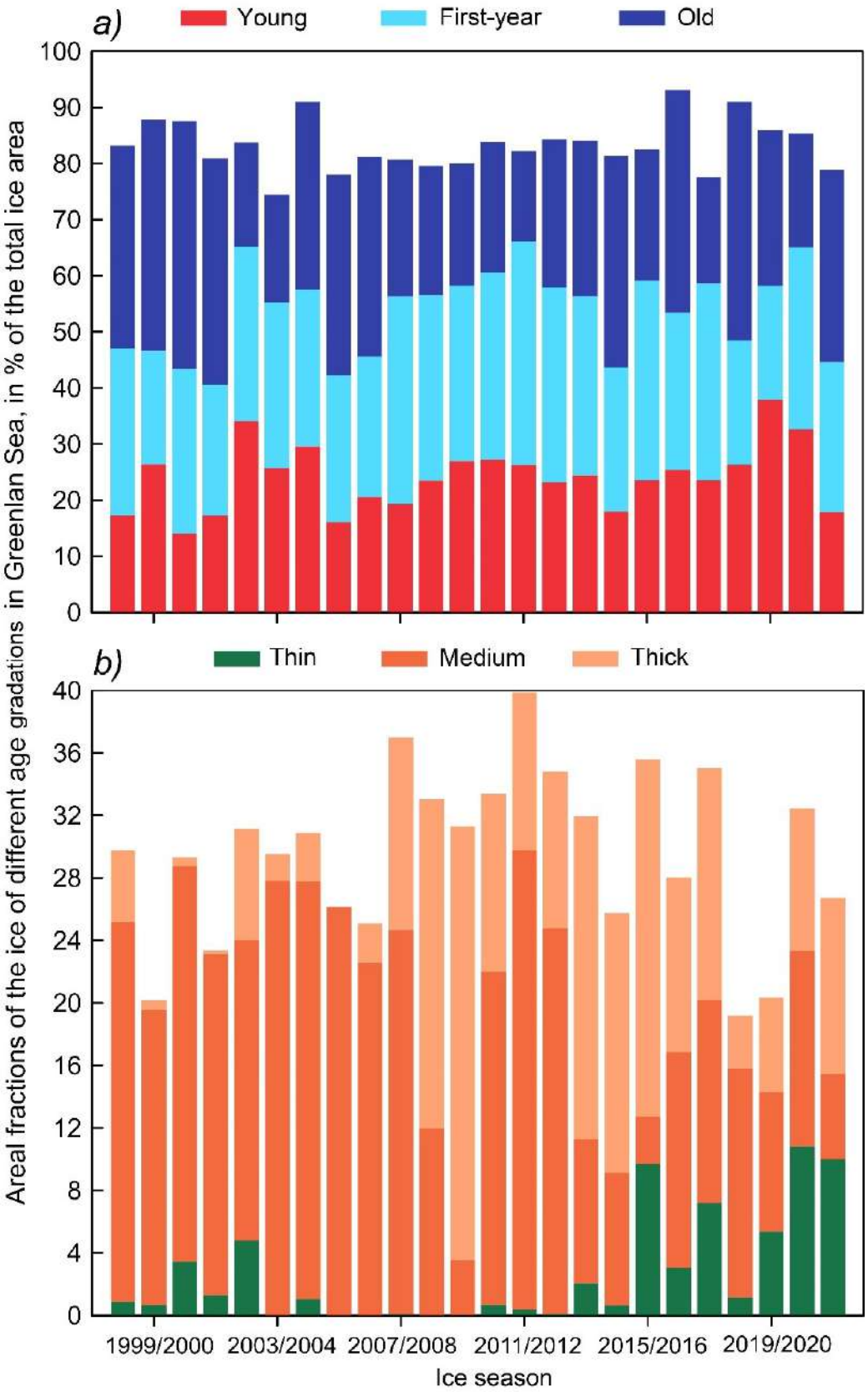


Figure 3.4. Interannual changes in the ice areas of different age gradations*: a)* young, first-year, and old ice*; b)* first-year thin, medium, and thick ice in the ice cover of the Greenland Sea in April (expressed as a percentage of its total area) on average for the period 1998/1999–2021/2022

The first-year thick ice is typically the least prevalent among the first-year ice age gradation throughout the winter season. However, for individual years in April, their area exceeds the amount of first-year thin and medium ice in the total ice area of the Greenland Sea, as noted in the ice seasons of 2009/2010, 2013/2014, 2014/2015, and 2015/2016 (see Figure 3.4b). Interannual changes in first-year medium and thick ice are usually in antiphase, i.e., with a relative increase the proportion of first-year medium and thick ice decreases as the quantity of first-year thin ice decreases. Following the observed minimum ice extent (area) in the Arctic in 2012 [Comiso et al., 2008; Ivanov et al., 2013], the area of first-year thin ice in the Sea began to increase rapidly, from 1% in the ice season of 2011/2012 to 10% in 2020/2021.

The year-round export of old ice from the Arctic basin to the Greenland Sea is one of the most important features of its ice regime, so frequency of occurrence assessment of the old ice was performed (see Figure 3.5b). Thus, with equal frequency of occurrence, in 25% of cases, old ice forms 20–25% and 35–40% of the Greenland Sea ice cover. Old ice occupies 15–20% of the total area of sea ice in 17% of all cases considered. Equally, in 13% of cases, old ice constitutes 25–30% and 40–45% of the sea ice cover. It is noted that old ice always occupies no less than 15% and no more than 50% of the total area of the Greenland Sea ice cover.

Next, linear and non-linear trends of the ice area of different age gradations in the Greenland Sea ice age structure in April were assessed for statistical significance. Table 3.8 presents the results of these assessments. The main criterion for evaluating the statistical significance of trends was the Student's t-test (at the 99% significance level) [Malinin, 2020a]. Thus, linear trends of ice area less than 30 cm thick (i.e., combined into a single general category of initial types, nilas, and young ice), as well as first-year and old ice, were found to be statistically insignificant. This means that against the backdrop of the observed reduction in the total Greenland Sea ice area, the areas of ice in these age gradations change within the range of natural seasonal variations. However, when first-year ice is divided into thin, medium, and thick, each of these categories exhibits a significant linear trend. The decrease in the relative area of first-year medium and thick ice, as well

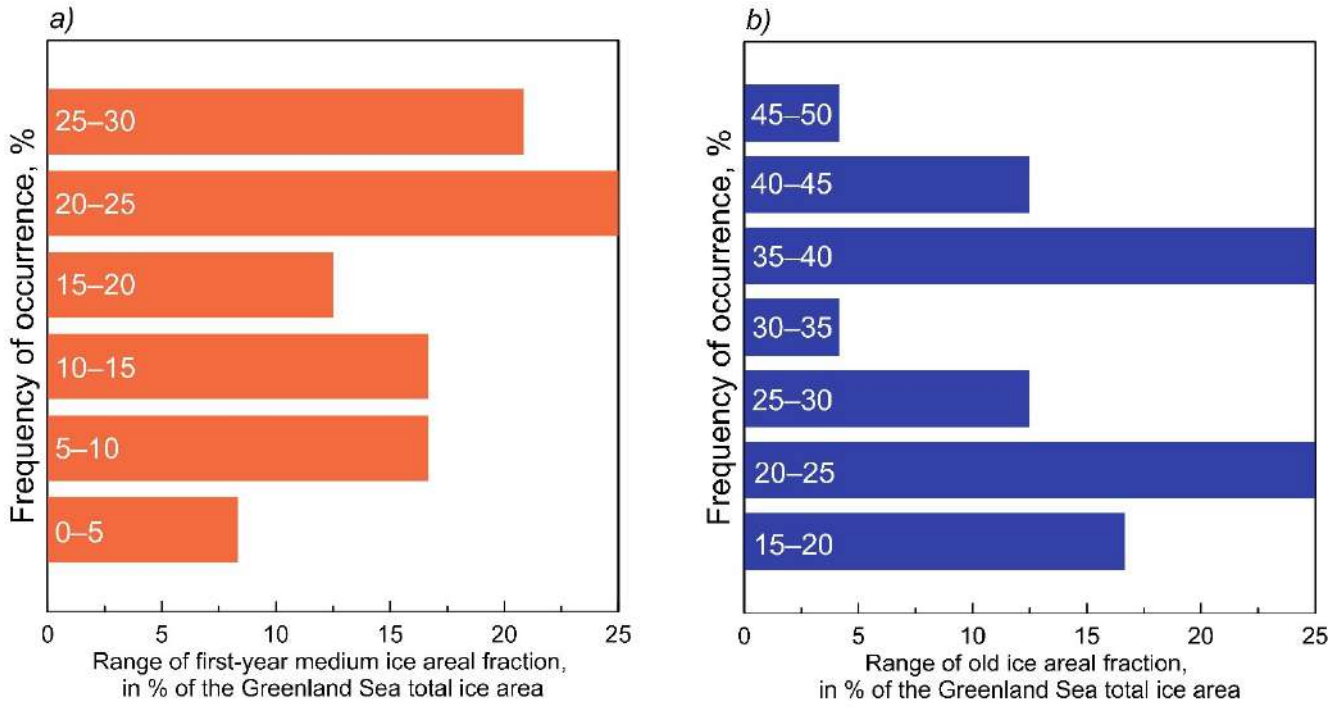


Figure 3.5. Frequency of occurrence of ice areas (expressed as a percentage of its total ice area): *a)* first-year medium ice; *b)* old ice from the total ice area of the Greenland Sea in April on average for the period 1998/1999–2021/2022

as the increase in the relative area of first-year thin ice, compensate for changes in the overall age distribution of first-year ice in the structure of the Greenland Sea ice cover. The rates of decrease in the relative amount of first-year medium and thick ice are –0.51% and –0.73% per ice season, respectively, while the increase in the area of first-year thin ice is already +0.31% per ice season (see Table 3.8). As for non-linear trends, trends of all age gradations, except initial types and young ice, are statistically significant. This indicates internal changes in the age composition of the Greenland Sea ice cover with a period shorter than the 24-year period considered.

Table 3.8. Statistically significant linear and non-linear trends in the relative amounts of ice of different age categories (expressed in % per ice season) in the Greenland Sea ice cover in April

| *Trend magnitude* / Age gradation | *Linear* | *Non-linear* |
|---|---|---|
| Young | Insignificant | |
| First-year thin | +0.31 | –0.78 |
| First-year medium | –0.73 | –0.24 |
| First-year thick | –0.51 | +2.52 |

| | | |
|---|---|---|
| First-year | Insignificant | +1.51 |
| Old | | –2.26 |

Next, we will proceed to compare the estimates of the age composition of the Greenland Sea ice cover obtained in this study with the results of earlier research. Table 3.9 presents the values of the relative amounts of ice of different age gradations in the sea area, calculated for the following periods: 1988–1992 [Mironov, 2004] and 1998/1999–2021/2022 (present study).

Starting from the 2000s, the age structure of the Greenland Sea ice cover underwent significant changes compared to the period of the late 1980s to early 1990s. In the 21st century, during the period of maximum growth of the sea ice cover, it is now equally formed from old and first-year ice: on average, they each occupy about 30% of the total ice cover area. However, in 1988–1992, old ice predominated in the Greenland Sea, accounting for up to 45% of the total ice area. Comparing the estimates indicates a decrease in the average thickness of the Greenland Sea ice cover: there is a decrease in the proportion of old ice by 15% (from 45% to 30%), as well as initial types and young ice by 8% (from 33% to 25%); in contrast, there is an 8% increase in first-year ice in the Greenland Sea ice cover (from 22% to 30%). Considering the statistical insignificance of the linear trends of interannual fluctuations in the relative amounts of ice of different age gradations in the Greenland Sea, it can be concluded that quantitative changes in the ice age structure began earlier than the 1998/1999 ice season.

Table 3.9. Estimates of the relative amount of ice of separate age gradations (expressed as a percentage of its total area) in the Greenland Sea ice structure in April

| *Age gradation* / Period | 1988–1992 [Mironov, 2004] | 1998/1999–2021/2022 (present study) |
|---|---|---|
| *Initial types and young* | 33 | 25 |
| *First-year* | 22 | 30 |
| *Old* | 45 | 30 |

*Note.* The calculation of the relative ice areas of different age gradations took into account the amount of landfast ice.

The main results of the research on the ice age structure of the Greenland Sea are presented in [Egorova, 2021; Egorova and Mironov, 2023a; Mironov and Egorova, 2024].

### 3.3.3. Ice age composition in Fram Strait

Additionally, this study provides estimates of seasonal changes in the ice age composition in the Fram Strait, which is the main source of old ice export from the Arctic basin [Ricker et al., 2018]. Initially, the widths of the ice flow in the Fram Strait (accounting for ice concentration) were obtained during the winter months (these data were used to calculate the volume of ice carried through the strait site). The seasonal cycle of changes in the ice flow width is reflected in Table 3.10. The average width (±SD) is 314 (±9) km. During the winter months, the maximum and minimum values of width are reached in April, 327 (±30) km, and in January, 299 (±26) km, respectively [Egorova and Mironov, 2023b].

Table 3.10. Average ratio of ice areas of different age categories (expressed as a percentage of the total ice flow width in km) at the Fram Strait during the winter months on average for the ice seasons from 1997/1998 to 2021/2022

| *Age composition* / Month | X | XI | XII | I | II | III | IV | V |
|---|---|---|---|---|---|---|---|---|
| **Ice flow width in the Fram strait site, km** | | | | | | | | |
| Summarized | 312 | 314 | 315 | 299 | 308 | 324 | 327 | 316 |
| **Ice age composition in the Fram strait site, % of the total ice flow width** | | | | | | | | |
| *Old* | 72 | 61 | 58 | 53 | 50 | 52 | 52 | 52 |
| *First-year thick* | 0 | 0 | 2 | 6 | 10 | 16 | 22 | 24 |
| *First-year medium* | 0 | 0 | 6 | 14 | 11 | 8 | 5 | 4 |
| *First-year thin* | 9 | 17 | 17 | 11 | 8 | 6 | 5 | 4 |
| *Young grey-white* | 8 | 9 | 6 | 8 | 10 | 11 | 8 | 9 |
| *Young grey* | 5 | 8 | 7 | 5 | 8 | 6 | 8 | 7 |
| *Initial types and nilas* | 6 | 5 | 4 | 3 | 3 | 1 | 0 | 0 |

The ratio of the amounts of first-year ice in the Fram Strait ice flow is logically linked to the processes of ice growth. In October-November, there are no first-year thick and medium ice at the strait site, but the presence of first-year thin ice is characteristic for all winter months. The quantity of first-year thin ice reaches its maximum in November-December (17% of the total ice flow width). Subsequently, their proportion gradually decreases as ice of other age gradations forms, reaching 4% by the end of the growth period in May. In December, first-year medium ice begins to form in the Fram Strait, reaching the highest proportion among all first-year ice in January (14% of the total ice flow

width). Afterward, their quantity also decreases, reaching 4% in May. The proportion of first-year thick ice in the total ice flow increases throughout the ice season, starting from 2% in December to 24% in May.

The presence of young grey-white and grey ice is characteristic of the ice cover in the Fram Strait during the winter period. Although it would be expected to have the highest amount during periods of intensive ice formation (October-November), the proportion of young ice in the ice flow during the winter season changes insignificantly, from 13% in October and December-January to 18% in February. This is explained by the fact that young ice in the Fram Strait forms in disturbances in the ice cover caused by dynamic factors (its cracks, rifts, and leads). The amounts of initial types of ice and nilas ice at the strait site reaches its maximum in October, at the beginning of the ice formation period, constituting 6% of the total ice flow width. The proportion of these age gradations in the total ice flow gradually decreases to 1% in March, and by the end of the winter period, in April-May, initial types and nilas ice are absent here.

### 3.4. Boundary of old ice prevalence

The spatial distribution of the ice cover of separate age categories in the Greenland Sea throughout the winter period can be visually demonstrated by the average position of their predominance boundaries. In this subsection, particular attention was given by the authors to the gradation of old ice, the changes of which are a factor determining the ice conditions of the Greenland Sea and an important climatic indicator.

#### 3.4.1. Seasonal variations

In Table 3.11, the seasonal variation of the boundary of old ice predominance in the Greenland Sea under average conditions is presented. Since the spatial characteristics of ice cover distribution are more effectively demonstrated on charts, Figure 3.6 illustrates the average position of the zone of old ice prevalence in November, February, and April. These months correspond to periods of active and stable ice formation in the Greenland Sea, as well as maximum ice development. It is noted that the boundary of old ice

predominance changes insignificantly throughout the winter period, as evident from both the curves presented in Figure 3.6 and the data in Table 3.11.

Table 3.11. Position of the boundary of old ice predominance in the Greenland Sea (expressed in degrees of longitude) at fixed transects averaged for the ice seasons from 1997/1998 to 2021/2022

| Latitude, ° N / Month | *Longitude, ° W (–) / ° E (+)* | | | | | | | |
|---|---|---|---|---|---|---|---|---|
| | X | XI | XII | I | II | III | IV | V |
| 80.0 | +0.3 | +0.1 | –0.1 | –0.7 | –1.4 | 0.0 | **+1.3** | +0.9 |
| 79.0 | –3.1 | –3.3 | –3.5 | –4.4 | –4.5 | –3.8 | **–2.8** | –4.2 |
| 78.0 | –6.7 | –6.5 | **–6.1** | –7.9 | –7.1 | –7.5 | –6.8 | –7.1 |
| 77.0 | –9.8 | –8.8 | –8.7 | –9.3 | –8.8 | –8.7 | –8.5 | **–8.4** |
| 76.0 | –13.6 | –12.2 | –11.4 | –11.9 | –11.4 | –11.8 | –11.7 | **–11.3** |
| 75.0 | –16.1 | –15.6 | –14.2 | –14.3 | –14.3 | –13.9 | **–13.6** | –13.9 |
| 74.0 | –18.5 | –18.2 | –16.9 | –16.5 | –16.9 | **–15.9** | **–15.9** | –16.1 |
| 73.0 | –20.2 | –20.2 | –19.2 | –18.6 | –19.0 | –17.6 | **–17.5** | **–17.5** |
| 72.0 | –21.3 | –21.4 | –20.4 | –19.9 | –20.1 | –19.2 | **–18.8** | –19.4 |
| 71.0 | –21.1 | –21.1 | –20.6 | –20.2 | –20.1 | –19.7 | **–19.5** | –19.7 |
| 70.0 | –21.9 | –21.8 | –21.4 | –21.2 | –21.0 | –20.7 | **–20.5** | –20.6 |
| 69.0 | –25.3 | –25.1 | –24.9 | –24.6 | –24.2 | –23.8 | –23.9 | **–23.5** |

*Note.* Bold font (underlining) highlights the fixed parallels where, during the average ice season, the maximum (minimum) predominance of old ice occurs.

As the ice cover area in the Greenland Sea expands, the zone of old ice prevalence widens. The boundary of old ice coincides with the area of the East Greenland Current, whose strong currents continuously transport old ice from the Arctic Basin via the Fram Strait. The maximum predominance of old ice, occurring on 67% of the transects, mostly aligns with the seasonal peak of ice coverage, typically observed in April (predominantly for transects south of 75° N). In 25% of cases, the period of maximum boundary establishment shifts to May (for stations at 77°, 76°, and 69° N). At the parallel 78° N, the maximum is observed in December (on 8% of the transects). The minimum predominance of old ice in the Greenland Sea occurs in October, less frequently in November, January, and February (in 67%, 8%, 8%, and 17% of cases, respectively). Discussion regarding the alignment of results with ice coverage data is irrelevant in September as age structure of ice are not depicted on ice charts. The boundary of predominance of old ice closest to

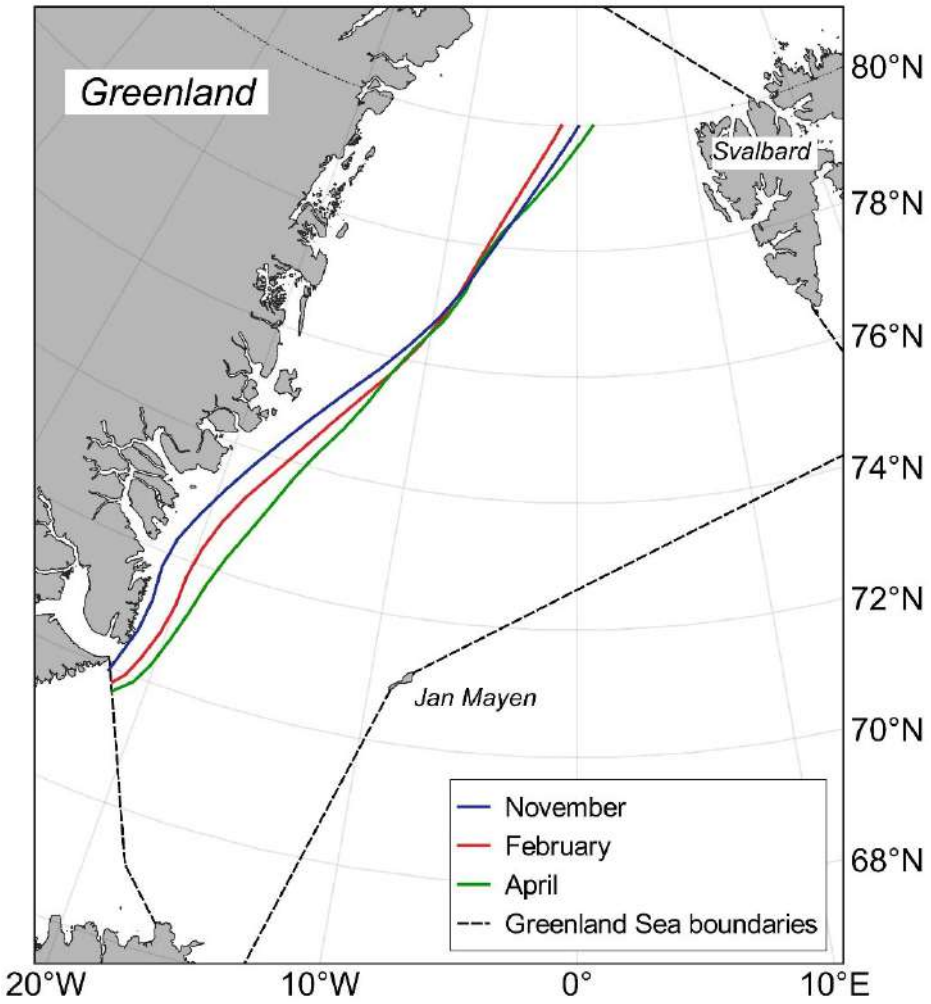


Figure 3.6. Average position of the boundary of old ice predominance in the Greenland Sea (expressed in ° longitude) in November, February, and April, averaged for the ice seasons from 1997/1998 to 2021/2022

the seasonal minimum in ice coverage is recorded in October for parallels south of 77° N. Conversely, on other stations, between 78° and 80° N, the boundary of their prevalence reaches a minimum in January-February. Thus, the analysis of seasonal changes in the spatial distribution of old ice in the Greenland Sea allows for a conditional division into northern and southern regions: in the *southern* region (stations at 69°–75° N), there is a correspondence between the seasonal changes in the boundary of old ice predominance and ice coverage, while in the *northern* region (stations at 76°–80° N), there is an inconsistency in the seasonal cycle characteristics.

The greatest seasonal changes in the position of the boundary of old ice prevalence of in the Greenland Sea are observed at latitudes 80° N and 72°–75° N, where maximum

seasonal ranges (2.5°–2.7° of longitude) and SD (±1.0° of longitude) are noted. Conversely, the smallest changes are characteristic at 78°–79° N and 69°–71° N: here, the seasonal range is <1.5° of longitude, with a SD of approximately ±0.5° of longitude. The obtained results do not complement the aforementioned division of the Greenland Sea into two regions.

### 3.4.2. Interannual variations

Figure 3.7 illustrates the distribution of maximum, minimum, and mean positions of the predominant old ice boundary for separate winter months. The area of the East Greenland Current determines the *mean* position of the old ice massif. In the marginal ice zone, small areas or fields of old ice may occur, resulting from the divergence of sea ice; however, during the winter period, first-year and young ice predominantly prevail there. The boundary of predominant old ice, reaching the southern boundary of the sea, extends southward of 70° N.

At the *minimum* position of the old ice dominance zone, its main massif is concentrated between 80° N and 78° N and between Greenland and meridians 8° W (April) or 9° W (October and February); first-year and young ice prevail to the south. In particular, the minimum or close to it spatial distribution of the old ice boundary is characteristic for the following ice seasons: 2003/2004, 2009/2010, 2013/2014, 2017/2018, 2018/2019, and 2021/2022 in November; 2007/2008, 2009/2010–2011/2012, and 2015/2016 in February; 2007/2008, 2009/2010, 2012/2013, 2017/2018, and 2020/2021 in April.

At its *maximum* position, analogous to the mean, the boundary of predominant old ice extends along the East Greenland Current. The deviation of the maximum from the mean position at fixed parallels averages from 4.5° longitude in November to 5.7° longitude in April. Although in February and April, the zone of old ice dominance extends southward of 70° N, it does not reach the southern boundary of the Greenland Sea, unlike November. The greatest deviation from the mean position in November, approximately 5.0° longitude, is noted on parallels from 72° N to 77° N, in February, about 7.5° longitude on the meridians of 73°–75° N, and in April, 11.0° longitude at 80° N. Among the studied

ice seasons, the maximum or close to maximum distribution of old ice positions was observed in 1997/1998 and 2006/2007 in November, in 2000/2001 and 2003/2004 in February, as well as in 2008/2009, 2016/2017, and 2019/2020 in April.

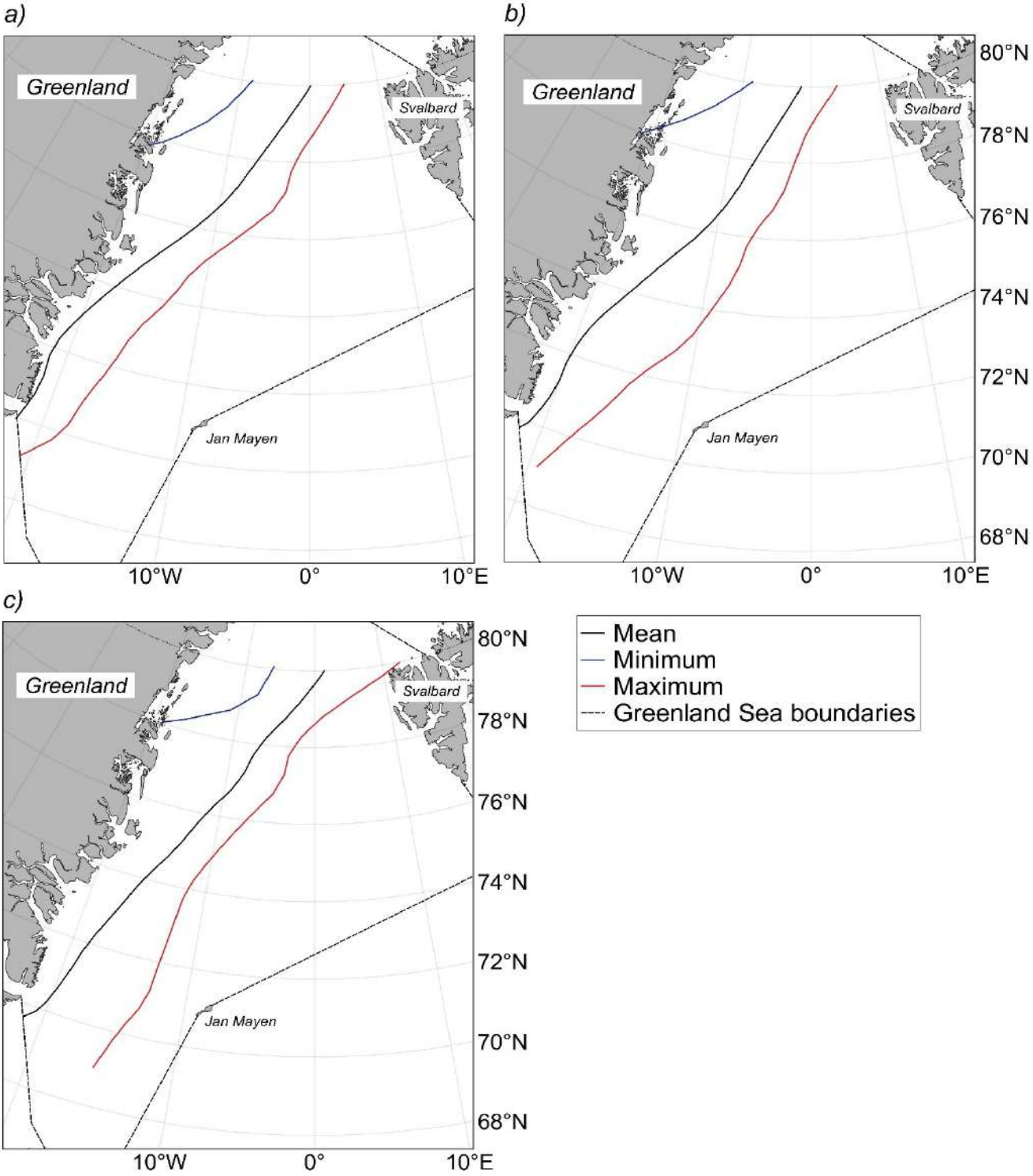


Figure 3.7. Spatial distribution of maximum, minimum, and mean positions of the predominant old ice boundary in the Greenland Sea (expressed in ° longitude): *a)* in November, *b)* in February, *c)* in April on average for ice seasons from 1997/1998 to 2021/2022

Subsequently, during the period of maximum ice development in the Greenland Sea (April), the obtained estimates of the old ice dominance boundary position were compared with the results of the study [Mironov, 2004] for the winter-spring period of 1989–1992. A significant difference lies in the position of the old ice dominance zone at minimal area: according to [Mironov, 2004], the boundary reaches the latitude of 74° N, while according to the results of present study, it reaches 80° N. Additionally, the boundary of old ice prevalence in the 1990s, at its mean and maximum positions, extends beyond the southern boundary of the Greenland Sea, whereas after the 2000s, it is concentrated within the sea basin.

### 3.5. Ice volume export from the Arctic Basin

In this study, a new method for assessing the ice volume exported through the Fram Strait is proposed, which accounts for the ice cover thickness at the strait site. This method is based on obtaining data on the average ice thickness distribution using information about its age structure; additionally, a correction for ridged ice formations was introduced. For the first time, this methodology for the Fram Strait was proposed in the author's article [Egorova and Mironov, 2023], where the first results of ice volume flux estimation are presented.

We begin with the assessment of the average ice cover thickness in the Fram Strait, considering ridges. Table 3.13 provides the values of level ice thickness and nominal ice thickness (the thickness obtained after applying the correction for ridged formations) for the old ice and first-year (thin, medium, and thick) ice age gradations. According to the methodology, this correction is not applied to the initial types and young ice.

Table 3.13. Level and nominal ice thickness (in cm) for age gradations of old and first-year ice in the Fram Strait on average for ice seasons from 1997/1998 to 2021/2022

| Month / *Age gradation* | X | XI | XII | I | II | III | IV | V |
|---|---|---|---|---|---|---|---|---|
| **Level ice thickness ($H_{lev}$), cm** | | | | | | | | |
| *Old* | 290 | | | | | | | |
| *First-year thick* | — | | 120 | 141 | 156 | 169 | 180 | 185 |
| *First-year medium* | 95 | | | | | | | |
| *First-year thin* | 50 | | | | | | | |

| Nominal ice thickness ($H_{nom}$), cm | | | | | | | |
|---|---|---|---|---|---|---|---|
| *Old* | 456 | | 487 | | | 518 | |
| *First-year thick* | — | 185 | 218 | 233 | 246 | 270 | 275 |
| *First-year medium* | — | 105 | 105 | 106 | | 108 | |
| *First-year thin* | 59 | | 61 | | | 63 | |

*Note.* Dashes indicate months in which ice of separate age gradations was not observed.

The assessment of the old ice thickness plays a crucial role in the ice cover thickness distribution in the Fram Strait, as old ice constitutes more than 50% of the total ice flow throughout the entire ice season. The average thickness of level old ice during the winter period is 290 cm, with the nominal old ice thickness varying from 456 cm to 518 cm. When considering the ridged nature of the ice cover, the thickness of old ice nearly doubles, which can significantly impact the final ice volume flux. The thickness of level first-year thick ice, ranging from 120 cm in December to 185 cm in May, also nearly doubles after the correction for ridged formations, increasing by an average of 65–90 cm in the winter months. In contrast, for first-year medium and thin ice, the nominal thickness differs from the level ice thickness by no more than 9–13 cm, which theoretically does not significantly contribute to the volume of ice exported via the Fram Strait.

The following subsections present assessments of seasonal and interannual changes in the volume of ice exported through the Fram Strait, utilizing ice drift data from the National Snow and Ice Data Center (hereinafter referred to as NSIDC).

### 3.5.1. Seasonal variations

Figure 3.8 demonstrates the seasonal variation of ice volume flux through the Fram Strait during the winter period. It exhibits a well-defined seasonal cycle. The maximum value (±SD) occurs in March, amounting to 375 km³ (±131 km³) per month, while the minimum value occurs in October, amounting to 159 km³ (±77 km³) per month. The greatest interannual changes in the volume of ice exported is observed from December to April, with a SD ranging from ±106 km³ per month (March) to ±130 km³ per month (December and April), whereas in October and May, it is approximately ±91 km³ and 88 km³ per month, respectively.

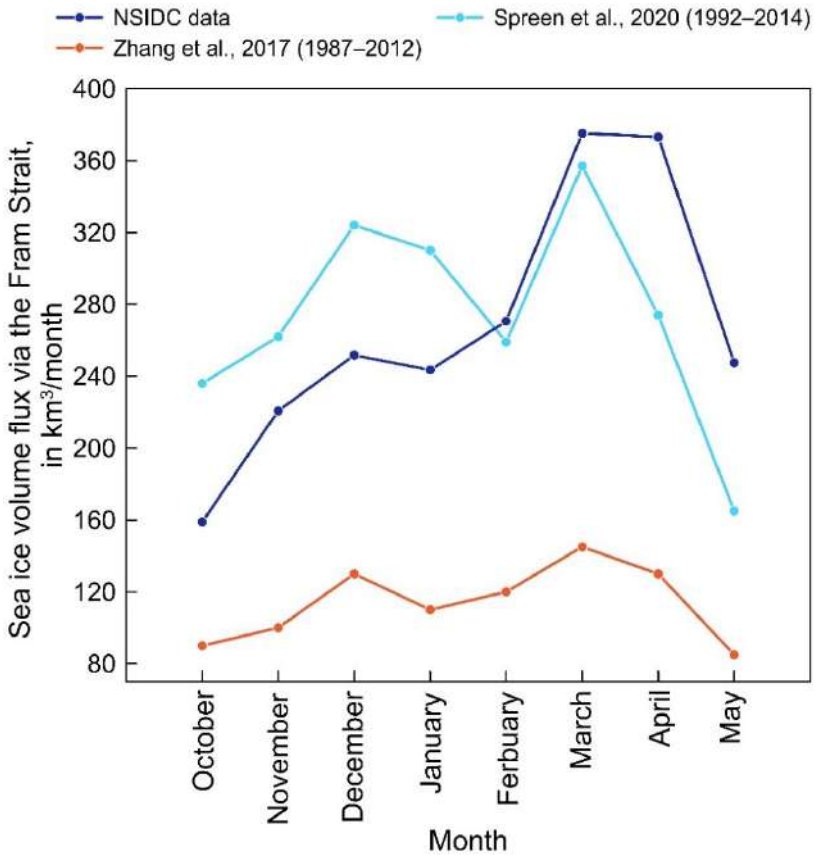


Figure 3.8. Estimates of the ice volume exported through the Fram Strait (expressed in km³ per month) according to the results of present study (on average for the ice seasons from 1997/1998 to 2021/2022) and previous research. The seasonal variation of volume for the periods 1987–2012 and 1992–2014 are shown in the works of [Zhang et al., 2017] and [Spreen et al., 2020], respectively.

Estimates of the volume of ice exported through the Fram Strait during the summer period are not presented in this study, as obtaining reliable data on ice thickness during these months is not feasible. However, estimates of the area of exported ice using a similar approach to determining ice drift velocity [Egorova and Vinogradnaya, 2019] indicate that the months from June to September account for no more than 10% of the annual ice export through the Fram Strait. Consequently, regarding the volume of ice export through the cross-section of the strait, a similar ratio can be inferred, with 90% occurring in the winter and 10% in the summer period. Therefore, the contribution of the summer months to the total annual area (volume) of ice exported through the Fram Strait can be considered relatively insignificant.

Subsequently, the ice volume export estimates obtained in present study were compared with the results of other research. Two estimates for the longest periods were selected for analysis: 1987–2012 [Zhang et al., 2017] and 1992–2014 [Spreen et al., 2020], for a proper comparison of average monthly values. It should be noted that the selected assessments were obtained using fundamentally different approaches to determining ice drift and thickness, as well as at different sites of the Fram Strait. In [Zhang et al., 2017], the same NSIDC ice drift data as in this study were used, while [Spreen et al., 2020] employed data from the Jet Propulsion Laboratory of the California Institute of Technology, which they considered closest to reality. Both databases include results from satellite microwave sensing and buoy stations. For ice thickness, the authors of [Zhang et al., 2017] used data from the PIOMAS model, while [Spreen et al., 2020] used data from profiling sonars and upward-looking sonars. Additionally, the position of site at 81° N in [Zhang et al., 2017] and this study coincides, whereas the assessments by [Spreen et al., 2020] were conducted at 79° N, where profiling sonars and upward-looking sonars were installed. Seasonal changes in the studied characteristic are also shown in Figure 3.8. Interestingly, the cited studies show significant discrepancies in the estimates of the seasonal variation of ice volume flux. Thus, the question of *which* estimate provides a more accurate representation of the seasonal variation in ice export volume remains open.

The timing of the seasonal maximum ice export volume via the Fram Strait aligns with the results of other studies, occurring in March. Quantitatively, the results of present study agree with the estimates of [Spreen et al., 2020]: 375 km³ and 350 km³ per month, respectively. In the study by [Zhang et al., 2017], the maximum export volume is 150 km³ per month, which is nearly three times lower than the other estimates. The curves in Figure 3.8 illustrate how closely the results of this study and [Spreen et al., 2020] align in other winter months. This suggests that using different data on drift and average ice thickness at strait site with a latitudinal difference of about 2° yields similar ice export volume estimates for the Fram Strait. The use of model data for ice thickness in [Zhang et al., 2017] leads to an underestimation of the final ice export volume.

The timing and magnitude of the observed seasonal minimum ice export volume through the strait vary significantly among different estimates. In this study, the minimum occurs in October, while in [Spreen et al., 2020], the lowest export volume is observed in May, at 165 km³ per month. The authors [Zhang et al., 2017] show very similar volumes in May and October, at 85 km³ and 89 km³ per month, respectively. It is noted that a spike in ice export volume is observed in December in the previous studies, which is also reflected in the results of this study.

The seasonal changes in the volume of ice exported via the Fram Strait is primarily influenced by the ice flow width and the ice drift velocity, rather than its thickness (see Figure 3.9). The correlation coefficients between the ice volume flux and ice drift velocity, ice flow width, and ice thickness are +0.89, +0.73, and +0.47, respectively. It is evident that both the area and volume of exported ice exhibit similar seasonal patterns of change. The timing of the seasonal maximum and minimum for both analyzed characteristics coincide, occurring in March and October, respectively.

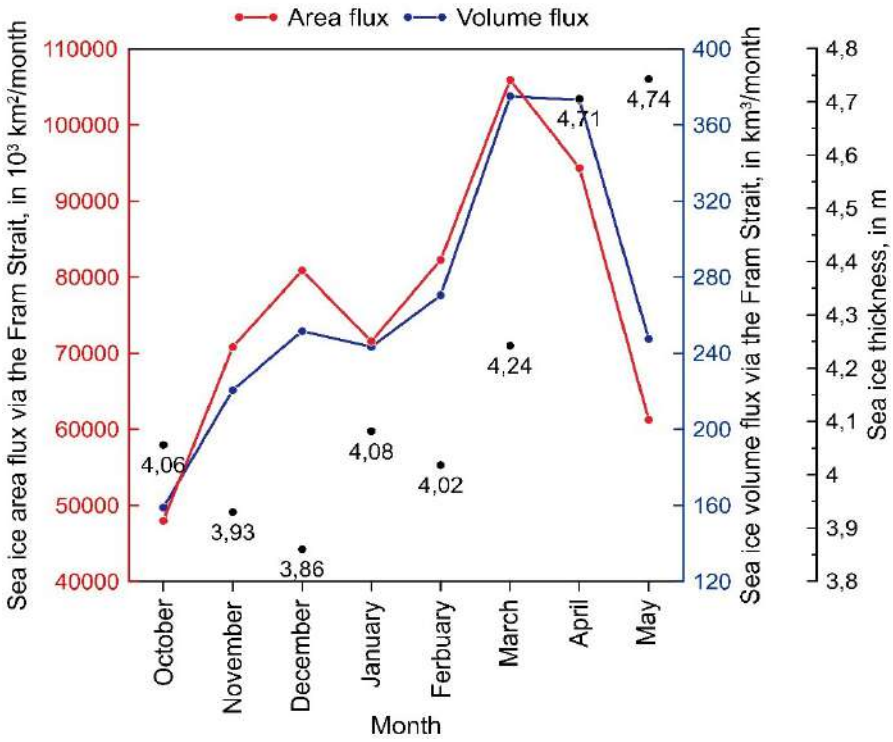


Figure 3.9. Comparison of the area (red curve, in thousand km²/month) and volume (blue curve, in km³/month) of ice exported via the Fram Strait, as well as their average-weighted thickness (points with corresponding values, in m) on average for the ice seasons from 1997/1998 to 2021/2022 using NSIDC data

### 3.5.2. Interannual variations

Figure 3.10 depicts interannual variations in the sea ice export volume via the Fram Strait. As a result, the total volume flux during the winter period (with ±SD) averages 2141 (±420) km³.

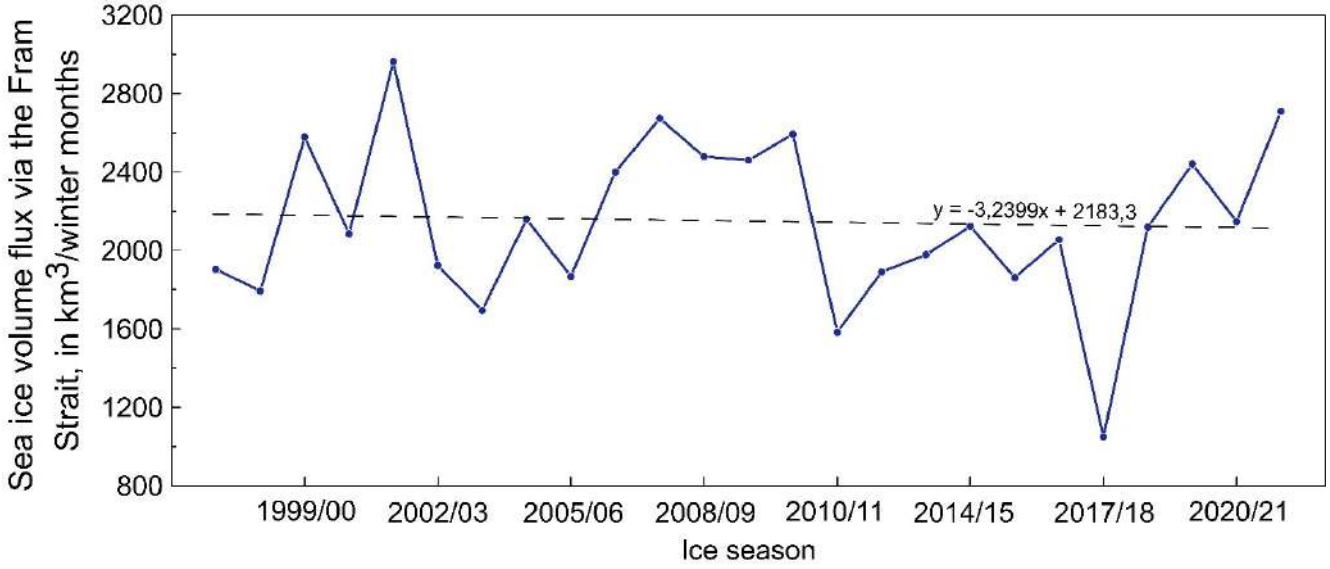


Figure 3.10. Interannual variations in the volume of ice exported through the Fram Strait during the winter months (expressed in km³), averaged over the ice seasons from 1997/1998 to 2021/2022, and their linear trend (indicated by a dashed line)

Interannual changes in the monthly mean values of ice volume transported through the Fram Strait are also illustrated in the form of a diagram of their *standardized* anomalies in Figure 3.11, where colours indicate the sign of the anomaly, ranging from negative (blue) to positive (red). The determination of standardized anomalies is achieved by dividing the difference between its monthly mean and the multi-year mean values by the standard deviation (the latter calculated for the entire observation period from 1997/1998 to 2021/2022).

As a result, out of 200 months, positive standardized anomalies of ice volume export are observed in 55% (110 cases), while negative anomalies are observed in 45% (90 cases). Several ice seasons stand out on the diagram, within which anomalies of one sign are noted: the seasons of 2001/2002 and 2007/2008 with positive anomalies, as well as 2017/2018 with negative anomalies of ice volume flux. In the overwhelming majority of seasons, there is an alternation of anomaly signs for the characteristic. The maximum positive anomalies

of exported ice volume, reaching +2.7 km³ per month, are observed in November 2010 and December 2013; the diagram also highlights March 2020 (with an anomaly magnitude of +2.3 km³ per month) and October 2009 (+2.2 km³ per month). The maximum negative anomaly, reaching –2.5 km³ per month, was observed in May 2018; notable negative anomalies of –2.1 km³ per month are observed in April 1998 and March 2018.

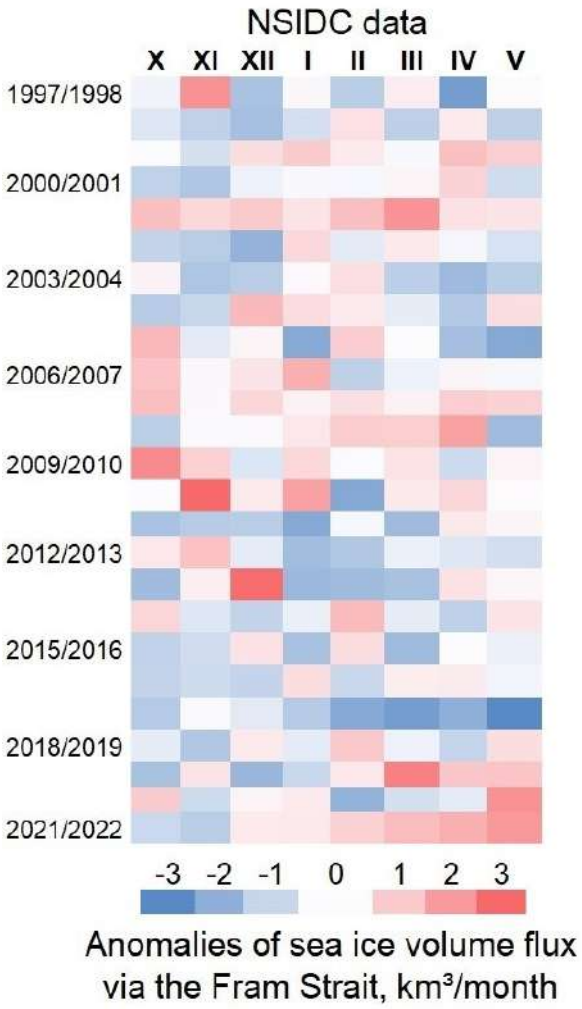


Figure 3.11. Standardized anomalies of the volume of ice exported via the Fram Strait during the winter months (expressed in km³ per month), averaged over the ice seasons from 1997/1998 to 2021/2022, obtained from NSIDC data

Subsequently, a statistical significance test was conducted on the linear trend of the ice volume flux through the Fram Strait. The primary criterion for assessing the statistical significance of the trend was the Student's t-test (at a significance level of 99%) [Malinin, 2020a]. The result indicated that the interannual changes in the ice export volume do not exhibit a statistically significant linear trend. This finding contradicts the results of studies

based on long-term observation records, notably [Zhang et al., 2017; Spreen et al., 2020], where a significant decreasing trend in the characteristic is identified. The presence of this trend is mainly attributed to a significant reduction in the thickness of the ice cover being transported from the Arctic Basin.

Turning to the interannual variations in the average-weighted ice thickness and ice drift velocity, as well as the ice flow width in the Fram Strait — they were utilized for calculating the ice volume export (see Figure 3.12). Statistical significance tests were conducted on the linear trends of the aforementioned characteristics, with the primary criterion for assessing the significance of the trend being the Student's t-test (at a significance level of 99%) [Malinin, 2020a]. As a result, a significant negative linear trend is identified for the average-weighted ice thickness, while non-significant trends with a tendency to increase are observed for the drift velocity of the ice cover and the width of the ice flow. Specifically, the magnitude of the significant linear trend in sea ice thickness amounts to –3.6 cm per ice season. Thus, since 1997, the reduction in the average ice

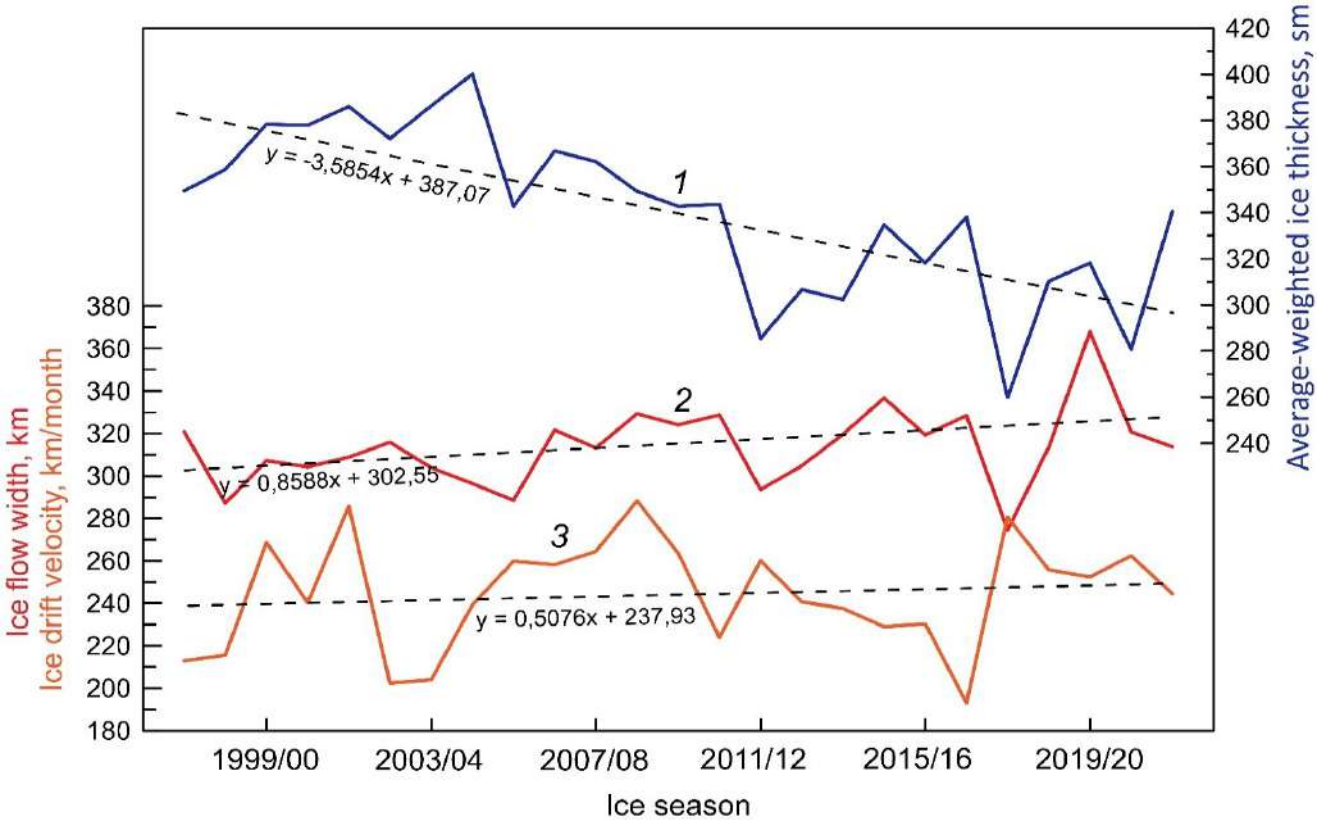


Figure 3.12. Interannual variations in the average-weighted ice thickness (*1*), ice flow width (*2*), and ice drift velocity (*3*), averaged over the ice seasons from 1997/1998 to 2021/2022, along with their linear trends (indicated by dashed lines)

thickness in the Fram Strait is offset by the maintenance of its drift velocity and the ice flow width. This is reflected in the non-significant linear trend of the volume of ice exported via the strait site. The highest correlation coefficients are observed between the ice flow width and the ice volume flux (+0.52), and between the average-weighted ice thickness and the ice volume flux (+0.48), while the mean ice drift velocity and the ice volume flux are associated with a correlation coefficient of +0.29.

In Table 3.14, estimates of the volume of sea ice exported through the Fram Strait, as compiled by various authors over extended time periods, are presented. The volume transport estimate derived in the present study, using data on mean sea ice thickness from AARI ice charts and ice drift velocity from NSIDC, is comparable to the findings of [Kwok et al., 2004; Spreen et al., 2020] for long-term observational series.

Table 3.14. Estimates of sea ice volume exported via the Fram Strait by different authors

| *Author(s) and publication year* | *Period* | *Ice volume flux via the Fram Strait, $km^3$ per ice season* |
|---|---|---|
| Lebedev and Uralov, 1981 | 1958–1976 | 2320* |
| Mironov, 1997 | 1958–1992 | 2100* |
| Vinje et al., 1998 | 1990–1996 | 2850* |
| Kwok et al., 2004 | 1991–1998 | 2218 |
| Spreen et al., 2009 | 2003–2008 | 1564 |
| Zhang et al., 2017 | 1987–2012 | 1041 |
| Ricker et al., 2018 | 2010–2017 | 1885 |
| Bi et al., 2018 | 2011–2015 | 1463 |
| | | 1029 |
| Spreen et al., 2020 | 1992–2014 | 2209 |
| Present study | 1997–2022 | 2141 |

*Note*. Summative estimates accounting for ice volume exported through the Fram Strait during the summer period are marked with an asterisk (*). In rows of the table where two estimates of ice volume flux are provided, authors employ two approaches to determine sea ice drift through the strait.

While the authors in the studies employ different approaches to determine ice drift and thickness, let us focus on the sources of data specifically regarding thickness (data on drift require further consideration, which is beyond the scope of this study), and examine the estimates obtained after 2000. In the works of [Spreen et al., 2009; Ricker et al., 2018;

Bi et al., 2018], ice volume estimates ranging from 1029 $km^3$ to 1885 $km^3$ were derived using data on ice thickness from the ICESat and CryoSat-2 satellites. Within the same range lies the estimate by [Zhang et al., 2017], where a joint PIOMAS model, accounting for ice pack ridging, was utilized. Authors [Kwok et al., 2004; Spreen et al., 2020] used ice draft measurements obtained through upward-looking sonars and profiling sonars to account for ice thickness in the Fram Strait. The ice volume in these studies, ranging from 2209 $km^3$ to 2218 $km^3$, are closely aligned with each other and correspond to the estimate presented in present study based on NSIDC data. As a result, the average-weighted ice thickness in the Fram Strait, derived from age structure data from AARI ice charts adjusted for ridged formations, are comparable to thickness from instrumental measurements. Modeling and satellite observations yielded relatively underestimated results.

### 3.6. Conclusions for Chapter 3

The chapter describes the patterns of seasonal and interannual variations in the main parameters of the Greenland Sea ice cover, which shape the unique ice conditions. Based on the results of the study, the following *key* conclusions were formulated:

- Seasonal maximum ice coverage is observed from February to April, with a minimum in September. After 2016, the largest ice area is consistently recorded in April. Additionally, the period of establishing the maximum position of drift ice edge is smoothed out until April.
- The modern period of climate change is defined from the ice season of 1999/2000, according to the distribution of ice coverage anomalies on their cumulative curves. The author suggests that the main portion of changes in the sea ice coverage during the ice season is contributed by the period of its stable formation in February when the ice area is already close to its maximum value within the season. Statistically significant linear trends of absolute ice coverage values in February confirm this.
- In the modern period of climate change, the seasonal range of drift ice edge position remains at the average level, which was obtained in the previous cold climate period (1958–1992), despite the observed absolute minimums in ice extent (area) in the Greenland Sea after the 2000s.

- The relative amount of old ice in the ice age structure since the beginning of the 21st century (compared to 1989–1992) has significantly decreased, from 50–62% to 30–44% during the winter period. In April, old ice occupies from 15% to 50% of the total ice area of the Greenland Sea.
- Among locally formed ice, age gradations of initial types and young ice are characteristic for the ice cover of all analyzed winter months (from October to May) in the Greenland Sea. In April, first-year medium ice predominates among the first-year ice gradations overall, while thick ice is encountered least frequently.
- In April, the decrease in the relative area of first-year medium and thick ice, as well as the increase in the relative area of thin ice, compensates for the overall changes in the entire first-year ice gradation in the Greenland Sea ice cover structure.
- The dominance boundary of old ice throughout the entire winter period changes insignificantly, not more than by 2° of longitude.
- The estimated volume of ice exported through the Fram Strait during the winter months, October-May, averaged over the period 1997–2022, is 2141 $km^3$. The estimate is comparable to the results of other studies where data on ice thickness obtained through upward-looking sonars and profiling sonars (i.e., instrumental observations) were used.
- Interannual variations of ice volume flux do not have a statistically significant linear trend, despite a significant linear trend indicating a decrease in the average-weighted ice thickness in the Fram Strait by –3.6 cm per ice season.

# CHAPTER 4. REGULARITIES OF SPATIO-TEMPORAL VARIATIONS OF ICE REGIME KEY CHARACTERICTISC IN BARENTS SEA

## 4.1. Ice coverage

### 4.1.1. Seasonal variations

Due to the inflow of warm Atlantic waters, the Barents Sea never completely freezes over, even in the harshest winters, which is a characteristic feature of its ice conditions, similar to the Greenland Sea. Table 4.1 presents the seasonal ice coverage variation for the entire Barents Sea and its sub-areas.

Under average long-term conditions, the formation of the ice cover in the Barents Sea begins with residual ice at 8% in October and reaches 53% in April, lasting for seven months. Conversely, the ice cover decreases from May (43%) to September (4%), lasting for five months each year. The maximum ice coverage in the Barents Sea occurs in April, while the minimum is in September, with the ice cover occupying 53% and 4% of the sea area, respectively. The timing of the seasonal peaks in sea ice area aligns with the results of other studies with a monthly accuracy for the following periods: 1934–1984 in [Hydrometeorology and..., 1990], 1928–1996 in [Mironov, 2004], and 1930–2018 in [Timokhov et al., 2019].

Further analysis of the ice coverage extremes is conducted by *ice seasons*. According to Table 4.1, the ice cover can occupy up to 86% of the Barents Sea, which was observed in April during the ice season of 1928/1929. Heavy ice conditions, with ice cover reaching 84% and 82%, were also noted in the 1941/1942 and 1963/1964 ice seasons, respectively. Although under average conditions, the seasonal maximum ice cover in the Barents Sea is established in April, during the 95-year observation period, the peak occurs in other winter months in 50% of the cases. Specifically, the maximum ice area occurs in March and February in 27% and 18% of the ice seasons, respectively, and in January and May in the remaining 3% and 2% of the cases, respectively. It is noted that up until the 1965/1966 ice season, the maximum ice coverage in the Barents Sea was recorded in April (with some

exceptions); however, after 1966, the timing of its seasonal maximum varies from January to May.

Table 4.1. Seasonal variation of ice coverage (expressed in %) over the entire Barents Sea and its sub-areas throughout the annual cycle, averaged over the period from 1928 to 2022

| Ice coverage, % / Month | X | XI | XII | I | II | III | IV | V | VI | VII | VIII | IX |
|---|---|---|---|---|---|---|---|---|---|---|---|---|
| **Barents Sea** | | | | | | | | | | | | |
| Mean | 8 | 18 | 30 | 40 | 48 | 52 | 53 | 43 | 28 | 13 | 5 | 4 |
| Maximum | 33 | 43 | 54 | 61 | 76 | 83 | 86 | 75 | 61 | 36 | 22 | 18 |
| Minimum | 0 | 1 | 5 | 20 | 27 | 30 | 22 | 10 | 1 | 0 | 0 | 0 |
| SD, % | ±6 | ±9 | ±9 | ±9 | ±10 | ±10 | ±12 | ±13 | ±12 | ±8 | ±5 | ±4 |
| Seasonal range, % | 33 | 42 | 49 | 41 | 49 | 53 | 64 | 65 | 60 | 36 | 22 | 18 |
| **Western sub-area of Barents Sea** | | | | | | | | | | | | |
| Mean | 12 | 23 | 32 | 38 | 43 | 46 | 47 | 42 | 33 | 19 | 8 | 6 |
| Maximum | 49 | 58 | 60 | 63 | 73 | 80 | 82 | 70 | 63 | 43 | 33 | 27 |
| Minimum | 0 | 0 | 2 | 7 | 18 | 23 | 10 | 10 | 2 | 0 | 0 | 0 |
| SD, % | ±9 | ±12 | ±11 | ±12 | ±11 | ±11 | ±12 | ±11 | ±12 | ±11 | ±7 | ±6 |
| Seasonal range, % | 49 | 58 | 58 | 56 | 55 | 57 | 72 | 60 | 61 | 43 | 33 | 27 |
| **North-eastern sub-area of Barents Sea** | | | | | | | | | | | | |
| Mean | 23 | 40 | 52 | 62 | 69 | 74 | 79 | 70 | 52 | 29 | 16 | 12 |
| Maximum | 49 | 76 | 77 | 90 | 99 | 99 | 99 | 99 | 99 | 64 | 43 | 36 |
| Minimum | 0 | 9 | 16 | 27 | 25 | 22 | 26 | 24 | 17 | 1 | 0 | 0 |
| SD, % | ±12 | ±14 | ±14 | ±15 | ±17 | ±17 | ±17 | ±18 | ±20 | ±14 | ±11 | ±9 |
| Seasonal range, % | 49 | 67 | 61 | 63 | 74 | 77 | 73 | 75 | 82 | 63 | 43 | 36 |
| **South-eastern sub-area of Barents Sea** | | | | | | | | | | | | |
| Mean | 0 | 8 | 25 | 45 | 60 | 64 | 63 | 45 | 17 | 2 | 0 | 0 |
| Maximum | 14 | 58 | 71 | 86 | 99 | 99 | 99 | 99 | 62 | 23 | 11 | 9 |
| Minimum | 0 | 0 | 0 | 16 | 26 | 27 | 4 | 0 | 0 | 0 | 0 | 0 |
| SD, % | ±2 | ±9 | ±13 | ±14 | ±16 | ±16 | ±20 | ±23 | ±16 | ±4 | ±1 | ±1 |
| Seasonal range, % | 14 | 58 | 71 | 70 | 73 | 72 | 95 | 99 | 62 | 23 | 11 | 9 |

*Note.* SD refers to the standard deviation. The seasonal range is defined as the difference between the maximum and minimum ice coverage values in the seasonal cycle.

The Barents Sea was completely free of ice cover for two to three summer months, as observed in August-October 1955, 2007, 2018, and 2020, as well as in July-August 2012, 2016, and 2022. These peaks coincide with periods of extremely low ice cover area (extent) in the Arctic [Ivanov et al., 2013]. Although instances of the Barents Sea being entirely ice-free number around a dozen throughout the observation period, seven of these occurred in the last decade, 2011–2021, as noted by the authors [Tyuryakov and Egorova,

2021]. In 61% (the majority) of cases, the seasonal minimum ice coverage in the Barents Sea is observed in September, consistent with the long-term average. However, in 32% of ice seasons, the minimum occurs in August, while in 5% and 2% of cases, it occurs in July and even October, respectively. Additionally, under light ice conditions, the seasonal maximum ice coverage shifts back by a month, occurring in March.

Subsequently, by calculating the difference between the ice coverage values for pairs of adjacent months within the ice season, the rates of change were determined. The highest rates of ice growth in the Barents Sea, on average, are observed from October to January — this period marks the active ice formation phase, with ice cover increasing by +9% per month. From February to April, the rate of ice coverage change significantly slows down, amounting to +1% to +3% per month. In April, the ice cover reaches its maximum under average conditions. The period of intensive melting begins in May: from May to July, the Barents Sea experiences the highest rates of ice cover reduction, at –10% to –15% per month. The rate of ice coverage reduction from August to September is around –5% per month.

When assessing the spatial heterogeneity of ice distribution in the Barents Sea, it is necessary to closely examine the changes in ice coverage in its sub-areas. In the western and north-eastern sub-areas, the seasonal maximum ice coverage occurs in April (47% and 79%, respectively), while in the south-eastern sub-area, it occurs in March (64%). The minimum ice coverage values in the annual cycle are reached in September in the western (6%) and north-eastern sub-areas (12%); in the south-eastern one, the ice cover completely melts by August under average conditions, with ice formation beginning on open water in October. The results of ice coverage changes analysis in the northern part of the Barents Sea align with data for the entire sea.

In the harshest winters, the seasonal ice coverage changes in the western sub-area of the Barents Sea are similar to the long-term average: the peaks of ice coverage occur in April and September (with maximum and minimum values of 82% and 27%, respectively). The same trend is observed in the ice seasons with the lightest ice conditions: here, the seasonal maximum occurs in March (23%), and the area is completely ice-free from July

to November (and for the entire sea from July to September). In the other sub-areas of the Barents Sea, the pattern of annual ice coverage variations differs from the average under extreme heavy and extreme light ice conditions. Thus, the changes in the ice cover area of the entire Barents Sea within the annual cycle are primarily driven by fluctuations in its western sub-area. This is due to the western sub-area: (1) having the largest area compared to other parts of the sea; (2) being most influenced by the Atlantic waters.

In the harshest years, the ice coverage in the north-eastern sub-area of the Barents Sea can reach 99% from February to June, as observed in the 1978/1979 and 1981/1982 ice seasons. In the south-eastern sub-area, the seasonal maximum ice coverage under extreme heavy ice conditions also extends from February to May, as noted in the 1965/1966 and 1978/1979 ice seasons. Minimum ice coverage values were observed in September, constituting 36% in the north-eastern sub-area and 9% in the south-eastern sub-area. Conversely, under extreme light ice conditions, the maximum ice coverage in the north-eastern sub-area occurs in January, and in the south-eastern sub-area, it occurs in March, with 27% for each sub-area. From August to October, the north-eastern part can be completely ice-free, as it was in the summer months of 2018; the ice conditions in 2012 and 2020 were close to the minimum distribution. The south-eastern sub-area can be ice-free from May to December, but in 1995, open water was noted only from May to October, while, for example, in 1959, it was from July to December, and in 1954, it was from June to November.

### 4.1.2. Interannual variations

Interannual changes in the ice coverage of the Barents Sea are also characterized by a statistically significant linear trend towards reduction, as noted by [Krasheninnikova and Krasheninnikova, 2019; Lis and Egorova, 2022]. This correlates with the results for the sea ice area (extent) in the Arctic overall [Serreze and Stroeve, 2015; Stroeve and Notz, 2018; Yulin et al., 2019]. Against the backdrop of this pronounced negative trend, SD values show large interannual fluctuations in the ice coverage of the Barents Sea. The highest SD values, ±10% and above, are observed from March to June, with a peak in May at ±13%. For August-September, the months with the minimum ice coverage in the Barents Sea within

the annual cycle, the SD values are the lowest, at ±4% and ±5%, respectively. A similar monthly distribution is typical for its sub-areas (SD values are not presented in the text).

In present study, ice coverage anomalies for the sub-areas of the Barents Sea were examined, and periods of cooling and warming were identified using the cumulative curve analysis method for anomalies, similar to the Greenland Sea [Girs and Kondratovich, 1978]. Although periods of cooling and warming were identified in various articles [Matishov et al., 2013; Zhichkin, 2015; Timokhov et al., 2019; Lis and Egorova, 2022], it is important to investigate the Barents Sea by its sub-areas and compare the results.

In accordance with the identified main periods of sea ice coverage changes within the ice season of Arctic Seas, as highlighted by [Zakharov, 1996; Alekseev et al., 2009], the following months were selected for the analysis of ice coverage anomalies in the sub-areas of the Barents Sea: *November*, the month of active ice formation; *February*, the period of stable ice formation; *April* and *September*, the months of maximum and minimum ice coverage, respectively. The cumulative curve plots of ice coverage anomalies for the sub-areas of the Barents Sea for these months, obtained relative to the long-term mean values for 1950–2022, are shown in Figures 4.1, 4.2, and 4.3 for the western, north-eastern, and south-eastern parts, respectively. For the south-eastern sub-area, the curve for September (see Figure 4.3) is not presented, as under average conditions, the ice cover in this month completely melts in its part. Anomalies of absolute ice coverage values at the identified stages of change are presented in Tables 4.2 (western), 4.3 (north-eastern), and 4.4 (south-eastern) — after indicating the magnitudes of positive and negative ice coverage anomalies in parentheses, the number of ice seasons characterized by predominance of anomalies of one or the other sign is provided. Thus, visually, up to three periods of anomaly changes in the sub-areas of the Barents Sea are distinguished: the stage of increase in ice coverage is indicated by the red curve, stability by the green curve, and decrease by the blue curve.

The analysis of cumulative curve anomalies in the ice coverage of the Barents Sea reveals that the duration of “cold” and “warm” periods, as well as the onset of the modern warming period, vary significantly not only for individual months within the annual cycle but also in different parts of the Sea. In the northern sub-area, two periods of ice coverage

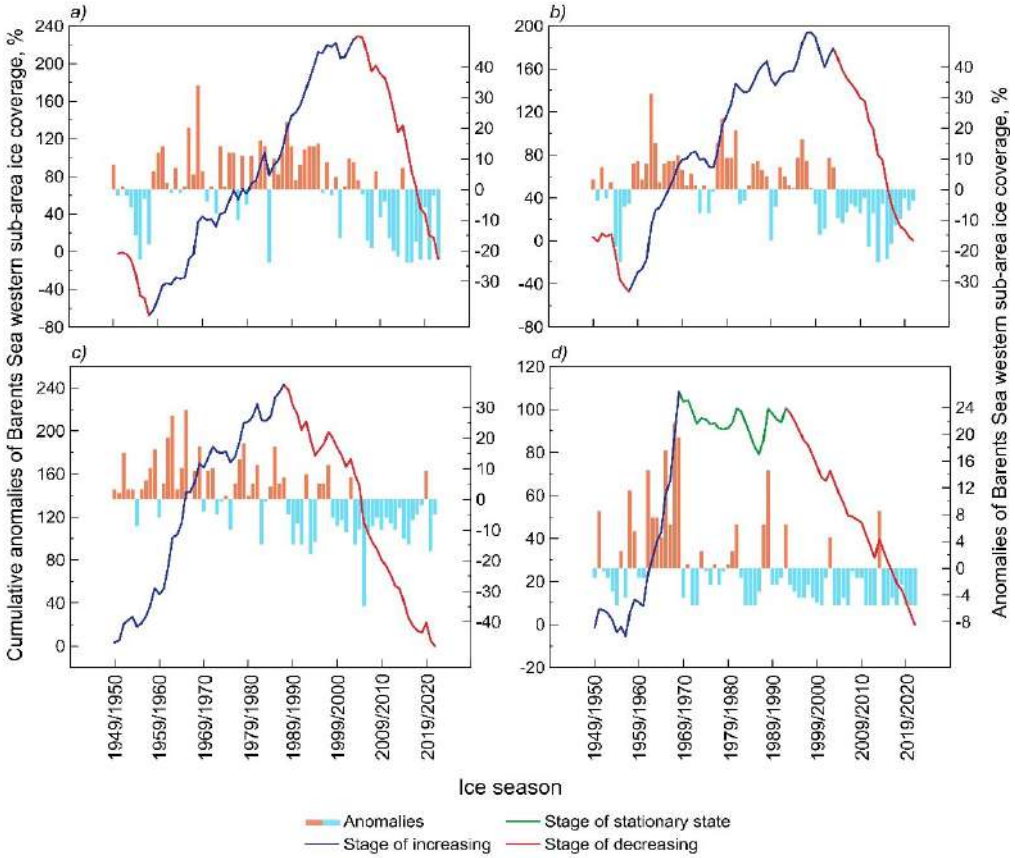


Figure 4.1. Cumulative curve anomalies of ice coverage in the western sub-area of the Barents Sea in: *a)* November, *b)* February, *c)* April, and *d)* September, calculated relative to the long-term mean values for 1950–2022

Table 4.2. Mean magnitude and prevailing sign of absolute ice coverage anomalies in the western sub-area of the Barents Sea (expressed in %) at the identified stages for the period 1950–2022

| *Stage of change* | Period | Ice cover anomaly, % | | |
|---|---|---|---|---|
| | | Mean | Positive | Negative |
| **November** | | | | |
| *Increasing* | 1957/1958–2003/2004 | +6% | +1%...+34% (35) | –24%...–1% (13) |
| *Decreasing* | 2004/2005–2022/2023 | –12% | +3%...+7% (3) | –24%...–2% (16) |
| **February** | | | | |
| *Increasing* | 1957/1958–2003/2004 | +3% | +1%...+31% (36) | –25%...–1% (11) |
| *Decreasing* | 2004/2005–2021/2022 | –10% | (0) | –24%...–3% (18) |
| **April** | | | | |
| *Increasing* | 1949/1950–1987/1988 | +6% | +1%...+27% (32) | –15%...–1% (7) |
| *Decreasing* | 1988/1989–2021/2022 | –7% | +5%...+9% (5) | –35%...–5% (29) |
| **September** | | | | |
| *Increasing* | 1949/1950–1967/1968 | +5% | +3%...+22% (12) | –5%...–1% (7) |
| *Stationary state* | 1968/1969–1991/1992 | 0% | +1%...+20% (10) | –5%...–1% (14) |
| *Decreasing* | 1992/1993–2021/2022 | –3% | +1%...+9% (4) | –5%...–1% (26) |

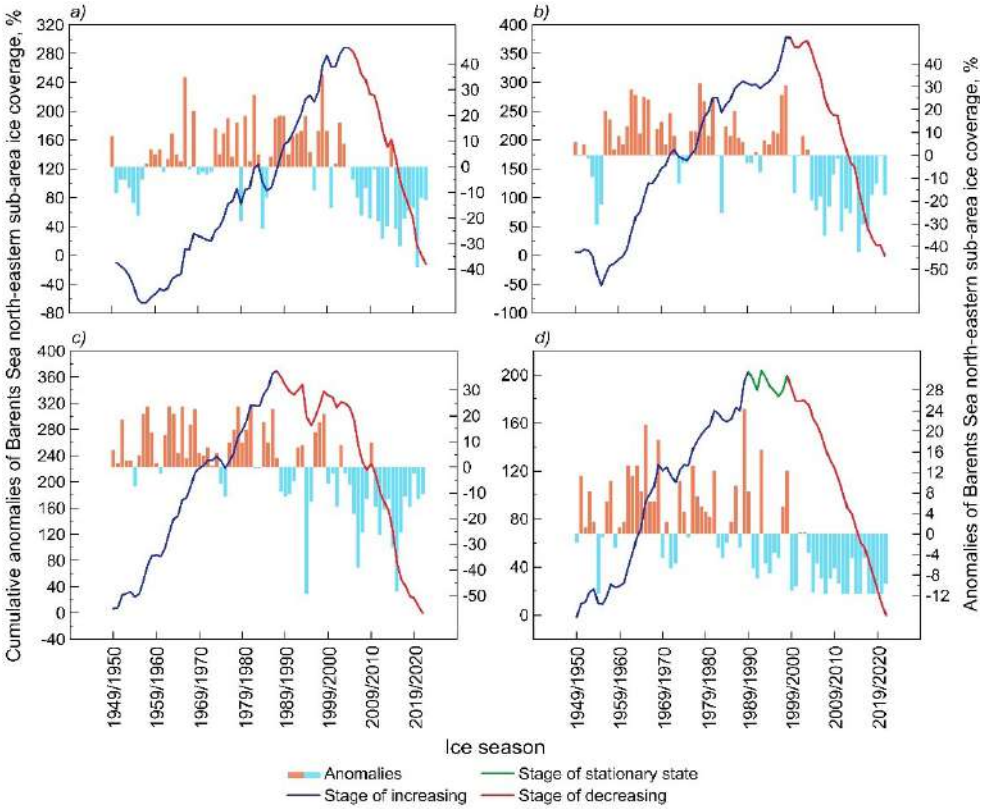


Figure 4.2. Cumulative curve anomalies of ice coverage in the north-eastern sub-area of the Barents Sea in: *a)* November, *b)* February, *c)* April, and *d)* September, calculated relative to the long-term mean values for 1950–2022

Table 4.3. Mean magnitude and prevailing sign of absolute ice coverage anomalies in the north-eastern sub-area of the Barents Sea (expressed in %) at the identified stages for the period 1950–2022

| *Stage of change* | Period | Ice cover anomaly, % | | |
|---|---|---|---|---|
| | | Mean | Positive | Negative |
| **November** | | | | |
| *Increasing* | 1949/1950–2003/2004 | +5% | +1%...+36% (39) | –24%...–1% (16) |
| *Decreasing* | 2004/2005–2022/2023 | –16% | +1%...+10% (2) | –39%...–1% (17) |
| **February** | | | | |
| *Increasing* | 1949/1950–1998/1999 | +6% | +1%...+32% (39) | –30%...–1% (11) |
| *Decreasing* | 1999/2000–2021/2022 | –16% | +1%...+9% (5) | –42%...–1% (18) |
| **April** | | | | |
| *Increasing* | 1949/1950–1987/1988 | +9% | +1%...+24% (36) | –7%...–1% (3) |
| *Decreasing* | 1988/1989–2021/2022 | –11% | +4%...+6% (6) | –48%...–2% (28) |
| **September** | | | | |
| *Increasing* | 1949/1950–1989/1990 | +5% | +1%...+24% (30) | –12%...–1% (11) |
| *Stationary state* | 1990/1991–1998/1999 | 0% | +5%... +16% (3) | –9%... –4% (6) |
| *Decreasing* | 1999/2000–2021/2022 | –9% | +1% (2) | –12%...–4% (21) |

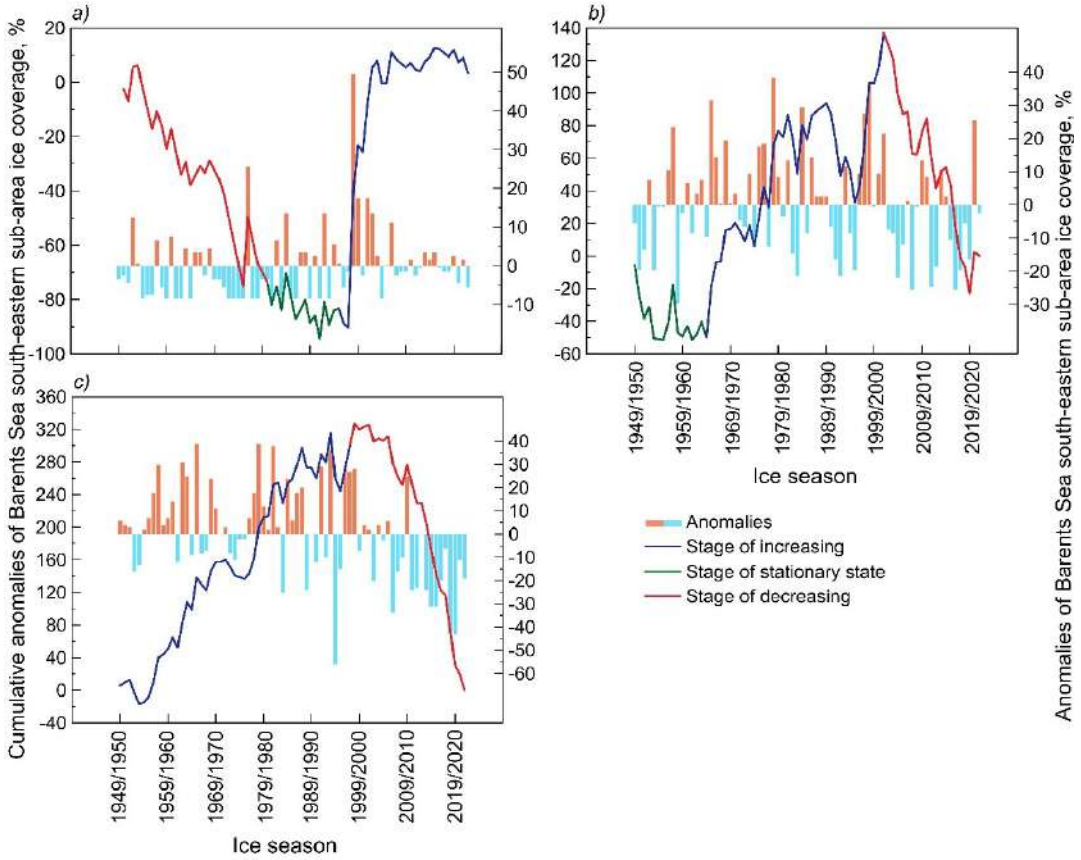


Figure 4.3. Cumulative curve anomalies of ice coverage in the south-eastern sub-area of the Barents Sea in: *a)* November, *b)* February, *c)* April, and *d)* September, calculated relative to the long-term mean values for 1950–2022

Table 4.4. Mean magnitude and prevailing sign of absolute ice coverage anomalies in the south-eastern sub-area of the Barents Sea (expressed in %) at the identified stages for the period 1950–2022

| *Stage of change* | Period | Ice cover anomaly, % | | |
|---|---|---|---|---|
| | | Mean | Positive | Negative |
| **November** | | | | |
| *Decreasing* | 1949/1950–1980/1981 | –2% | +1%...+26% (7) | –8%...–2% (25) |
| *Stationary state* | 1981/1982–1995/1996 | 0% | +1%...+14% (8) | –8% (7) |
| *Increasing* | 1996/1997– 2022/2023 | +3% | +1%...+50% (15) | –8%...–1% (12) |
| **February** | | | | |
| *Stationary state* | 1949/1950–1964/1965 | 0% | +4%...+24% (9) | –29%...–5% (7) |
| *Increasing* | 1965/1966–2001/2002 | +5% | +1%...+37% (24) | –21%...–3% (13) |
| *Decreasing* | 2002/2003– 2021/2022 | –7% | +1%...+14% (6) | –25%...–2% (14) |
| **April** | | | | |
| *Increasing* | 1949/1950–1998/1999 | +7% | +1%...+39% (34) | –56%...–2% (16) |
| *Decreasing* | 1999/2000–2021/2022 | –14% | +1%...+6% (5) | –34%...–3% (18) |

anomaly changes are distinguished in November, February, and April, and three periods (including the stability stage) in September. In November and April, the onset of the warming stage coincides for the western and north-eastern sub-areas up to a single ice season, 2004/2005 (November) and 1988/1989 (April). In February, the "warm" period starts significantly later in the western part, from the ice season 2004/2005, compared to 1999/2000 in the north-eastern part of the Barents Sea. It is also noted that in the western sub-area, the stage of increasing ice coverage in November and February started from the ice season 1957/1958, while in the north-eastern sub-area, it started from 1949/1950 (or earlier, but the studied sample is limited to 1950). In September, both in the western and north-eastern sub-areas of the Barents Sea, three periods of ice coverage changes are identified, but their durations significantly differ. In the western part, the modern "warm" period of climate change has been ongoing for the past 30 years (since the ice season 1992/1993); here, there is also a relatively long period of relative stability in ice cover changes, approximately 24 years. In the north-eastern part, the period of increasing ice cover lasted for 41 years, with relatively short 8-year periods of stability. The decreasing stage started later than in the western sub-area, specifically from the ice season 1999/2000, and has been ongoing for 23 years.

In the south-eastern sub-area of the Barents Sea, not only the timing of the onset of cold and warm phases, but also the sign of prevailing ice coverage anomalies during the investigated period differ. Thus, in November, the distribution of anomalies begins with a decrease stage, rather than an increase, as in other parts of the Sea. It turns out that during the modern period of climate change, since the ice season of 1996/1997, an increase in characteristic anomalies, specifically the "cold" period, is observed here. In February and April, the picture is more familiar: in recent years, there has been a stage of decreasing ice coverage in the south-eastern sub-area, which began in the ice seasons of 2002/2003 and 1999/2000, respectively.

The contribution of separate months to interannual changes in ice coverage can be assessed by constructing a similar cumulative curve for the average ice season (see Figure 4.4). Three stages are distinguished on the cumulative curve for the entire Barents Sea:

1949/1950–1987/1988, 1988/1989–2003/2004, and 2004/2005–2021/2022. For the first period, the average anomaly magnitude is +5% (–9%...+31%), for the second, it is close to zero (–6%...+10%), and for the third, it is –9% (–16%...–4%). The first period out of the total (39) ice seasons is characterized by 8 negative (–9%... –1%) and 31 positive anomalies of ice coverage (+1%...+31%). In the second stage, out of 16 ice seasons, 8 cases correspond to negative and positive signs of ice coverage anomalies (–6%...–1% and +1%...+10%). In the third period, all 18 ice seasons are characterized by only negative anomalies of Barents Sea ice coverage (–16%...–4%). Similar durations of the stage of decreasing anomalies are highlighted on cumulative curves for the western part in November and February, and for the north-eastern one, only in November, the months of active or stable ice formation in the Barents Sea. Thus, it is assumed that the main share of changes in ice coverage anomalies during the ice season is contributed by November and February. In this case, April determines these changes to a much lesser extent: the period of decreasing ice coverage anomalies in the western and north-eastern sub-areas occurs earlier in this month, namely, in the late 1980s, while in November and February, it occurs in the early 2000s.

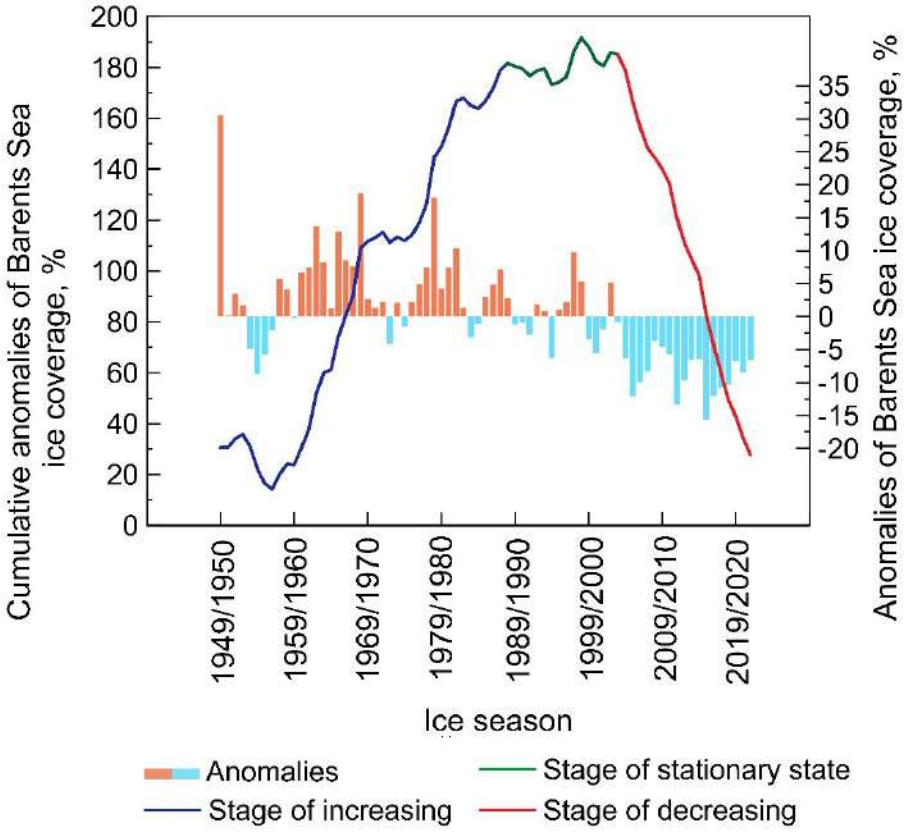


Figure 4.4. Cumulative curve anomalies of ice coverage in the Barents Sea, calculated relative to the long-term mean values for 1950–2022

It is noted that the stages of ice coverage changes identified by cumulative curves on average for the ice season do not correspond to the results of the analysis of its absolute values in [Lis and Egorova, 2022], where a warming period in the sub-areas of the Barents Sea is established from 1986. The analysis of cumulative curves in present study shows that from the mid-1980s, a period of relative stability in ice coverage anomalies begins, which is replaced by a stage of predominance of negative anomalies (a warming period, respectively) after the 2000s.

Next, let's turn to the absolute values of Barents Sea ice coverage and its sub-areas. The main statistical characteristics of ice coverage within the identified stages, calculated for individual months as well as on average for the season, are summarized in Tables 4.5 (western and north-eastern parts) and 4.6 (southeastern part). In the northern region of the Sea, a reduction (in percentages) in ice coverage is observed in September: on average, in its western sub-area, ice cover decreased by 80% (from 10% to 2%), and in the north-eastern sub-area, by 82% (from 17% to 3%). At the same time, a similar regularity in changes in the SD and seasonal range of the analyzed characteristic is not observed (they decreased only by 2–3 times). Ice coverage in the north-eastern sub-area of the Barents Sea decreased significantly more than in the western one: by 14–24% compared to 8–18% (in absolute values of ice coverage, %). In the western sub-area, ice coverage is subject to smaller changes in September (SD up to ±8%), and larger changes occur in November (up to ±11%); for the north-eastern sub-area, smaller changes are typical for September (up to ±9%), and larger changes are observed in April (up to ±17%). The greatest seasonal range values for the northern region of the Barents Sea are observed in winter months (up to 58% in the western part and up to 70% in the northeastern part). In the south-eastern sub-area, maximum SD and seasonal range values are observed in April (up to ±19% and up to 95%, respectively), and minimum values are observed in November (up to ±11% and up to 58%, respectively). In November, ice coverage here increased by 2 times (from 6% to 12%), while in February and April, on the contrary, it decreased by 1.2 times (from 66% to 54%) and by 1.5 times (from 67% to 46%), respectively.

Table 4.5. Statistical characteristics of ice coverage in the western (W) and north-eastern (NE) sub-areas of the Barents Sea (in %) during its stages of change for the period 1950–2022, identified by cumulative curves of its anomalies

| *Stage of change* | Mean, % | | SD, % | | Seasonal range, % | |
|---|---|---|---|---|---|---|
| | **W** | **NE** | **W** | **NE** | **W** | **NE** |
| **November** | | | | | | |
| *Increasing* | 30 | 46 | ±11 | ±13 | 58 | 60 |
| *Decreasing* | 12 | 24 | ±11 | ±12 | 31 | 49 |
| **February** | | | | | | |
| *Increasing* | 46 | 75 | ±9 | ±14 | 48 | 62 |
| *Decreasing* | 32 | 51 | ±7 | ±14 | 21 | 51 |
| **April** | | | | | | |
| *Increasing* | 51 | 85 | ±9 | ±10 | 44 | 35 |
| *Decreasing* | 38 | 65 | ±9 | ±17 | 46 | 70 |
| **September** | | | | | | |
| *Increasing* | 10 | 17 | ±8 | ±8 | 27 | 36 |
| *Stationary state* | 6 | 11 | ±5 | ±9 | 20 | 25 |
| *Decreasing* | 2 | 3 | ±4 | ±4 | 14 | 12 |

Table 4.6. Statistical characteristics of ice coverage in the south-eastern sub-area of the Barents Sea (in %) during its stages of change for the period 1950–2022, identified by cumulative curves of its anomalies

| *Stage of change* | Mean, % | SD, % | Seasonal range, % |
|---|---|---|---|
| **November** | | | |
| *Decreasing* | 6 | ±8 | 34 |
| *Stationary state* | 8 | ±8 | 22 |
| *Increasing* | 12 | ±11 | 58 |
| **February** | | | |
| *Stationary state* | 57 | ±13 | 53 |
| *Increasing* | 66 | ±16 | 60 |
| *Decreasing* | 54 | ±14 | 51 |
| **April** | | | |
| *Increasing* | 67 | ±19 | 95 |
| *Decreasing* | 46 | ±17 | 68 |

*Note to Tables 4.5 and 4.6.* SD stands for the standard deviation. Seasonal range refers to the difference between the maximum and minimum values of ice coverage within one stage (increase, stability, or decrease).

Additionally, statistically significant linear trends of interannual changes in the Barents Sea ice coverage were evaluated (see Table 4.7, which presents the values of statistically significant linear trends). The t-Student criterion with a significance level of 99% [Malinin, 2020a] was used as the main criterion for assessing the statistical significance of trends. As a result, significant linear trends are determined in all analyzed periods for the entire observation series (from 1950 to 2022) only in the western and northeastern sub-areas. Moreover, the maximum magnitude of the linear trend is observed in April, amounting to –0.29% for the ice season in the western part and –0.46% for the ice season in the north-eastern part. Thus, the obtained results do not confirm the previously suggested assumption that interannual changes in Barents Sea ice coverage in February determine its fluctuations for the entire ice season. The analysis of the significance of linear trends in the absolute values of ice coverage in the sub-areas indicates a greater contribution to interannual fluctuations in April, the month of maximum ice development in the Barents Sea. It is noted that in "warm" periods, significant linear trends are observed only in April and September throughout the sea basin (for the south-eastern sub-area, only in April). Overall, ice cover decreases faster over the ice season in the north-eastern sub-area, where the magnitude of the linear trend is –0.38% for the ice season (compared to –0.22% and –0.13% for the ice season in the western and south-eastern parts, respectively). Interestingly, during the identified stage of increasing ice coverage anomalies in the western part of the Barents Sea in February, the linear trend of absolute values is negative (–0.18% for the ice season).

Table 4.7. Magnitudes of statistically significant linear trends of absolute ice coverage values in the sub-areas of the Barents Sea (in % per ice season) for various stages of its anomalies change

| Stage of change / *Month* | *November* | *February* | *April* | *September* | *Ice season* |
|---|---|---|---|---|---|
| **Western sub-area of Barents Sea** | | | | | |
| Increasing | Insignificant | –0.18 | Insignificant | +0/86 | — |
| Stationary state | — | | | Insignificant | |
| Decreasing | Insignificant | | –0.16 | –0.46 | |
| Entire observational series | –0.18 | –0.20 | –0.29 | –0.13 | –0.22 |
| **North-eastern sub-area of Barents Sea** | | | | | |
| Increasing | +0.25 | Insignificant | | | — |

| | | | | | |
|---|---|---|---|---|---|
| Stationary state | — | | | Insignificant | |
| Decreasing | Insignificant | | | –0.25 | |
| Entire observational series | –0.24 | –0.40 | –0.46 | –0.25 | –0.38 |
| **South-eastern sub-area of Barents Sea** | | | | | |
| Increasing | Insignificant | | Insignificant | — | — |
| Stationary state | | | — | | |
| Decreasing | | | –1.25 | | |
| Entire observational series | | | –0.40 | | –0.13 |

*Note.* A dash indicates that no such stage of change was identified for that month.

According to the results of the analysis of cumulative curves of ice coverage anomalies, the warming stage in the Barents Sea begins from the ice season of 2004/2005. As noted earlier, in other seas of the Russian Arctic (the Kara Sea, Laptev Sea, East Siberian Sea, and Chukchi Sea), this ice season is also pivotal [Egorov, 2020; Timofeeva and Sharatunova, 2021; Timofeeva et al., 2024]. This means that the response to ongoing climate changes, reflected particularly in ice coverage, has been observed since 2004/2005 in all the Russian Arctic Seas.

### 4.2. Drift ice edge position in annual cycle

Seasonal variations in the drift ice edge position in the Barents Sea are illustrated in Figure 4.5. The onset of the seasonal minimum of the drift ice edge position occurs in September, consistent with ice coverage data and observed across all fixed sections. In this month, from 20° E to 47.5° E, the ice edge lies beyond the boundaries of the Barents Sea, while from 50° E to 65° E, it resides in its north-eastern sub-area near the archipelago of Franz Josef Land, initiating ice formation against the backdrop of residual ice. In August, the drift ice edge is similarly observed north of the northern boundary of the Sea, extending closer to the archipelagos of Svalbard and Franz Josef Land. It is worth noting that under average conditions, from August to October, the south-eastern part of the Barents Sea lacks sea ice cover (see Table 4.1), corresponding to the drift ice edge position (see Figure 4.5a). Hence, the seasonal minimum is observed here in July. In other months of the year, the drift ice edge remains within the boundaries of the Barents Sea. In its northern region, the period of seasonal maximum is observed in April, and in the south-eastern sub-area, in March, correlating with ice coverage, although not uniformly across fixed sections. A more

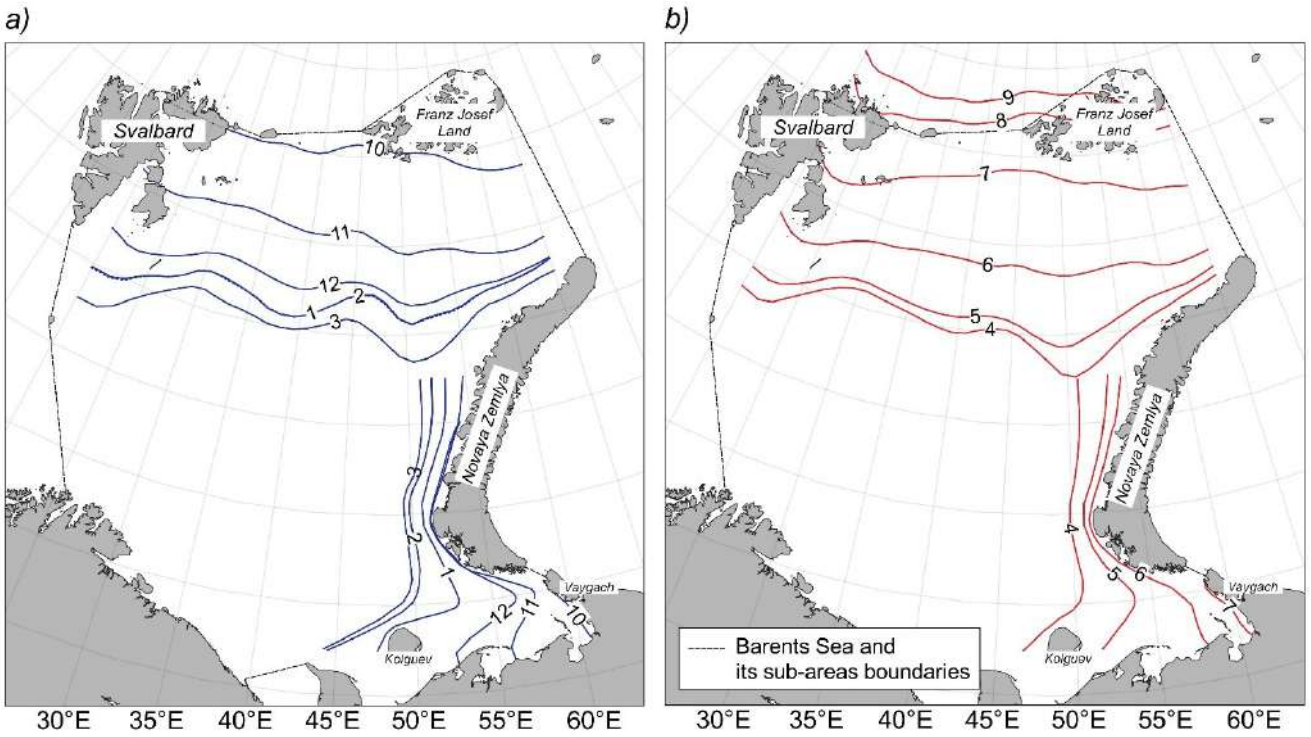


Figure 4.5. Seasonal variation of the drift ice edge position in the Barents Sea (expressed in ° longitude and ° latitude) on fixed parallels and meridians averaged for the ice seasons of 1982/1983–2021/2022 for months: *a)* October through March, *b)* April through September. Months are indicated by numbers along the curves.

detailed analysis of the spatial distribution of sea ice cover in the Barents Sea and its sub-areas will refine the main patterns of its state changes (see Table 4.8 for the northern region of the Barents Sea and Table 4.9 for the south-eastern sub-area).

The onset of the seasonal maximum ice edge position in the western region of the Barents Sea (on sections from 20° E to 42.5° E) is observed in March-April, while in the northeastern region (east of 45° E), it occurs only in April (see Figure 4.5b). On the meridians 25°–27.5° E and 32.5°–37.5° E, the ice edge position remains at its maximum for two months. The ice edge position in the southeastern region of the Barents Sea reaches its maximum value in the seasonal cycle in March (on sections 69°–72° N), while north of 73° N, i.e., already in the northeastern region, it occurs in April. In the northern regions of the sea, seasonal fluctuations in the standard deviation do not exhibit pronounced spatial regularities; their magnitude varies on average by ±1.9° latitude. The smallest values, up to ±1.6° latitude, are observed only on the westernmost meridians, from 60° E to 65° E. This holds true for the seasonal range as well: the average magnitude

is 5.2° latitude, with a maximum of over 5.9° latitude observed on meridians 20°–22.5° E and 47.5°–52.5° E, and a minimum of less than 4.0° latitude observed on the section at 65° E (see Table 4.8). Additionally, in the southeastern region of the Barents Sea, parallels with maximum standard deviation and seasonal range of the ice edge position are identified—these are the southern sections at 69° N and 70° N (see Table 4.9).

Table 4.8. Characteristics demonstrating seasonal changes of the drift ice edge in the western and north-eastern sub-areas of the Barents Sea averaged for the ice seasons of 1982/1983–2021/2022

| *Transect, ° E* | *Period of seasonal maximum* | *SD, ° latitude* | *Seasonal range, ° latitude* |
|---|---|---|---|
| 20.0 | March | ±2.2 | 6.1 |
| 22.5 | | ±2.1 | 5.9 |
| 25.0 | March-April | ±1.9 | 5.3 |
| 27.5 | | ±1.8 | 4.9 |
| 30.0 | April | ±1.7 | 4.6 |
| 32.5 | March-April | ±1.7 | 4.8 |
| 35.0 | | ±1.8 | 4.9 |
| 37.5 | | ±1.9 | 5.2 |
| 40.0 | April | ±2.0 | 5.3 |
| 42,5 | | ±2.0 | 5.2 |
| 45.0 | | ±2.0 | 5.4 |
| 47.5 | | ±2.1 | 5.9 |
| 50.0 | | ±2.2 | 6.5 |
| 52.5 | | ±2.2 | 6.1 |
| 55.0 | | ±2.0 | 5.6 |
| 57.5 | | ±1.7 | 5.0 |
| 60.0 | | ±1.6 | 4.5 |
| 62.5 | | ±1.5 | 4.1 |
| 65,0 | | ±1.4 | 3.9 |

Table 4.9. Characteristics demonstrating seasonal changes of the drift ice edge in the south-eastern and partially north-eastern sub-areas of the Barents Sea averaged for the ice seasons of 1982/1983–2021/2022

| *Transect, ° N* | *Period of seasonal maximum* | *SD, ° longitude* | *Seasonal range, ° longitude* |
|---|---|---|---|
| 69.0 | March | ±6.6 | 16.8 |
| 70.0 | | ±3.8 | 9.7 |
| 71.0 | | ±1.5 | 3.9 |
| 72.0 | | ±0.8 | 2.1 |
| 73.0 | April | ±1.0 | 2.7 |
| 74.0 | | ±1.4 | 3.7 |
| 75.0 | | ±1.9 | 5.1 |

*Note to Tables 4.8 and 4.9.* SD stands for the standard deviation. Seasonal range refers to the difference between the maximum and minimum values of the drift ice edge position coordinate in the seasonal cycle.

Based on the analysis of the drift ice edge position from 1934 to 1991, the northern region of the Barents Sea was divided into three homogeneous groups of meridians [Mironov, 2004]. For the first group (20°–30° E), located in the western sub-area, a seasonal maximum occurs in March-April, with a minimum in September, along with the smallest seasonal range. The second group, the central (35°–45° E), occupying an intermediate position, exhibits average range values. The third group (50°–60° E) in the north-eastern part of the Sea demonstrates a clearly defined seasonal maximum (minimum) in April (September), along with the largest seasonal range. According to [Mironov, 2004], in the south-eastern sub-area of the Barents Sea, the establishment of the seasonal maximum occurs in April. Additionally, the sea ice cover undergoes the greatest changes on the sections at 69° N and 70° N.

Comparing the classification of sea ice distribution in the Barents Sea over a 60-year observation period in the 20th century with the results of present study reveals: (1) *coincidence* for the northern region in the timing of seasonal peaks of the drift ice edge position (March-April in the western and April in the north-eastern sub-area); (2) an *earlier onset* of the seasonal maximum sea ice coverage in the south-eastern sub-area (March for the period 1982/1983–2021/2022 compared to April for the period 1934–1991); (3) a *smoothing* of the magnitude of the seasonal range of the drift ice edge position in the northern region of the Sea, despite the apparently greater influence of warm Atlantic waters on the sea ice distribution in the western sub-area, which, by hindering its southward expansion, determines significant seasonal changes in the western sections.

### 4.3. Ice age composition

#### 4.3.1. Seasonal variations

The average ratio of the relative ice amount in separate age gradations, delineated by the structure of the sea ice in the sub-areas of the Barents Sea during its growth period

from October to May, is presented in Table 4.10. Relative quantity refers to the *percentage of the area occupied by ice in a particular age gradation relative to the total area of the sea ice cover in a sub-area of the sea*. The proportion of landfast ice is included in the total ice area of the Barents Sea and is taken into account when calculating the ratios of ice of different age gradations. Throughout the winter period, landfast ice is most developed in the south-eastern sub-area: ice area gradually increases from 9% in October to 22% in May, with a sharp jump from April to May (from 13% to 22%, a 9% increase). Landast ice accounts for no more than 10% of the sea ice cover in the north-eastern part of the Barents Sea, and in the western part, landfast ice occupies no more than 2% of its total area throughout all winter months (see Table 4.10). Under average conditions, the following features of the ice age composition in the Barents Sea during the seasonal cycle are distinguished.

Table 4.10. Average ratio of areas of drift and landfast ice in the sea ice cover of sub-areas of the Barents Sea during winter months (expressed as a percentage of its total area) for the period from 1997/1998 to 2021/2022

| Ice cover / Month | X | XI | XII | I | II | III | IV | V |
|---|---|---|---|---|---|---|---|---|
| **Western sub-area of the Barents Sea** | | | | | | | | |
| Drift ice | >99 | | | | 99 | | | 98 |
| Landfast ice | <1 | | | | 1 | | | 2 |
| **North-eastern sub-area of the Barents Sea** | | | | | | | | |
| Drift ice | 96 | 93 | 92 | 91 | | | | 90 |
| Landfast ice | 4 | 7 | 8 | 9 | | | | 10 |
| **South-eastern sub-area of the Barents Sea** | | | | | | | | |
| Drift ice | 91 | 90 | 88 | | 89 | 88 | 87 | 78 |
| Landfast ice | 9 | 10 | 12 | | 11 | 12 | 13 | 22 |

*Initial and young ice*. In the Barents Sea, the ice formation process begins in October. At this time, the sea ice cover in its sub-areas mainly consists of initial and young ice: in the western and north-eastern parts, it accounts for 78%, while in the south-eastern part, it accounts for 91%. Then, the north-eastern and south-eastern sub-areas of the Sea experience the maximum seasonal development, while in the western sub-area, the highest amount of ice of the considered gradations is observed in November, constituting 81% of the total ice area. From October-November to May, their proportion in the total ice area

of the Barents Sea gradually decreases across its entire basin, without jumps, to 26%, 24%, and 23% in the western, north-eastern, and south-eastern sub-areas, respectively. Initial ice and young ice are observed in the sea ice cover of the Barents Sea throughout the entire winter period. Among ice with a thickness of up to 30 cm, the gradation of grey-white predominates (except for November in the south-eastern part of the sea). In October, their proportion in the total ice area is 28% and 31% for the western and north-eastern parts, respectively, and in November, with the intensification of the ice formation process, it sharply increases to 41% and 39%, respectively. Subsequently, the quantity of grey-white ice gradually decreases from November to May from 41% to 22% (western) and from 39% to 20% (north-eastern) of the total area of the sea ice cover. The proportion of initial ice and grey ice in the western sub-area of the Sea decreases from October to May, from 26% to 2% of the total area of ice for both age gradations, respectively. In the north-eastern sub-area of the Barents Sea, the relative quantity of initial ice decreases from October to May from 18% to 2%, and grey ice from 28% to 2%, respectively.

In the south-eastern sub-area of the Barents Sea, unlike other parts of it, the peaks of development of initial ice and grey ice, reaching 31% and 37% of the total sea ice area, respectively, occur in November, while in October they occupy 24% and 23% of the sea ice area, respectively. Subsequently, from October to May, their proportion in the total ice area gradually decreases to 3% (initial ice) and 2% (gray ice). It is noted that the proportion of grey-white ice in the sea ice cover of the south-eastern part of the Barents Sea changes abruptly throughout all winter months. Under average conditions, the highest relative quantity of grey-white ice is recorded in January-February, while the lowest is in November and May (45% and 18% of the total sea ice area, respectively). However, the quantity of ice in other age gradations with thicknesses up to 30 cm smoothens these jumps, and the total area of initial ice and young ice in the south-eastern sub-area of the Barents Sea also gradually decreases.

*First-year thin ice*. First-year thin ice is observed in the northern region of the Barents Sea as early as October, although its proportion (about 3%) of the total ice area is insignificant. A sharp increase in their relative quantity is characteristic for November, so

it is assumed that the formation of ice of this age gradation in the northern region of the Sea begins in November. However, the first-year thin ice observed in October was most likely carried in small quantities from the Arctic Basin and the Kara Sea through the Shilling and Makarov straits. In the south-eastern part of the Barents Sea, first-year thin ice is not observed in October under average conditions.

Since the formation of first-year thin ice on the Barents Sea has begun, its proportion of the total ice area in the western sub-area increases from 16% in November to 25% in March, reaching its maximum area of 28–29% in April-May. In the north-eastern part, the maximum (23% of the total area of the ice cover) relative quantity of first-year thin ice occurs in December-January, while in other winter months its proportion is 17–18%. In the south-eastern sub-area of the Barents Sea, the quantity of first-year thin ice increases gradually, ranging from 4% (November) to 25% (March) of its total area and reaching its highest values of 26–27% in April-May.

*First-year medium ice*. In December, part of the first-year thin ice in the western part of the Barents Sea transitions to the next age gradation of first-year medium ice; then its proportion of the total ice area does not exceed 2%. The quantity of first-year medium ice in the ice cover of the western sub-area then increases from 7% (January) to 26% (April), reaching a maximum in May (37% of its total area). In the north-eastern sub-area of the Sea, first-year medium ice is observed throughout the winter period, but in October-December its proportion does not exceed 3% of the total ice cover area. Presumably, part of the first-year medium ice was carried from neighboring basins (the Kara Sea and the Arctic Basin), while another part was formed directly in the research area. A noticeable jump in the relative amount of medium ice indicates that its formation in the north-eastern sub-area of the Barents Sea occurs in January. Starting from January, first-year medium ice is observed in the south-eastern sub-area, the quantity of which increases from 1% in January to a maximum of 28% in May relative to the total ice area.

*First-year thick ice*. On average, first-year thick ice is absent in the south-eastern part of the Barents Sea; however, it may occur here only in the harshest years [Mironov,

2004], none of which were observed during the entire 25-year period under study. In the northern region of the Sea, first-year thick ice is recorded in small quantities (less than 1%) in January-February (in the western region - in January-March). Both in the western and north-eastern sub-areas, their largest proportion of the total ice area is observed in May, comprising 6% and 14%, respectively. A jump of 7% in the relative quantity of first-year thick ice is characteristic for the north-eastern sub-area from April to May (from 7% to 14%).

*Old ice*. In October, at the beginning of ice formation in the Barents Sea, the quantity of old ice (mostly residual) in the ice cover of the northern region ranges from 15% to 19%. However, as ice of other age gradation appears during the winter months, the proportion of old ice begins to decrease, remaining within 1% to 4% (western) and 1% to 3% (north-eastern) of the total ice cover area. In the south-eastern sub-area, old ice is not encountered under average conditions. An exception was the case of 1998/1999 when residual ice was carried from the south-eastern part of the Kara Sea, against the background of which ice formation began in the autumn months in the Barents Sea. This phenomenon was influenced by a number of hydrometeorological conditions discussed by the authors [Tyuryakov et al., 2020].

It is noted that according to the results of this study and the assessments of [Mironov, 2004], the average periods of formation of first-year ice of different thickness (thin, medium, and thick) when transitioning from one age gradation to another coincide in most cases with an accuracy of up to a month. The months of formation of first-year thin and thick ice in the northern region of the Barents Sea are consistent. However, in the south-eastern part, according to the estimates obtained here, the onset of thin ice formation falls in November, while according to [Mironov, 2004], it falls in January, on average two months later.

### 4.3.2. Interannual variations

The author conducted an analysis of interannual changes in the ice age composition of sub-areas of the Barents Sea for April, the month of maximum ice cover development.

As a result, the following distribution of the relative quantity of ice of different age gradation in the Barents Sea was obtained, which is presented in Figure 4.6 (old ice is not represented in the figure).

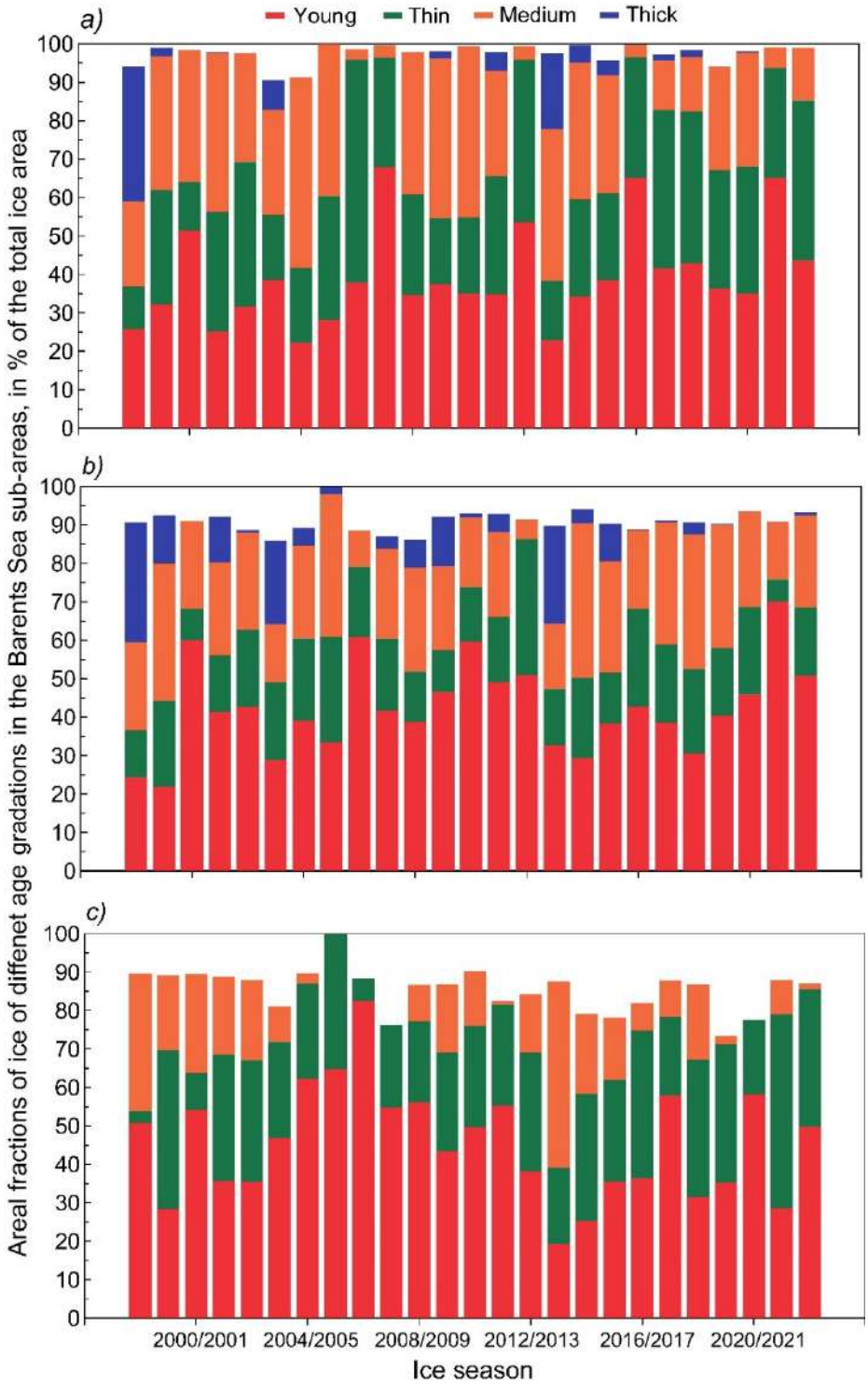


Figure 4.6. Interannual changes in the areas of young, as well as first-year thin, medium, and thick ice in the ice cover of: *a)* the western, *b)* north-eastern, *c)* south-eastern sub-areas of the Barents Sea in April (expressed as a percentage of its total area) on average for the period from 1998/1999 to 2021/2022

The areas of ice of all age gradations present in the Barents Sea ice cover are subject to significant interannual fluctuations (quantitative assessments are provided in [Egorova and Mironov, 2022a]). It is noted that with the relative increase in the proportion of young and first-year thin ice in the age structure, the area covered by first-year medium and thick ice decreases, and vice versa. After the minimum ice extent (area) in the Arctic in 2012 [Comiso et al., 2008; Ivanov et al., 2013], there was a significant reduction in the quantity of first-year thick ice in the ice cover of the northern region of the Barents Sea.

In recent years, the presence of old ice in the northern region of the Barents Sea has become a relatively rare phenomenon (see Figure 4.7). Over the studied period, at the time of maximum ice cover development in April, old ice was observed in the western sub-area in eight ice seasons (1997/1998, 2002/2003–2003/2004, 2008/2009, 2014/2015, 2016/2017, 2018/2019, and 2019/2020) — twice as often as in the north-eastern sub-area (1997/1998, 2001/2002, 2002/2003, and 2014/2015). The maximum values of old ice were recorded in the western and north-eastern sub-areas of the Barents Sea in 2002/2003, constituting 8% and 6% of their total ice cover area, respectively. In the ice seasons listed above, old ice on average occupies from 1% to 5% of the ice cover area of the Barents

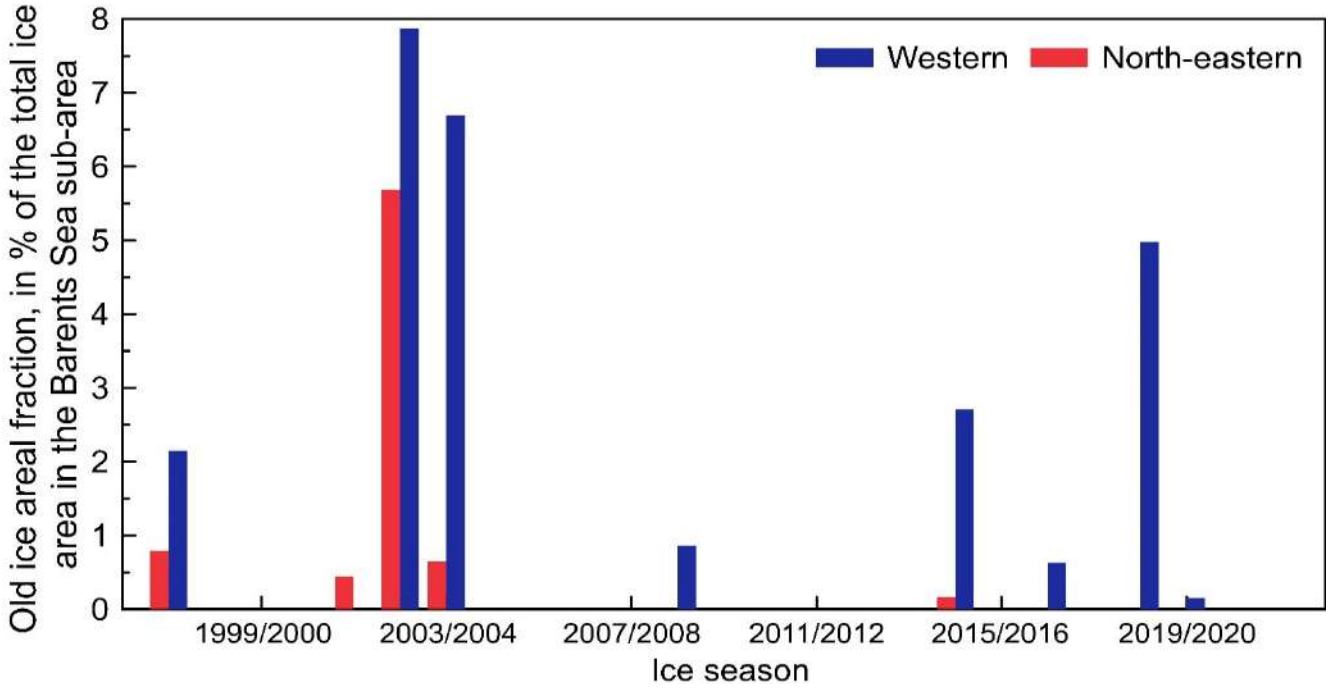


Figure 4.7. Interannual changes in the old ice area in the ice cover of the western and north-eastern sub-areas of the Barents Sea in April (expressed as a percentage of its total area) on average for the period from 1998/1999 to 2021/2022

Sea sub-areas. Interannual fluctuations in the amount of old ice are determined by the following SD: ±2% (western part) and ±1% (north-eastern part).

Among the first-year ice in the Barents Sea in April, the prevailing gradation is first-year medium ice, with an average thickness ranging from 70 cm to 120 cm. An assessment of their frequency of occurrence was conducted for sub-areas (see Figure 4.8). In the western part, first-year medium ice occupies an area of 25–30% and 35–40% of the total ice cover in 20% and 16% of cases, respectively. For the north-eastern sub-area, in the predominant 40% of cases, the relative amount of first-year medium ice ranges from 20% to 25%. In the south-eastern part of the sea, first-year medium ice occurs with equal frequency in 20% of cases, comprising 5–10% and 15–20% of the total ice area.

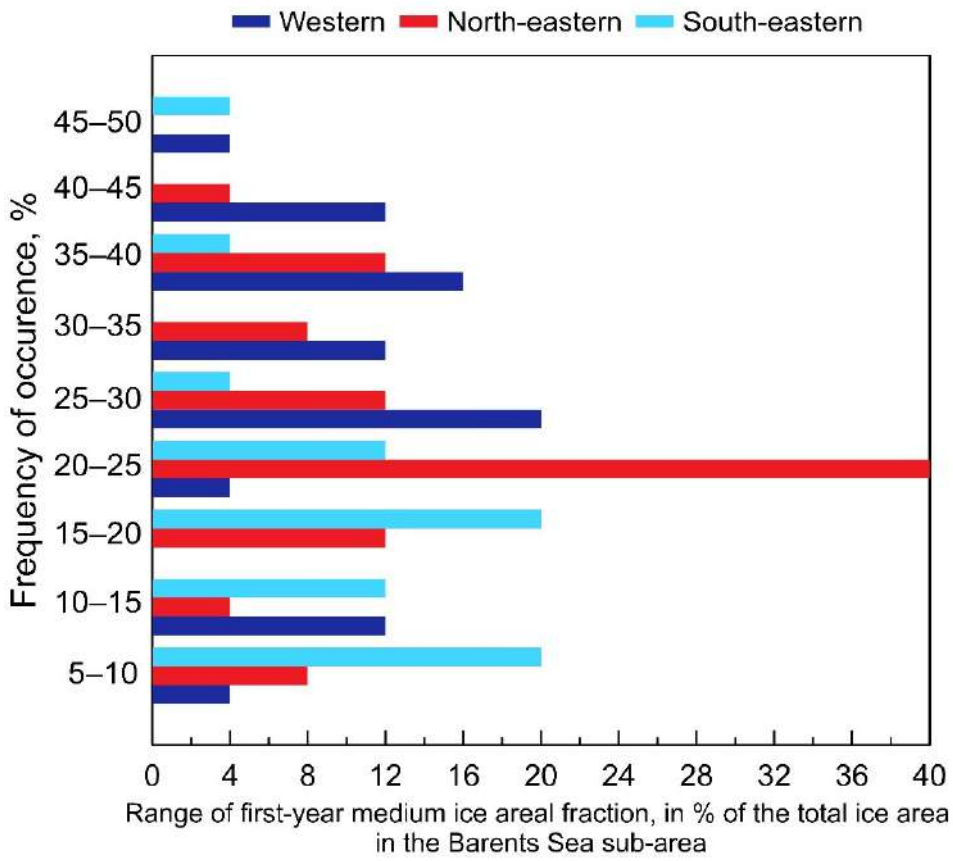


Figure 4.8. Frequency of occurrence of the first-year medium ice area (expressed as a percentage of the total ice cover area) in the sub-areas of the Barents Sea in April, averaged over the period from 1998/1999 to 2021/2022

Further, linear and nonlinear trends (the latter expressed by second-degree polynomials) in the area of ice of different age gradations within the ice age structure of

the Barents Sea sub-areas in April were assessed for statistical significance. The main criterion for evaluating the significance of trends was the Student's t-test (at a significance level of 99%) [Malinin, 2020a]. As a result, trends identified over the entire observation period (both linear and nonlinear) were found to be statistically insignificant. This indicates that amid the observed reduction in the total area of the Barents Sea ice cover, the area of ice of various age gradations in its sub-areas fluctuates within the bounds of natural seasonal variations.

However, conclusions about interannual changes in the ice age structure of the Barents Sea by age gradations can be drawn by comparing the results of the present study with earlier assessments for separate sub-areas. Table 4.11 presents estimates of the relative quantity of ice of various age gradations in the Barents Sea obtained for the periods 1971–1976 (from [Mironov, 2004]) and 1997–2022 (this study).

In April, the ice cover of the Barents Sea is predominantly composed of locally formed first-year ice, as confirmed by the results of present study. However, estimates of their relative quantity vary significantly. According to the estimates of [Mironov, 2004] and the present study, in the south-eastern part of the Barents Sea, the proportion of first-year ice to its total area is 80% and 42%, respectively; in the north-eastern sub-area, it is 86% and 50%, and in the western sub-area, it is 64% and 60%. In the 1970s [Mironov, 2004], the quantity of young ice is considerably less than the estimates: in the south-eastern part, it occupies 20% and 45% of the total ice area, respectively; in the north-eastern part, it is 13% and 41%, and in the western part, it is 12% and 38%.

Thus, the average thickness of the Barents Sea ice cover in the early 21st century compared to the mid-1970s, based on data on its age composition, has decreased. There is a significant reduction in the quantity of first-year thick ice and, conversely, an increase in the proportion of first-year thin and medium ice in the Barents Sea ice cover. Additionally, the area of young ice has increased. Considering the identified statistical insignificance of linear trends in the interannual fluctuations of the area of ice of different age gradations in the Barents Sea, it should be considered that quantitative changes in the age structure of sea ice began before the ice season of 1997/1998.

Table 4.11. Estimates of the relative amount of ice of different age gradations in the ice age structure of the Barents Sea sub-areas (expressed as a percentage of its total area) in April

| *Age gradation* / Barents Sea sub-area | **«1»** | **«2»** | **«1»** | **«2»** | **«1»** | **«2»** |
|---|---|---|---|---|---|---|
| | Western | | North-eastern | | South-eastern | |
| *Initial types and young* | 12 | 38 | 13 | 41 | 20 | 45 |
| *First-year thin* | 0 | 29 | 0 | 18 | 64 | 26 |
| *First-year medium* | 10 | 26 | 17 | 24 | 16 | 15 |
| *First-year thick* | 54 | 4 | 69 | 7 | 0 | 0 |
| *Old* | 24 | 1 | 1 | 1 | 0 | 0 |

*Note.* Numbers "1" and "2" denote estimates from [Mironov, 2004] and estimates in present study, respectively.

The difference in the ratio of old ice in the western part ice cover is of interest (24% according to [Mironov, 2004] and only 1% according to the estimates of present study; see Table 4.10). Most likely, the work of [Mironov, 2004] presents inflated values of the area of ice of the analyzed age gradation, which were caused by increased ice export from the Arctic Basin during the period 1971–1976. However, this issue requires further detailed consideration and is beyond the scope of this study.

The main results of the study of the age composition of the ice cover in sub-areas of the Barents Sea are published in [Egorova and Mironov, 2022a; Egorova and Mironov, 2022b].

### 4.4. Boundaries of old ice and first-year ice prevalence

The spatial distribution of the ice cover of different age gradations in the Barents Sea area throughout the winter season can be visually represented by the mean position of their boundary predominance. In this subsection, particular attention was paid by the author to the gradations of first-year and old ice.

#### 4.4.1. Seasonal variations

*Old ice.* Seasonal changes in the boundary of old ice predominance in the Barents Sea area under average conditions are provided in Table 4.12. Since the spatial characteristics of ice distribution are best demonstrated on charts, the mean position of the boundary of

old ice prevalence in typical winter months, November, February, and April, was depicted in Figure 4.9. The selected months correspond to periods of active and stable ice formation in the Barents Sea, as well as maximum ice cover development, respectively.

Table 4.12. Position of the boundary of old ice predominant in the Arctic Basin (expressed in ° latitude) on fixed meridians averaged over ice seasons from 1997/1998 to 2021/2022

| Longitude, ° E / Month | *Latitude, ° N* | | | | | | | |
|---|---|---|---|---|---|---|---|---|
| | X | XI | XII | I | II | III | IV | V |
| 20.0 | **81.9** | **81.9** | **81.9** | 82.4 | 82.7 | 82.5 | 82.5 | 82.3 |
| 22.5 | **81.8** | 81.9 | 81.9 | 82.5 | 82.8 | 82.6 | 82.5 | 82.3 |
| 25.0 | **81.7** | 81.9 | 81.9 | 82.4 | 82.9 | 82.6 | 82.5 | 82.3 |
| 27.5 | **81.6** | 81.9 | 81.9 | 82.4 | 83.0 | 82.8 | 82.4 | 82.3 |
| 30.0 | **81.7** | 81.9 | 82.0 | 82.5 | 83.0 | 82.9 | 82.6 | 82.5 |
| 32.5 | **81.7** | 82.0 | 82.0 | 82.7 | 83.3 | 83.1 | 82.7 | 82.9 |
| 35.0 | **81.9** | 82.0 | 82.0 | 82.8 | 83.4 | 83.3 | 83.0 | 83.1 |
| 37.5 | **82.0** | 82.1 | 82.1 | 83.0 | 83.5 | 83.6 | 83.4 | 83.3 |
| 40.0 | **82.0** | 82.1 | 82.3 | 83.2 | 83.7 | 83.8 | 83.6 | 83.4 |
| 42.5 | **82.2** | 82.3 | 82.5 | 83.2 | 83.8 | 84.0 | 83.7 | 83.5 |
| 45.0 | **82.4** | **82.4** | 82.6 | 83.3 | 83.9 | 84.1 | 83.8 | 83.6 |
| 47.5 | **82.4** | 82.5 | 82.7 | 83.4 | 84.0 | 84.4 | 83.9 | 83.8 |
| 50.0 | **82.5** | **82.5** | 82.8 | 83.5 | 84.1 | 84.4 | 84.0 | 84.0 |
| 52.5 | 82.5 | **82.4** | 82.8 | 83.7 | 84.1 | 84.4 | 84.1 | 84.1 |
| 55.0 | **82.4** | **82.4** | 82.8 | 83.7 | 84.2 | 84.5 | 84.2 | 84.3 |
| 57.5 | **82.4** | **82.4** | 82.8 | 83.7 | 84.3 | 84.5 | 84.3 | 84.5 |
| 60.0 | **82.1** | 82.4 | 82.9 | 83.7 | 84.3 | 84.6 | 84.4 | 84.5 |
| 62.5 | **81.9** | 82.3 | 82.8 | 83.6 | 84.4 | 84.5 | 84.4 | 84.7 |
| 65.0 | **81.8** | 82.2 | 82.8 | 83.6 | 84.3 | 84.5 | 84.5 | 84.7 |

*Note*. Bold font (underlining) highlights fixed meridians where the maximum (minimum) dominance of old ice occurs during the average ice season.

During the winter months, the boundary of old ice predominance is observed beyond the Barents Sea, in the part of the Arctic Basin adjacent to its northern boundary. As the ice cover expands in the western and north-eastern sub-areas of the Barents Sea, the position of the old ice massif shifts northward from the northern boundary of the Barents Sea. The zone of old ice prevalence in the winter months is located south of 85° N. In October-November, its boundary is approximately at 82° N, corresponding to the maximum position of old ice in the seasonal cycle. Only on one meridian, 52.5° E, which represents 5% of the area, does the maximum occur in November; on other meridians, the peak is in

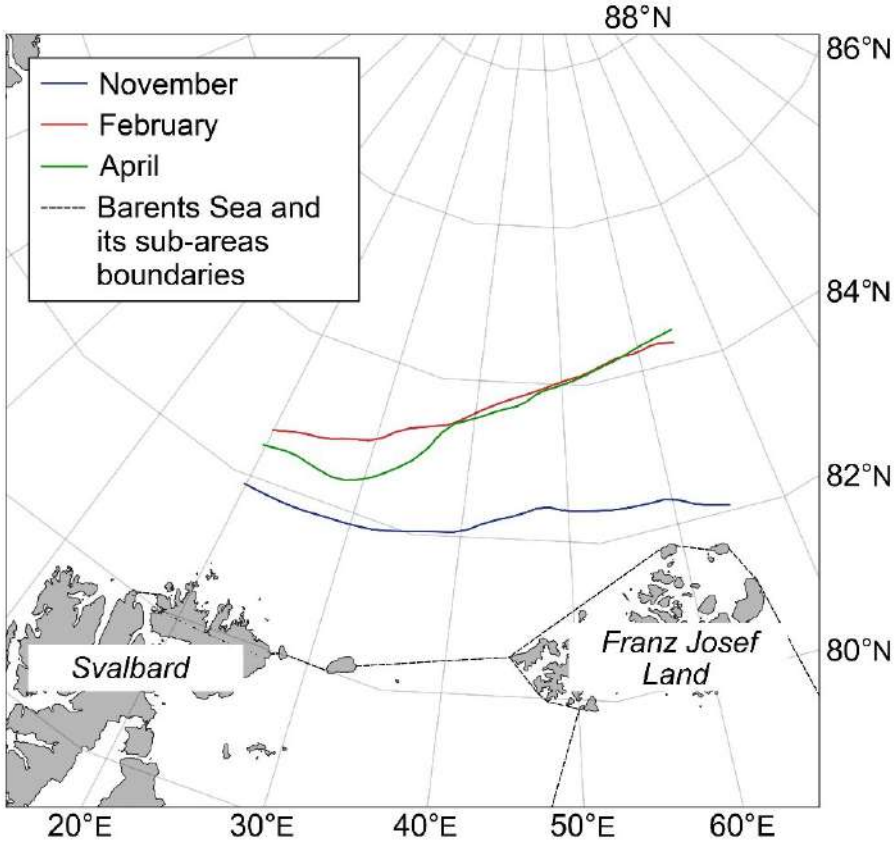


Figure 4.9. Mean position of the boundary of old ice predominance in the part of the Arctic Basin adjacent to the Barents Sea area (expressed in ° latitude) in November, February, and April averaged from 1997/1998 to 2021/2022

October. By February, the boundary of old ice predominance rises north of 82.5° N on fixed meridians 20°–30° E, north of 83.0°N on 32.5°–40° E, and north of 84.0° N on 42.5°–65° E. The distribution of the period when the seasonal minimum boundary predominance is established varies considerably: in the western sub-area of the considered Arctic Basin area, on 20°–35° E, the old ice prevalence zone shifts to its minimum in February (representing 37% of the meridians); in its main part, located between 37.5° E and 60° E, the boundary reaches its seasonal minimum by March (i.e., in 53% of cases); only on meridians 62.5° E and 65° E, i.e., on the easternmost meridians, the minimum distribution of the boundary of old ice predominance is observed in May (in 10% of cases).

It is noted that the boundary of old ice predominance undergoes the least seasonal fluctuations on meridians from 20° E to 35° E, where minimal seasonal range (from 0.8° to 1.5° of latitude) and SD (up to ±0.6° of latitude) are observed. The greatest changes in this spatial characteristic, on the contrary, are typical for eastern meridians, 60°–65° E:

here, the seasonal range is 2.5°–2.9° of latitude, and the SD ranges from ±1.0° to ±1.2° of latitude. The central part of the Sea area shows average seasonal range (1.5°–2.1° of latitude) and SD (from ±0.6° to ±0.9° of latitude). Thus, the obtained results allow for the division of the considered part of the Arctic Basin adjacent to the Barents Sea into three homogeneous regions. In the *western* region (20°–35° E), the seasonal minimum prevalence boundary of old ice occurs in February, with the smallest seasonal changes in its position. In the *eastern* region (from 62.5° E to 65° E), the largest fluctuations in the position of the predominant boundary of old ice are observed, which reaches its minimum only in May. In the *central* region (from 37.5° E to 60° E), the maximum of the characteristic occurs in March, and the position of the old ice massif changes within its average values (judging by the seasonal range and SD).

*First-year ice*. Seasonal changes in the boundary of first-year ice predominance in the Barents Sea under average conditions are presented in Tables 4.13 and 4.14. Figure 4.10 shows the mean position of their prevalence boundaries for November, February, and April. During the winter period, the boundary of first-year ice predominance naturally expands as the ice cover area in the Barents Sea grows gradually. On all meridians, the minimum boundary of first-year ice predominance occurs in October: in the western and north-eastern sub-areas, it is located north of 89° N, i.e., beyond the Barents Sea, while in the south-eastern part, ice of this age gradation is not yet represented at all. However, by November, the position of the boundary of first-year ice predominance significantly shifts southward, reaching the northern boundary of the sea on meridians from 55° E in its northern region; in the south-eastern sub-area, first-year ice passes along a narrow strip along Vaigach Island and the coast of the Yugorsky Peninsula. From April to May, there is a maximum boundary of first-year ice prevalence in the western and north-eastern parts of the Sea: in 63% of cases, it falls on May (meridians 20°–25° E, 32.5° E, and 47.5°–65° E), and in the remaining 37% of cases, it occurs in April (on 27.5°E, 30°E, and 35°–45° E). The maximum area of first-year ice in the age ice structure of the Barents Sea is reached in May, which is consistent with the results of the analysis of changes in their boundary predominance on most calculated meridians.

Table 4.13. Position of the boundary of first-year ice predominance in the northern region of the Barents Sea (expressed in ° latitude) on fixed meridians averaged over ice seasons from 1997/1998 to 2021/2022

| Longitude, ° E / Month | *Latitude, ° N* | | | | | | | |
|---|---|---|---|---|---|---|---|---|
| | X | XI | XII | I | II | III | IV | V |
| 20.0 | 89.4 | 85.3 | 82.8 | 81.2 | 80.0 | 78.8 | 77.7 | **77.5** |
| 22.5 | 89.2 | 84.9 | 81.9 | 80.4 | 79.6 | 78.2 | 77.1 | **76.8** |
| 25.0 | 89.1 | 83.8 | 80.8 | 79.8 | 78.9 | 77.8 | 76.7 | **76.6** |
| 27.5 | 89.1 | 83.2 | 80.3 | 79.6 | 78.9 | 77.7 | **76.9** | 77.0 |
| 30.0 | 89.1 | 83.1 | 80.2 | 79.5 | 78.9 | 77.8 | **77.1** | **77.1** |
| 32.5 | 89.1 | 82.7 | 80.0 | 79.6 | 78.8 | 77.8 | 77.1 | **76.9** |
| 35.0 | 89.0 | 82.4 | 80.0 | 79.6 | 78.8 | 77.7 | **76.9** | **76.9** |
| 37.5 | 89.0 | 82.3 | 80.0 | 79.4 | 78.6 | 77.6 | **76.8** | **76.8** |
| 40.0 | 89.0 | 82.2 | 80.0 | 79.2 | 78.5 | 77.6 | **76.7** | 76.8 |
| 42.5 | 88.9 | 82.3 | 80.0 | 79.2 | 78.5 | 77.6 | **76.8** | 76.9 |
| 45.0 | 89.0 | 82.3 | 80.1 | 79.2 | 78.4 | 77.7 | **76.8** | 77.0 |
| 47.5 | 88.8 | 82.2 | 80.1 | 79.0 | 78.1 | 77.3 | 76.5 | **76.4** |
| 50.0 | 88.9 | 81.8 | 80.0 | 78.8 | 77.9 | 77.4 | 76.7 | **76.4** |
| 52.5 | 88.8 | 81.8 | 79.8 | 78.7 | 78.1 | 77.6 | 77.0 | **76.8** |
| 55.0 | 88.7 | 81.4 | 79.6 | 78.7 | 78.3 | 77.8 | 77.2 | **77.1** |
| 57.5 | 88.7 | 81.2 | 79.5 | 78.7 | 78.4 | 78.0 | 77.3 | **77.2** |
| 60.0 | 88.7 | 81.1 | 79.4 | 78.7 | 78.4 | 78.0 | 77.4 | **77.2** |
| 62.5 | 88.7 | 80.8 | 79.3 | 78.7 | 78.4 | 78.1 | 77.5 | **77.3** |
| 65.0 | 88.8 | 81.1 | 79.3 | 78.7 | 78.4 | 78.1 | 77.6 | **77.4** |

Table 4.14. Position of the boundary of first-year ice predominance in the north-eastern and south-eastern sub-areas of the Barents Sea (expressed in ° longitude) on fixed meridians averaged over ice seasons from 1997/1998 to 2021/2022

| Latitude, ° N / Month | *Longitude, ° E* | | | | | | | |
|---|---|---|---|---|---|---|---|---|
| | X | XI | XII | I | II | III | IV | V |
| 69.0 | 61.0 | 60.7 | 59.8 | 56.6 | 53.1 | 51.0 | 50.2 | **52.3** |
| 70.0 | 58.7 | 58.4 | 58.3 | 56.1 | 53.8 | **52.4** | **52.4** | 53.6 |
| 71.0 | 53.6 | 53.5 | 53.5 | 53.1 | 52.2 | 51.7 | **51.3** | 51.8 |
| 72.0 | 51.5 | 51.5 | 51.5 | 51.3 | 50.9 | **50.7** | **50.7** | 50.9 |
| 73.0 | 53.1 | 53.1 | 53.1 | 52.9 | 52.5 | 52.2 | **52.1** | 52.3 |
| 74.0 | 54.6 | 54.6 | 54.6 | 54.4 | 53.9 | 53.1 | **52.8** | 53.1 |
| 75.0 | 55.9 | 55.9 | 55.9 | 55.6 | 54.6 | 53.5 | 53.3 | **53.2** |

*Note for Tables 4.13 and 4.14*. Bold font (underlining) highlights fixed meridians where the maximum (minimum) predominance of first-year ice occurs during the average ice season.

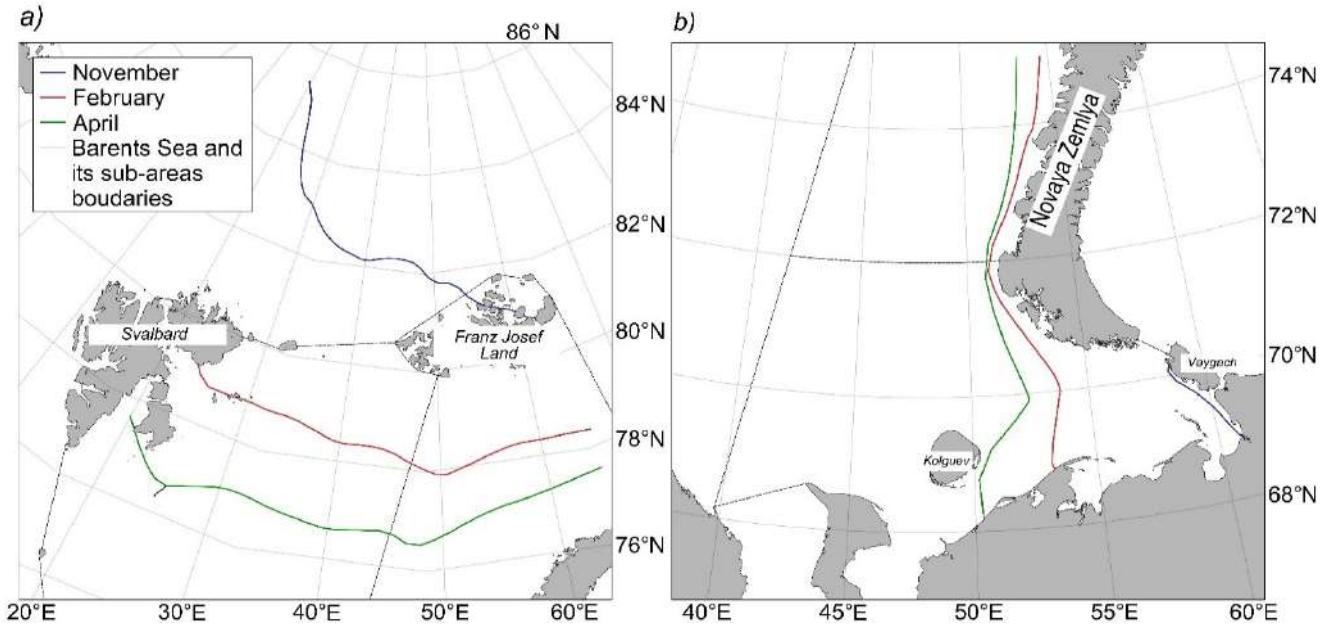


Figure 4.10. Mean position of the boundary of first-year ice predominance in November, February, and April (expressed in ° longitude or ° latitude): *a)* in the western and north-eastern sub-areas of the Barents Sea, as well as in the adjacent part of the Arctic Basin; *b)* in the south-eastern sub-area of the Barents Sea averaged over ice seasons from 1997/1998 to 2021/2022

On all fixed meridians for the western and north-eastern sub-areas of the Barents Sea, the values of seasonal range vary from 11.4° to 12.5° of latitude, with SD ranging from ±3.7° to ±4.3° of latitude, indicating a relative homogeneity in the changes in the position of the boundary of first-year ice prevalence during the winter months (see Table 4.13). In the south-eastern part (see Table 4.14), the maximum seasonal changes are characteristic of the meridians at 69° N and 70° N, where the seasonal range reaches 10.8° and 6.3° of longitude, with SD around ±4.5° and ±2.7° of longitude, respectively. These variations are also noted in the seasonal cycle fluctuations of the drift ice edge. On other meridians, the seasonal range averages 1.7° of latitude, varying from 0.8° of latitude (at 72° N) to 2.7° of latitude (at 75° N); the average SD of ±0.7° of latitude ranges from ±0.4° of latitude (72°–73° N) to ±1.2° of latitude (75° N).

### 4.4.2. Interannual variations

*Old ice*. Figure 4.11 presents the distribution of the maximum, minimum, and average positions of the boundary of old ice predominance in the Barents Sea for separate

winter months (specifically, this considers the part of the Arctic Basin adjacent to the northern boundary of the Barents Sea area). Only during the *maximum* distribution does the boundary of old ice prevalence lie within the Barents Sea, ranging between parallels 78°–80° N in November, and between 76°–79° N in February and April. In November, old ice is evenly concentrated in both the western and north-eastern sub-areas of the Sea, showing a spatial distribution in the form of a wave. In February and April, on the contrary,

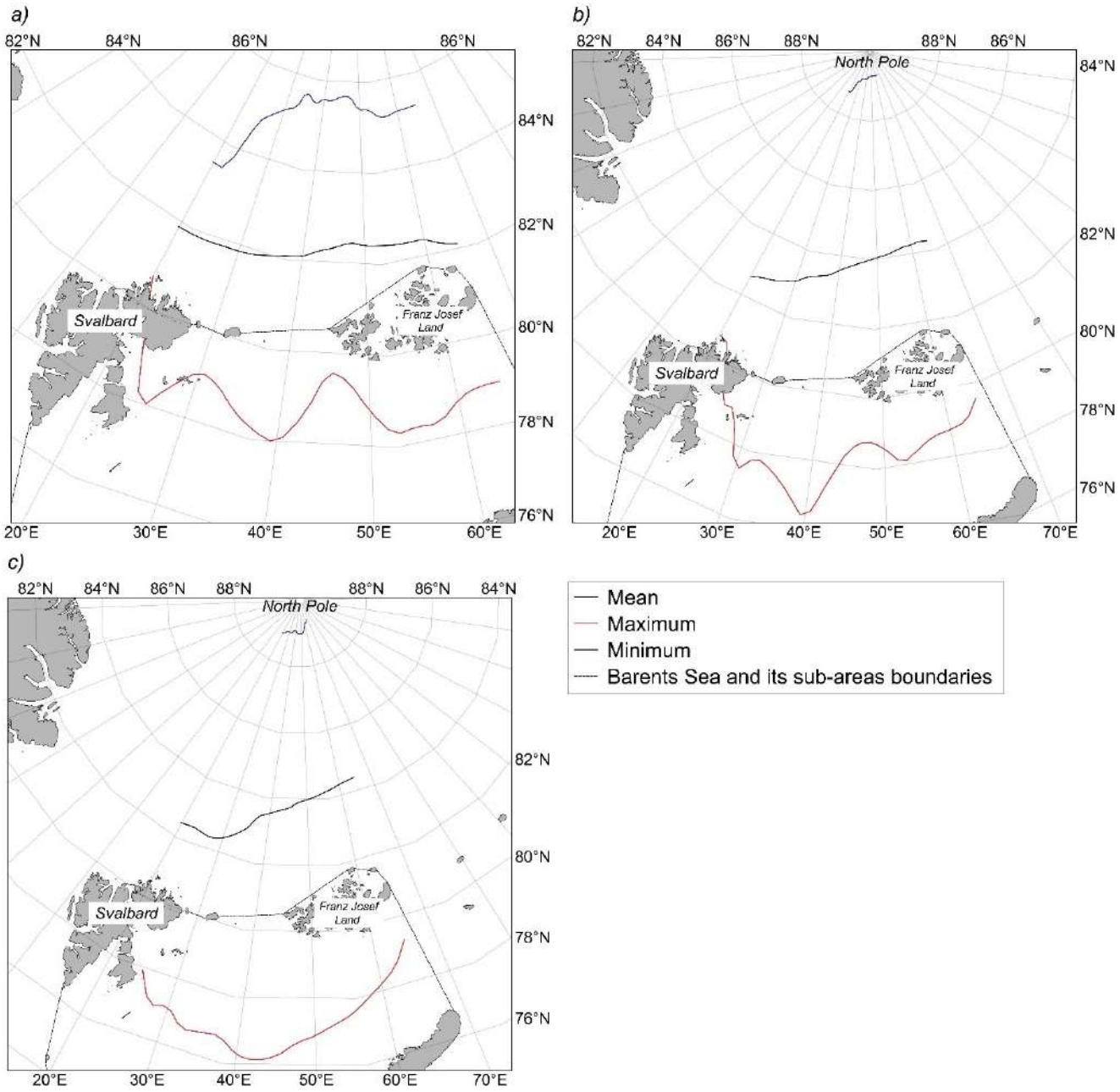


Figure 4.11. Spatial distribution of the maximum, minimum, and average positions of the boundary of old ice predominance in the Barents Sea and the adjacent part of the Arctic Basin (expressed in ° latitude): *a)* in November, *b)* in February, *c)* in April, averaged over the ice seasons 1997/1998–2021/2022

the ice of this age gradation is more concentrated in the western part than in the north-eastern part. For February, the average position of the boundary of old ice predominance is at 78° N, descending to 76° N closer to the eastern boundary of the western part of the Barents Sea (at 40° E); in the north-eastern sub-area, the boundary is located north of 78° N. The dominance boundary of old ice in April, averaging at 77° N, extends from 40°–45° E to 76° N in the western sub-area of the Sea, and then rises to 78° N and further north at the eastern boundary of the Barents Sea area. During the ice seasons of 1997/1998, 2002/2003, and 2003/2004, the old ice mass occupied the maximum area of the Barents Sea compared to the other analyzed years —this is characteristic for all the considered winter months.

For the *average* and *minimum* distributions, the boundaries of old ice predominance are observed outside the Barents Sea area. Under average conditions, they are concentrated in the part of the Arctic Basin adjacent to the Barents Sea, along 82° N (in November) and between 84° N and 82° N (in February and April). At its minimum position in November, old ice is mainly found between 86° N and 84° N, not reaching the 84 parallel only between 20°–22.5° E, in the western part of the studied area. Among the analyzed ice seasons, the smallest or nearly smallest distribution of the old ice position in November was observed during the 2009/2010 and 2013/2014 ice seasons. In February and April, the boundary of old ice prevalence is almost at 89° N, close to the geographic North Pole. Only one ice season from the study period, specifically 2012/2013, was characterized by the minimum position of the boundary for this ice age category predominance.

*First-year ice.* The spatial distribution of the average, maximum, and minimum positions of the boundary of first-year ice prevalence in the Barents Sea is shown in Figure 4.12. At the *maximum* position of first-year ice, the predominance boundary in November is fixed between 76° N and 78° N, evenly distributed across the entire sea area. The only exceptions are the westernmost transects between 20° E and 22.5° E, where the boundary predominance is marked along the eastern coast of the Svalbard archipelago; it appears that young ice predominates between the islands. In February and April, first-year ice covers about 80% of the Barents Sea, with the ice coverage in the north-eastern and south-

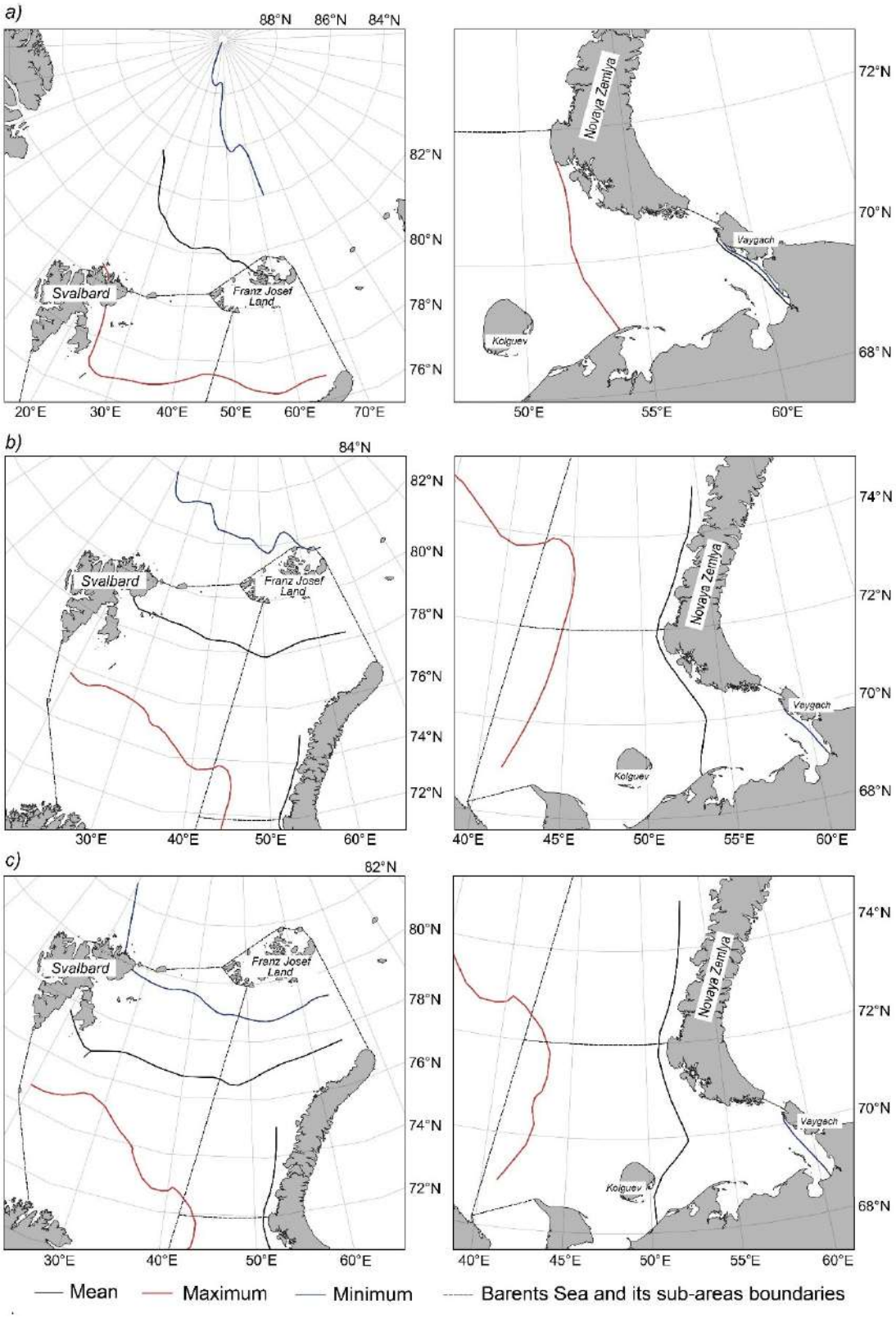


Figure 4.12. Spatial distribution of the maximum, minimum, and average positions of the boundary of first-year ice predominance in the western and north-eastern sub-areas (left), as well as in the south-eastern sub-area (right) of the Barents Sea (expressed in ° longitude and latitude): *a)* in November, *b)* in February, *c)* in April, averaged over the ice seasons from 1997/1998 to 2021/2022

eastern sub-areas approaching 90–100%. During this period, in the western part of the Barents Sea, the boundary of first-year ice predominance runs along 75° N, descending to 74° N in February and further to 73° N in April near the boundary with the north-eastern part of the sea. Such severe ice conditions were typical for the ice seasons of 1997/1998 and 1998/1999. It is noted that in recent years, the boundary of first-year ice predominance (the drift ice edge) in February and April has not extended as far south. South of the boundary of first-year ice prevalence, under any development scenario (maximum, minimum, or average) in all the considered months, young ice, as well as initial types and nilas ice, can be observed.

At the *minimum* extent, the boundary of first-year ice predominance in November and February is located beyond the northern boundary of the Barents Sea. In November, this boundary sees first-year ice aligning along the meridian 60° E, reaching the geographic North Pole at the transect 20° E, and reaching the meridian 84° N at 65° E. In February, the dominance boundary drops to 83° N, with transects between 20° E and 30° E located closer to 83°–84° N, and on the eastern meridians, it descends closer to the Franz Josef Land archipelago.

In April, the dominance boundary of first-year ice is observed within the Barents Sea, between 79° N and 80° N, though on the western transects, the boundary extends northwards up to 83° N. It is noted that in the western part of the Barents Sea, first-year ice concentrates closer to the northern boundary, while in the north-eastern part, it is somewhat southward at 79° N. In the southeastern part of the sea, the dominance boundary of first-year ice is observed between the transects of 69° N and 70° N, forming a narrow strip near Vaygach Island and the Yugorsky Shar Strait, without reaching the Kara Gates Strait. This spatial distribution of the boundary of first-year ice predominance is typical for all the considered months of the year. The most indicative ice seasons, characterized by the minimum position of the first-year ice boundary predominance, are the ice seasons of 2008/2009 and 2021/2022 (in November), 2011/2012 and 2020/2021 (in February), and 2015/2016 and 2020/2021 (in April).

### 4.5. Drivers of interannual variations of sea ice age composition in homogeneous sub-areas of Barents Sea

To reproduce the interannual changes in the ice age composition in the sub-areas of the Barents Sea and determine the main factors shaping them, the author developed a set of statistical equations. The selection of potentially significant predictors during the preparation of the electronic data archive was based on physically interconnected and stable processes within the "ocean-ice-atmosphere" system. Previously, similar studies were conducted only for the ice coverage of the Barents Sea, the most studied element of the ice regime, with a detailed review prepared by authors [Lis et al., 2023]. Therefore, the initial focus of the work was on the results related to ice coverage. As a result, the *following* set of hydrometeorological and ice characteristics was formed, constituting the base of possible predictors (for description, see Chapter 2):

(1) Climate indices AO, AD, and NAO;
(2) Water temperature at the standard oceanographic section "Kola Meridian" (in °C) — a factor necessary to account for the influence of warm Atlantic waters entering the Barents Sea;
(3) (3) Surface air temperature (in °C) in sib-areas of the Barents Sea and all the Barents Sea;
(4) Ice coverage (in %) in sub-areas of the Barents Sea and its previous values, as well as previous values of the ice area of various age gradations, which indicate the inertia of ice processes;
(5) Ice area export between the Barents Sea and surrounding waters (in thousand km² per month), calculated using a method similar to that for the Fram Strait, utilizing NSIDC drift data for the Shilling, Makarov, and Kara Gates straits.

It should be noted that in the formulation of statistical equations, the initial types of ice and nilas ice, as well as grey and grey-white ice, were combined into a general age gradation of young ice, forming an ice cover up to 30 cm thick. Moreover, the age gradation of old ice is not presented here. This is due to the fact that since the beginning of the 21st century, old ice in the northern region of the Barents Sea has become significantly rarer,

even in small quantities, meaning that its area is almost always zero (see Figure 4.7 and its description). First-year thick ice under average conditions is not found in the south-eastern sub-area of the Barents Sea, so this ice age category is also not considered in this work.

Exploring various combinations of statistically significant factors allowed for the formulation of the following equations, which shape the interannual changes in the age structure of the ice cover in the Barents Sea (see Table 4.15). To demonstrate the results of the multiple regression analysis, the statistical equations for April, the month of maximum sea ice development in the Barents Sea, with the highest correlation and determination coefficients, are provided.

Table 4.15. Statistical equations describing interannual changes in the area of ice of different age gradations (in thousand km²) in the sub-areas of the Barents Sea in April

| | |
|---|---|
| **Western sub-area of the Barents Sea** | |
| **(4.1)** | $\text{Пл(Мол)}_{3_{IV}} = -61{,}11 \cdot \text{ПТВ}_{3_{III}} - 59{,}94 \cdot \text{КМ}_{II-III}^{1-3} + 33{,}35 \cdot AO_{VI(-1)} - 2{,}86 \cdot \text{Обм}_{\text{Шил}_{VII(-1)}} + 290{,}95$ |
| **(4.2)** | $\text{Пл(Тонк)}_{3_{IV}} = 0{,}56 \cdot \text{Пл(Тонк)}_{3_{III}} + 9{,}32 \cdot NAO_{IV(-1)} - 7{,}25 \cdot AD_{XII(-1)} + 28{,}97$ |
| **(4.3)** | $\text{Пл(Ср)}_{3_{IV}} = -49{,}01 \cdot \text{КМ}_{XI-I}^{1-3} + 20{,}97 \cdot NAO_{V(-1)} - 27{,}06 \cdot AO_{IV(-1)} + 353{,}79$ |
| **(4.4)** | $\text{Пл(Тол)}_{3_{IV}} = -37{,}87 \cdot \text{КМ}_{II-III}^{3-7} - 10{,}52 \cdot NAO_{VI(-1)} + 36{,}59 \cdot AD_{VIII(-1)} + 156{,}27$ |
| **North-eastern sub-area of the Barents Sea** | |
| **(4.5)** | $\text{Пл(Мол)}_{\text{СВ}_{IV}} = -2{,}87 \cdot \text{Обм}_{\text{Шил}_{VIII(-1)}} - 22{,}77 \cdot NAO_{IV(-1)} + 8{,}82 \cdot AD_{II} + 107{,}64$ |
| **(4.6)** | $\text{Пл(Тонк)}_{\text{СВ}_{IV}} = -11{,}48 \cdot \text{ПТВ}_{\text{Бар}_{XI(-1)}} + 1{,}37 \cdot \text{Обм}_{\text{Мак}_{X(-1)}} + 9{,}53 \cdot NAO_{IV(-1)} + 56{,}12$ |
| **(4.7)** | $\text{Пл(Ср)}_{\text{СВ}_{IV}} = -1{,}65 \cdot \text{Обм}_{\text{Шил}_{X(-1)}} + 0{,}25 \cdot \text{Обм}_{\text{Мак}_{I(-1)}} - 26{,}16 \cdot AO_{IV(-1)} - 10{,}54 \cdot AD_{X(-1)} + 56{,}23$ |
| **(4.8)** | $\text{Пл(Тол)}_{\text{СВ}_{IV}} = 0{,}79 \cdot \text{Обм}_{\text{Мак}_{XI(-1)}} - 18{,}68 \cdot NAO_{XI(-1)} + 9{,}31 \cdot AO_{II(-1)} + 8{,}28 \cdot AD_{XII(-1)} + 14{,}62$ |
| **South-eastern sub-area of the Barents Sea** | |
| **(4.9)** | $\text{Пл(Мол)}_{\text{ЮВ}_{\text{IV}}} = 0{,}95 \cdot \text{Пл(Мол)}_{\text{ЮВ}_{\text{III}}} - 11{,}12 \cdot \text{ПТВ}_{\text{ЮВ}_{VI(-1)}} - 9{,}59 \cdot \text{NAO}_{\text{X}(-1)} + 23{,}60 \cdot \text{AD}_{\text{X}(-1)} + 8{,}28$ |
| **(4.10)** | $\text{Пл(Тонк)}_{\text{ЮВ}_{IV}} = 0{,}57 \cdot \text{Пл(Тонк)}_{\text{ЮВ}_{III}} + 5{,}18 \cdot \text{Л}_{\text{ЮВ}_{IX(-1)}} + 3{,}79 \cdot AD_{II} + 8{,}63$ |
| **(4.11)** | $\text{Пл(Ср)}_{\text{ЮВ}_{IV}} = -29{,}49 \cdot \text{КМ}_{III}^{3-7} - 4{,}64 \cdot \text{Обм}_{\text{КВ}_{III}} - 14{,}67 \cdot AD_{IV(-1)} + 143{,}19$ |

*Note.* In equations (4.1)–(4.11), the following notations were adopted: *Пл(Мол)*, *Пл(Тонк)*, *Пл(Ср)*, and *Пл(Тол)* represent the areas of young ice, first-year thin ice, first-

year medium ice, and first-year thick ice, respectively. *Л* represents the ice coverage in specific regions of the Barents Sea. $Обм_{КВ}$, $Обм_{Шил}$, and $Обм_{Мак}$ denote the ice area export of the Sea with the surrounding waters: with the Kara Sea through the Kara Gate Strait, with the Arctic Basin through the Shilling Strait, and the Makarov Strait, respectively. $КМ^{1-3}$ and $КМ^{3-7}$ refer to the water temperature along the "Kola Meridian" transect at stations 1–3 and 3–7, respectively. The subscripts "*З*", "*СВ*", and "*ЮВ*" indicate the western, north-eastern, and south-eastern sub-areas of the Barents Sea, respectively. Subscripts marked with Roman numerals indicate the months for which the predictors were taken, and Arabic numerals indicate their lead time relative to the predictands in years.

Further, Table 4.16 specifies the contributions of each significant factor included in the final equations (summing up to 100%). The primary factor, accounting for 46% of cases, determining interannual changes in the ice age composition in the sub-areas of the Barents Sea, is the nature of large-scale atmospheric circulation, expressed by various climate indices. To a lesser extent, in 18% of cases, these changes are influenced by the intensity of the inflow of warm Atlantic waters. In 27% of cases, the previous state of the ice cover in the sub-areas of the Barents Sea is the most significant factor in reproducing interannual changes in the ice area of various age gradations. The remaining 9% of cases are attributed to the factor of ice area export between the Barents Sea and adjacent basins.

Table 4.16. Contribution of factors determining interannual changes in the age structure of the ice cover in various sub-areas of the Barents Sea (%)

| Determining factors / *Ice gradation* | *Young* | *First-year* | | |
|---|---|---|---|---|
| | | *Thin* | *Medium* | *Thick* |
| **Western sub-area of the Barents Sea** | | | | |
| Atmospheric circulation (AO, AD, NAO indices) | **46** | 46 | 40 | **53** |
| Advection of warm Atlantic waters | 30 | — | **60** | 47 |
| Surface air temperature | 18 | | — | — |
| Previous state of ice cover | — | **54** | | |
| Ice area export with adjacent basins | 6 | — | | |
| **North-eastern sub-area of the Barents Sea** | | | | |
| Atmospheric circulation (AO, AD, NAO indices) | **72** | 29 | **68** | **68** |
| Advection of warm Atlantic waters | — | — | — | — |
| Surface air temperature | | 35 | | |

| | | | | |
|---|---|---|---|---|
| Previous state of ice cover | | — | | |
| Ice area export with adjacent basins | 28 | **36** | 32 | 32 |
| **South-eastern sub-area of the Barents Sea** | | | | |
| Atmospheric circulation (AO, AD, NAO indices) | 22 | 7 | 25 | Factors were not determined |
| Advection of warm Atlantic waters | — | — | **49** | |
| Surface air temperature | 36 | | — | |
| Previous state of ice cover | **42** | **93** | | |
| Ice area export with adjacent basins | — | — | 26 | |

*Note.* The most significant factor for each investigated age gradation is highlighted in bold.

In the north-eastern sub-area of the Barents Sea, interannual changes in the ice age structure are mainly described by two key factors: the character of atmospheric circulation (contributing from 29% for first-year thin ice to 72% for young ice) and ice export with the neighboring Arctic Basin (from 28% for young ice to 36% for first-year thin ice). Here, the ice export factor is dominant only for first-year thin ice; interannual changes in the ice area for other age gradations are determined by large-scale atmospheric processes. Parameters such as the advection of warm Atlantic waters and the previous state of the ice cover are not statistically significant for the considered sub-area of the Barents Sea.

It is noted that in both the western and south-eastern sub-areas of the Barents Sea, interannual changes in the first-year thin ice area are more dependent on the previous state of the ice cover, while first-year medium ice is more influenced by the advection of warm waters of Atlantic origin. However, the contributions of each predictor significantly differ: the contribution the previous state of the ice cover is 54% (western part) and 93% (south-eastern part), while that of the Atlantic waters is 60% (western part) and 49% (south-eastern part). Additionally, the area of young ice in the south-eastern sub-area of the Sea is determined by the previous state of the ice cover by 42%. As a result, a relatively greater influence of warm Atlantic waters entering the Barents Sea is characteristic of its western sub-area, while the age composition of the south-eastern part of the sea is more dependent on its previous state.

Next, the *presumed* impact schemes of various statistically significant natural factors on changes in the ice age structure in the sub-areas of the Barents Sea are presented.

In the western sub-area of the Barents Sea, the *young ice* area increases under the influence of the negative phase of the AO in June of the previous year (with a positive sign in equation 4.1). The persistence of this negative phase enhances the poleward transport of cold air masses from the North Pole, leading to increased ice formation and growth of young ice. Additionally, the *first-year thin ice* area increases: the influence of the persistent positive phase of the NAO in April of the previous year, included in equation 4.2 with a positive sign, weakens the meridional circulation and reduces the transport of warmth from the North Atlantic into higher latitudes, altering the distribution of sea surface temperature and contributing to the thickening of the ice cover already in April of the current year [Nesterov, 2013]. The reduction in the of *first-year medium ice* area is more likely associated with the prevailing positive phase of AO in April and negative phase of NAO in May, respectively — their impact on the ice cover is opposite to the described above (see equation 4.3). Changes in the *first-year thick ice* area are characterized by the dominance of the positive phase of the AD in August and the negative phase of NAO in June of the preceding year. The positive phase of AD, on one hand, shows reduced pressure over Eurasia (in the region of the Kara and Laptev Seas), and on the other hand, increased pressure over the Arctic region of North America (specifically over the Canadian Arctic Archipelago). Such a baric situation promotes the intensification of the southward movement of air masses into the Barents Sea, leading to enhanced ice melting and, consequently, may decrease the amount of first-year thick ice (see equation 4.4).

In the north-eastern sub-area of the Barents Sea, the changes in the *young ice* area are predominantly determined by the negative phase of the AD in February and the positive phase of the NAO in April (see equation 4.5). The negative phase of the AD in February, according to [Watanabe et al., 2006], corresponds to positive anomalies of downward long-wave radiation north of Western Europe, hindering further sea ice growth in April across the entire Barents Sea. The influence of the positive phase of NAO in April of the previous year (included in equation 4.6 with a positive sign) leads to a reduction in the *first-year thin ice* area. The combined effect of the positive phase of AO

in April and the negative phase of AD in October of the preceding year determines changes in the *first-year medium ice* area, included in equation 4.7 with negative signs. The positive phase of AO inhibits the intrusion of cold air masses from the North Pole into the sea, slowing down the ice formation process in April (similarly to the negative phase of AD). The joint influence of AO and NAO indices in the positive phase, as well as AD in the negative phase, results in the slowing of the reduction in the *first-year thick ice* area (see equation 4.8).

In the south-eastern sub-area of the Barents Sea, the negative phases of AD and NAO in October of the preceding year have a characteristic impact on *young ice* — their area gradually decreases (see equation 4.9). Here, the same negative phase of AD in February leads to a decrease in the *first-year thin ice* area (the index is included with a positive sign in equation 4.10), while the positive phase of AD in April of the previous year, conversely, leads to an increase in the *first-year medium ice* area (negative sign in equation 4.11).

However, a significant contribution to the interannual changes in the ice age composition in the north-eastern sub-area of the Barents Sea is made by the factor of ice area export with neighboring basins. Annual estimates [Egorova et al., 2023b] indicate a prevailing influx of sea ice into the Barents Sea from adjacent basins through the Makarov Strait and a predominant outflow of ice beyond its boundaries — through the Shilling Strait. The area of *young* and *first-year medium ice* is determined by ice area export via the Shilling Strait in August and October of the previous year, respectively — predictors are included with negative signs in equations 4.5 and 4.7. Accordingly, intensive ice area export occurs during these months, preventing an increase in the amount of young and first-year medium ice in April. The quantity of *first-year thin*, *medium*, and *thick ice*, in turn, depends on ice area export through the Makarov Strait in October, January, and November of the previous year, respectively. Since the predictors in equations 4.6, 4.7, and 4.8 are positive, this means that the increase in the first-year ice area in April occurs due to the sea ice outflow from the Arctic Basin through the Makarov Strait several months earlier.

Ice area export through the Kara Gate in March is one of the significant predictors describing interannual changes in the quantity of *first-year medium ice* in the south-eastern sub-area of the Barents Sea (see equation 4.11). Although in March, ice of this age gradation comes from the south-western part of the Kara Sea, thereby increasing its quantity, against the backdrop of the overall reduction in the first-year medium ice area, the predictor's sign in the equation is negative.

Table 4.17 presents the quality parameters (correlation coefficients and determination coefficients, as well as availability and efficiency) of the obtained statistical equations. As a result, they describe from 52% to 79% of the variance of ice area of various age gradations in the sub-areas of the Barents Sea, with the lowest correlation coefficient being 0.72. The highest determination coefficient was achieved in describing interannual changes in the ice age composition in the south-eastern part of the Sea, ranging from 0.64 for first-year medium ice to 0.79 for young and first-year thin ice (with correlation coefficients ranging from 0.80 to 0.89, respectively). The presented equations relatively poorly reproduce changes in the ice age structure in the northern region: their determination coefficients range from 0.55 (for first-year medium ice) to 0.74 (for first-year thick ice) in the western sub-area and from 0.52 (for young ice) to 0.72 (for first-year thick ice) in the north-eastern sub-area. It is noted that for the north-eastern and western parts of the Sea, maximum correlation and determination coefficients are characteristic of first-year thick ice, the thickest age gradation considered: apparently, in the north of the Barents Sea, they are characterized by relatively greater inertia of interannual changes compared to other gradations.

In accordance with [Instruction on…, 2011], the practical use of the long-term forecast method is deemed appropriate if its efficiency is at least 10%. As a result, most of the presented statistical equations could potentially be applicable for forecasting the ice area of various age gradations in the sub-areas of the Barents Sea with a lead time of one month (see Table 4.17). For the age gradations of young, first-year thin, and first-year medium ice, the method's efficiency varies from 11% (young ice in the south-eastern sub-area) to 38% (first-year thin ice in the same south-eastern sub-area). In the case of

first-year thick ice, the method's effectiveness does not reach the required 10%, being 7% for the north-eastern and 0% for the western parts. Despite high availability, 90% or more, the method's efficiency may be zero if the actual values of the ice area for the analyzed age gradations are close to zero and/or exhibit low interannual variability. It is noted that statistical equations are unable to forecast a complete absence of ice of separate age gradation; the calculated values will always be either greater or less than zero. Although assuming a negative prognostic ice area value as zero does not improve the method's efficiency (less frequently, it may improve marginally, but still won't reach the required 10%).

Table 4.17. Availability *P* (in %), efficiency *Эф* (in %), as well as correlation coefficients *R* and determination coefficients $R^2$ of statistic equations of ice area of different age gradations in the sub-areas of the Barents Sea in April

| Barents Sea sub-area | | R | $R^2$ | P | Эф | Barents Sea sub-area | | R | $R^2$ | P | Эф |
|---|---|---|---|---|---|---|---|---|---|---|---|
| *Young ice* | | | | | | *First-year thin ice* | | | | | |
| **(4.1)** | W | 0,77 | 0,59 | 78 | 32 | **(4.2)** | W | 0,75 | 0,56 | 75 | 25 |
| **(4.5)** | NE | 0,72 | 0,52 | 73 | 12 | **(4.6)** | NE | 0,75 | 0,57 | 75 | 29 |
| **(4.9)** | SE | 0,89 | 0,79 | 60 | 11 | **(4.10)** | SE | 0,89 | 0,79 | 92 | 38 |
| *First-year medium ice* | | | | | | | *First-year thick ice* | | | | |
| **(4.3)** | W | 0,74 | 0,55 | 76 | 26 | **(4.4)** | W | 0,86 | 0,74 | 92 | 0 |
| **(4.7)** | NE | 0,81 | 0,65 | 79 | 21 | **(4.8)** | NE | 0,85 | 0,72 | 90 | 7 |
| **(4.11)** | SE | 0,80 | 0,64 | 80 | 18 | — | SE | Factors were not determined | | | |

*Note.* In the columns “Barents Sea sub-area”, “W” stands for the western, “NE” for the north-eastern, and “SE” for the south-eastern sub-area of the Barents Sea.

Actual and calculated values of the ice area for various age gradations in the sub-areas of the Barents Sea are provided in Figure 4.13. Negative prognostic values of ice area, if encountered, were set to zero. Three ice seasons, 2020/2021, 2021/2022, and 2022/2023, were utilized as an independent dataset. As a result, on the dependent dataset, the statistical equations satisfactorily reproduce interannual changes in the Barents Sea ice age composition, describing not only the overall observed tendency for change but also most peaks of the studied characteristic. However, it was not possible to model the peaks of the young ice area in 2000/2001, 2010/2011 for the north-eastern sub-area, and

2005/2006 for the south-eastern sub-area, as well as the of first-year medium ice area in 2009/2010, 2012/2013 for the western sub-area, and 2010/2011, 2012/2013 for the south-eastern sub-area with the selected predictors. Although calculated values are often less than actual values, for first-year thick ice in the north of the Barents Sea, when their area is close to or equal to zero, the reverse situation is observed.

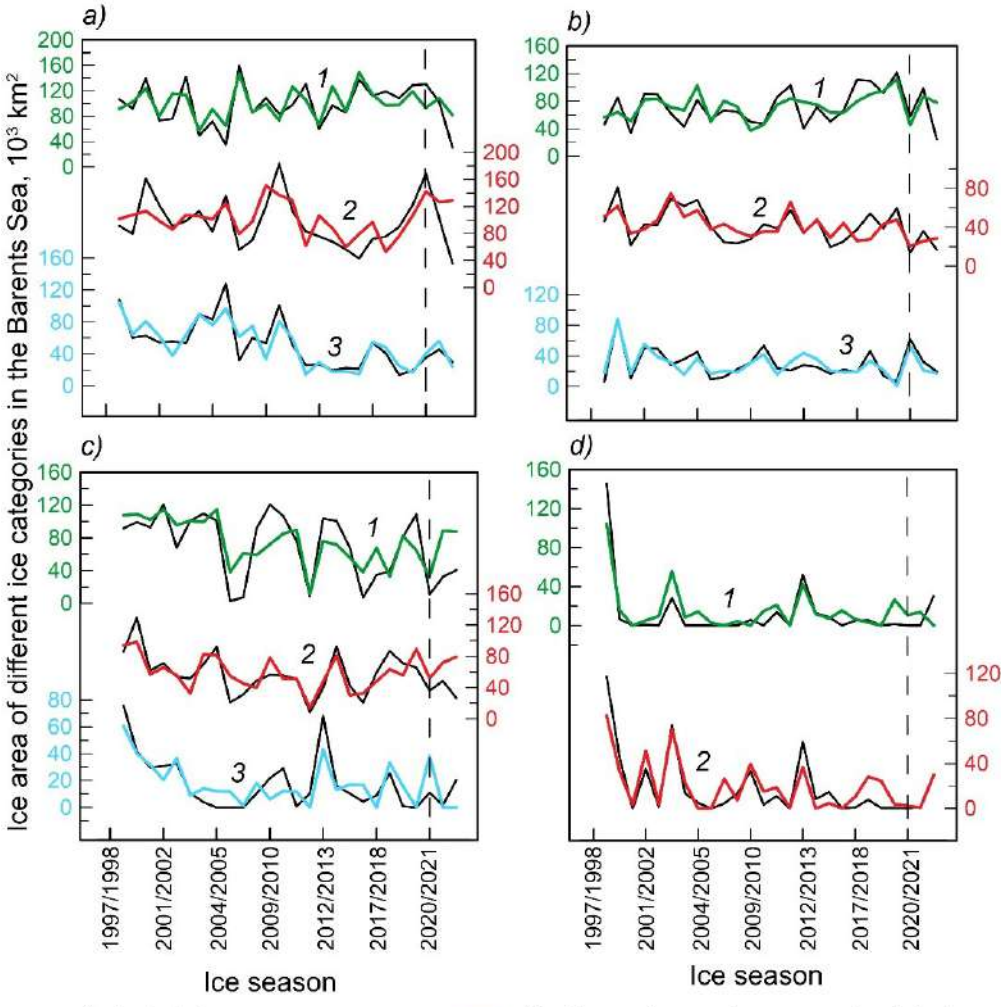


*1* — western (green), *2* — north-eastern (red), *3* — south-eastern (turquoise) sub-areas of the Barents Sea

Figure 4.13. Comparison of actual (shown in black line) and calculated (colored lines) values of area: *a)* young, *b)* first-year thin, *c)* first -year average, and *d)* first -year thick ice the Barents Sea in April for the period from 1998 to 2023. The vertical dashed line separates the dependent and independent datasets.

Analysis of the results obtained on the independent dataset showed that, overall, the presented statistical equations capture the trend of increasing or decreasing ice area of various age gradations (young ice in the western and south-eastern sub-areas, first-year

thin ice in the north-eastern and south-eastern sub-areas, and first-year thick ice in the south-eastern sub-area). The forecast for first-year medium ice showed discrepancies in the direction of area change for all regions of the Barents Sea; similarly, the results for first-year thin ice in the north-eastern sub-area and first-year thick ice in the western sub-area are not consistent. There is a complete match between the actual and forecasted area of young and first-year thin ice in the south-eastern part, as well as first-year thick ice in the north-eastern part of the Sea. To improve the quality of statistical equations, further research is important, particularly expanding the list of potential predictors.

The works of [Egorova et al., 2023a; Egorova et al., 2024] have published the main results of the study on the influence of natural factors on interannual changes in the ice age composition in the sub-areas of the Barents Sea.

### 4.6. Conclusions for Chapter 4

In this chapter, the regularities of seasonal and interannual changes in the main characteristics of the ice cover of the Barents Sea are described, which form a distinct ice regime. The following *key* conclusions were obtained from the analysis:

- The timing of the seasonal maximum ice coverage in April and the its seasonal minimum in September, accurate to the month, corresponds to the results of other studies. The analysis of changes in ice coverage in the western and north-eastern sub-areas of the Barents Sea is consistent with data for the entire basin, unlike the south-eastern one. The maximum ice coverage is observed here in March, and the ice cover completely melts by August, so ice formation always begins against a backdrop of clear water.
- Changes in the Barents Sea ice area throughout the annual cycle are influenced by fluctuations occurring in the western part. This is because it has the largest area compared to other sub-areas of the Sea and is most influenced by Atlantic waters.
- The onset of the modern warming climate period for the Barents Sea dates back to the early 20th century, with results varying depending on the sub-area. Analysis of the cumulative curve of ice coverage anomalies for the entire Barents Sea shows

that the “warm” phase began with the ice season of 2004/2005. The author assumes that the majority of changes in the sea ice coverage during the ice season are attributed to the period of stable formation in February. However, significant linear trends in the absolute values of ice coverage do not confirm this.

- Seasonal maximum and minimum positions of drift ice edges in the annual cycle generally correspond to the results obtained for ice coverage in the sub-areas of the Barents Sea.
- Among locally formed ice, age gradations of initial types and young ice are characteristic of the ice cover during all analyzed winter months (from October to May) in the sub-areas of the Barents Sea.
- The presence of old ice in the northern Barents Sea has become a relatively rare phenomenon. In April, old ice occupies no more than 8% of the total ice cover area; they were last observed in the western sub-area in 2020.
- After the minimum ice extent (area) in the Arctic in 2012, the amount of first-year thick ice in the ice cover of the western and north-eastern sub-areas of the Barents Sea significantly decreased, and under average conditions, they do not form at all in the south-eastern part.
- During the winter months, the boundary of old ice predominance is fixed outside the Barents Sea, while the boundary of first-year ice prevalence predictably expands with the increase in ice cover area.
- In the western sub-area of the Barents Sea, the factors determining changes in the ice age structure are the atmospheric circulation, the inflow of warm Atlantic waters, and the previous state of the ice cover. In the north-eastern sub-area, the predominant factors are large-scale atmospheric processes and ice area export with the Arctic Basin. In the south-eastern sub-area, the previous state of the ice cover and advection of the Atlantic water determine the ice area of various age gradations.

## CONCLUSIONS

The dissertation research *results* in the generalization of the spatial distribution patterns, as well as seasonal and interannual variations of the key parameters of the sea ice cover in the Greenland and Barents Seas.

The main findings and conclusions can be summarized as *follows*:

1. Working electronic data archives of the following sea ice parameters in the Greenland and Barents Seas have been compiled: ice age composition and boundaries of ice age gradations predominance (1997–2022 for both seas), positions of drift ice edge (1982–2022 and 1997–2022 for the Barents and Greenland Seas respectively during the year, and 1953–2022 for the Barents Sea in April), ice flow width and ice concentration (1997–2022 for the Greenland Sea).
2. It has been demonstrated that the seasonal maximum development of sea ice in the Greenland Sea occurs from February to April, while in the Barents Sea, it peaks in April. The seasonal minimum ice coverage is observed in September. It is noted that the establishment of the seasonal maximum in the Greenland Sea extends over three months, whereas during a colder climatic period (1958–1996), the peak ice coverage was observed in February-March. The identified periods of seasonal ice coverage changes in the Barents Sea coincide with the results of previous studies.
3. Characteristic periods of interannual ice coverage changes have been identified based on the analysis of cumulative curves of their anomalies for the Greenland Sea and the Barents Sea: 1949/1950–1981/1982 and 1999/2000–2021/2022 (Greenland Sea), as well as 1928/1929–1986/1987 and 2004/2005–2021/2022 (Barents Sea) respectively.
4. Seasonal patterns of spatial changes in the drift ice edge have been established for the Greenland Sea and the Barents Sea. In the Greenland Sea, unlike ice coverage, there is a smoothing of the period of establishing the seasonal maximum position of the drift ice edge up to one month, in April. In the Barents Sea, the timing of seasonal peak positions of the drift ice edge varies depending on the sub-area:

March-April in the western, April in the north-eastern, and March in the south-eastern part. Furthermore, an earlier establishment of the seasonal maximum ice coverage in the south-eastern sub-area of the Sea is noted, one month earlier compared to the results of the study for the colder climatic period of 1934–1991.

5. For the first time, regularities in seasonal and interannual changes in the ice age structure in the Greenland Sea and the Barents Sea have been identified. The ice formation process is observed throughout the winter period (from October to May). In the Greenland Sea, the total amount of first-year and young ice predominates in the age structure of the sea ice cover only in October, while in the Barents Sea, it predominates from October to March. First-year ice dominates in both the Greenland Sea and the Barents Sea in April-May. Old ice, prevailing from November to March, occupies at least 30% of the total area of the Greenland Sea ice cover. The presence of old ice in the ice structure becomes a rare phenomenon for the Barents Sea (less than 4% of its total area).
6. It has been shown that the age structure of the sea ice cover in the research region has undergone significant changes since the early 2000s compared to the period of the 1970s–1990s. Against the backdrop of the observed decrease in the total ice area in the Greenland Sea and the Barents Sea, the relative amount of ice of various age gradations changes within the bounds of natural variability.
7. Spatial regularities in the distribution of the sea ice of various age gradations in the Greenland Sea and the Barents Sea, specifically old and first-year ice, have been identified for the first time. In the Greenland Sea, the maximum boundary of old ice predominance occurs in April, coinciding with the seasonal peak of ice coverage, and the minimum in October. The timing of the seasonal maximum of old ice predominance in the Barents Sea varies considerably from February to May, depending on the analyzed area, with the minimum usually observed in October-November. The maximum boundary of first-year ice predominance in the western and north-eastern sub-areas of the Barents Sea is observed in April-May, and in the south-eastern one, it is observed in March-May. The minimum of their prevalence always falls in October.

8. Data on the age composition of the Greenland Sea ice cover and ice flow width from AARI ice charts and ice drift data from the National Snow and Ice Data Center (NSIDC) were utilized to assess the volume of ice carried out of the Arctic Basin through the Fram Strait. It was determined that the ice volume export exhibits a distinct seasonal cycle, peaking in March and reaching a minimum in October: the seasonal peaks are 375 km³ per month and 159 km³ per month respectively, with a total value of 2141 km³ for the winter months. The magnitude order coincides with the results of studies using ice thickness data from instrumental measurements. However, the interannual variations in the ice volume flux do not show a statistically significant linear trend, which contradicts the findings of other authors.
9. The main natural factor influencing interannual changes in the age composition of the sea ice cover in the sub-areas of the Barents Sea is the large-scale atmospheric circulation, expressed by different combinations of climate indices such as AO, AD, and NAO (contributing from 42% to 76%). The advection of warm Atlantic waters affects the amount of first-year medium ice in the western (60%) and south-eastern (49%) parts of the Sea. Furthermore, the previous state of the ice cover determines changes in the first-year thin ice area in the western (54%) and south-eastern (93%) sub-areas, as well as young ice in the south-eastern sun-area (42%). Mostly, the ice area export with the Arctic Basin determines the amount of first-year thin ice (36%) in the north-eastern part of the Barents Sea.
10. Most statistical equations describing interannual changes in the age structure of the sea ice cover in the sub-areas of the Barents Sea are potentially applicable in practice for long-term forecasting of the ice area of different age gradations, as the method's efficiency exceeds 10%, ranging from 11% to 38%.

*Acknowledgments*. The author expresses deep gratitude to their scientific supervisor, Dr. Mironov Yevgeny Uarovich, for his attentive guidance, comprehensive assistance, and valuable advice during the dissertation preparation. The author is grateful to the members of the AARI scientific departments for their helpful comments, which contributed

to the improvement of the manuscript. The author sincerely thanks her husband Pavel for his support and motivation.

## LIST OF ADOPTED ABBREVIATIONS

SD — standard deviation,

AARI — Arctic and Antarctic Research Institute,

NSIDC — National Snow and Ice Data Center,

AMO — Atlantic Multidecadal Oscillation,

AO — Arctic Oscillation,

AD — Arctic Dipole,

NAO — North Atlantic Oscillation.

**REFERENCES**


1. Alexandrov, V.Yu. Changes in Arctic Ice Thickness Since the Late 19th Century / V.Yu. Alexandrov, O.M. Johannessen // Arctic and Antarctic Research. – 2012. – Vol. 94. – No. 4. – P. 63-73. (In Russian).
2. Alekseev, G.V. Sea Ice of the Northern Hemisphere in Relation to Climate Changes in the 20th and 21st Centuries Based on Observational and Modeling Data / G.V. Alekseev, A.I. Danilov, V.M. Katzov [et al.] // Proceedings of the Russian Academy of Sciences. Earth Science Section. – 2009. – Vol. 45. – No. 6. – P. 723-735. (In Russian).
3. Alekseev, G.V. Arctic Amplification: The Role of Interhemispheric Exchange in the Atmosphere / G.V. Alekseev, N.E. Kharlanenkova, A.E. Vyazilova // Fundamental and Applied Climatology. – 2023. – Vol. 9. – No. 1. – P. 13-32. (In Russian).
4. Alekseeva, T.A. Ice Conditions for Navigation in the Arctic Basin in the Summer Period of 2018 / T.A. Alekseeva, S.S. Serovetnikov, S.V. Frolov [et al.] // Russian Arctic. – 2018. – No. 2. – P. 31-40. (In Russian).
5. Alekseeva, T.A. Review of Methods and Main Results of Sea Ice Thickness Measurements in the Arctic / T.A. Alekseeva, S.V. Frolov, S.S. Serovetnikov // Russian Arctic. – 2021. – Vol. 12. – No. 1. – P. 33-49. (In Russian).
6. Archive of the World Data Center for Sea Ice AARI [Electronic resource]. – Access mode: http://wdc.aari.ru/datasets/, free. (In Russian).
7. Atlas of the Oceans. The Arctic Ocean. Adm. No. 9501. – St. Petersburg: Publishing house of the State Hydrographic Office and Oceanography, 1980. – 200 p. (In Russian).
8. Afanasyeva, E.V. AARI Methodology for Sea Ice Charts Composition / E.V. Afanasyeva, T.A. Alekseeva, J.V. Sokolova [et al.] // Russian Arctic. – 2019. – No. 7. – P. 5-20. (In Russian).
9. Climate Monitoring Database of the National Oceanic and Atmospheric Administration (NOAA) [Electronic resource]. – Access mode: https://www.ncei.noaa.gov/climate-monitoring/#all, free.

10. Borzenkova, I.I. History of Sea Ice in the Arctic Basin: Lessons from the Past for Future / I.I. Borzenkova // Ice and Snow. – 2016. – Vol. 56. – No. 2. – P. 221-234. (In Russian).
11. Borodachev, V.E. Dictionary of Sea Ice Terms / V.E. Borodachev, V.P. Gavrilo, M.M. Kazansky. – St. Petersburg: Hydrometeoizdat, 1994. – 127 p. (In Russian).
12. Buzin, I.V. On Spreading of the Multiyear Ice in the Barents Sea in the Second Half of 20th – Beginning of 21 Century / I.V. Buzin // Arctic and Antarctic Research. – 2009. – Vol. 83. – No. 3. – P. 114-126. (In Russian).
13. Buzin, I.V. Seasonal Features of Climatic Change in the Barents Sea / I.V. Buzin, Z.M. Gudkovich // Arctic and Antarctic Research. – 2011. – Vol. 89. – No. 3. – P. 20-32. (In Russian).
14. Vaynovsky, P.A. Methods of Processing and Analysis of Oceanographic Information. Multidimensional Analysis: Manual / P.A. Vainovsky, V.N. Malinin. – St. Petersburg: Publishing House of RGGMI, 1992. – 96 p. (In Russian).
15. Vize, V.Yu. Climate of the Seas of the Soviet Arctic / V.Yu. Vize. – Leningrad-Moscow: Glavsevmorput Publishing House, 1940. – 124 p. (In Russian)
16. Vize, V.Yu. Fundamentals of Long-Term Ice Forecasting for Arctic Seas / V.Yu. Vize. – Moscow: Glavsevmorput Publishing House, 1944. – 273 p. (In Russian).
17. Volkov, V.A. Relation of Large-Scale Variations of the Sea Ice Drift Fields in the Arctic Ocean with Climatic Changes of Total Ice Concentrations During Last Decades / V.A. Volkov, A.V. Mushta, D.M. Demchev [et al.] // Arctic and Antarctic Research. – 2016. – No. 2. – P. 50-63. (In Russian).
18. Viazigina, N.A. Informativeness (Information-Bearing) of Hydrometeorological and Astrogeophysical Factors in the Problem of Describing Interannual Fluctuations of the Greenland Sea Ice Coverage / N.A. Viazigina, L.A. Timokhova, E.S. Egorova [et al.] // Ice and Snow. – 2021. – Vol. 61. – No. 3. – P. 431-444. (In Russian).
19. Hydrometeorology and Hydrochemistry of the Seas of the USSR. Volume I. Barents Sea, Issue 1. Hydrometeorological Conditions / Ed. by F.S. Terziev, G.V.

Girdyuk, G.G. Zykovaya, S.L. Dzhenyuk. – Leningrad: Hydrometeoizdat, 1990. – 281 p. (In Russian).

20. Girs, A.A. Methods of Long-Term Weather Forecasting / A.A. Girs, K.V. Kondratovich. – Leningrad: GMI, 1978. – 344 p. (In Russian).
21. Gordeeva, S.M. Practical Manual on the Discipline “Statistical Methods of Processing and Analysis of Hydrometeorological Information” / S.M. Gordeeva. – St. Petersburg: RGGMU, 2010. – 74 p. (In Russian).
22. Boundaries of Oceans and Seas. Adm. No. 9031. – Moscow: Publishing house of the State Hydrographic Office and Oceanography, 2000. – 208 p. (In Russian).
23. Gudkovich, Z.M. Fundamentals of Methodology for Long-Term Ice Forecasting for Arctic Seas / Z.M. Gudkovich, A.A. Kirillov, E.G. Kovalev [et al.]. – Leningrad: Hydrometeoizdat, 1972. – 348 p. (In Russian).
24. Gudkovich, Z.M. Interconnection of Modern Climatic Changes in the Atmosphere, Ocean, and Ice Cover / Z.M. Gudkovich, V.F. Zakharov, E.O. Aksenov [et al.] // Proceedings of AARI. – 1997. – Vol. 437. – P. 7-17. (In Russian).
25. Data from Polar Stations of Roshydromet Network in the Form of Bulletins [Electronic resource]. – Access mode: http://193.227.232.57/meteo/default/bulluten, free.
26. Diansky, N.A. Predictive Estimates of Climate Changes in the Arctic Based on the Combined Scenario / N.A. Diansky, I.V. Solomonova, A.V. Gusev // Russian Arctic. – 2019. – No. 4. – P. 24-33. (In Russian).
27. Dobrovolskiy, A.D. Seas of the USSR / A.D. Dobrovolskiy, B.S. Zalogin. – M.: Moscow University Publishing House, 1982. – 192 p. (In Russian).
28. Egorov, A.G. The Russian Arctic Seas Ice Age Composition and Thickness Variation in Winter Periods at the Beginning of the 21st Century / A.G. Egorov // Arctic and Antarctic Research. – 2020. – Vol. 66. – No. 2. – P. 124-143. (In Russian).
29. Egorova, E.S. Assessment of Ice Drift through the Fram Strait Based on Various Models / E.S. Egorova, E.S. Vinogradnaya // Comprehensive Studies of the World

Ocean: Materials of the V All-Russian Scientific Conference of Young Scientists. – Kaliningrad: AB IO RAS, 2020. – P. 60-61. (In Russian).

30. Egorova, E.S. Main Patterns of Changes in the Age Composition of Ice in the Greenland Sea / E.S. Egorova // Comprehensive Studies of the World Ocean: Materials of the VI All-Russian Scientific Conference of Young Scientists. – Moscow: P.P. Shirshov IO RAS, 2021. – P. 65-66. (In Russian).
31. Egorova, E.S. The Shipborne Sea-Ice Condition Observations in The Arctic Basin During the Summer 2021 / E.S. Egorova, N.A. Filippov, T.A. Alekseeva [et al.] // Russian Arctic. – 2021. – No. 15. – P. 68-80. (In Russian).
32. Egorova, E.S. Ice Age Composition in the Barents Sea / E.S. Egorova, Ye.U. Mironov // Arctic and Antarctic Research. – 2022a. – Vol. 68. – No. 3. – P. 216-233. (In Russian).
33. Egorova, E.S. Formation of the Age Composition of Ice in the Southeastern Part of the Barents Sea in the Winter Period / E.S. Egorova, Ye.U. Mironov // Seas of Russia: Challenges of Domestic Science: Abstracts of the All-Russian Scientific Conference. – Sevastopol: FSBSI FRS MHI RAS, 2022b. – P. 83-84. (In Russian).
34. Egorova, E.S. Assessment of Seasonal and Interannual Changes in the Age Structure of Ice in the Greenland and Barents Seas / E.S. Egorova, Ye.U. Mironov // Comprehensive Studies of the World Ocean: Materials of the VII All-Russian Scientific Conference of Young Scientists. – St. Petersburg: Own publishing house, 2023a. – P. 47-48. (In Russian).
35. Egorova, E.S. Drivers of Interannual Variations of Ice Age Composition in Sub-Areas of the Barents Sea / E.S. Egorova, N.A. Lis, Ye.U. Mironov // Arctic and Antarctic Research. – 2023a. – Vol. 69. – No. 3. – P. 290-309. (In Russian).
36. Egorova, E.S. Seasonal and Interannual Changes in Ice Export between the Greenland and Barents Seas with Adjacent Areas / E.S. Egorova, Ye.U. Mironov, I.A. Ilyushenkova // Oceanological Research: Materials of the X Conference of Young Scientists. – Vladivostok: POI FEB RAS, 2023b. – P. 20-21. (In Russian).
37. Egorova, E.S. Drivers of the Interannual Variations of Sea Ice Age Composition in the Barents Sea During Its Maximum Extent / E.S. Egorova, N.A. Lis, Ye.U.

Mironov // Marine Research and Education: Materials of the XII International Scientific and Practical Conference. Volume II (IV). – Tver: LLC PolyPRESS, 2024. – P. 142-148. (In Russian).

38. Daily Ice Drift Vectors EASE-Grid, Polar Pathfinder Database Version 4 from the National Snow and Ice Data Center (NSIDC) [Electronic resource]. – Access mode: https://nsidc.org/data/nsidc-0116/versions/4, free.
39. Weekly Ice Drift Vectors EASE-Grid, Quicklook Arctic Database Version 1 from the National Snow and Ice Data Center (NSIDC) [Electronic resource]. – Access mode: https://nsidc.org/data/nsidc-0748/versions/1, free.
40. Zhichkin, A.P. Dynamics of Inter-annual and Seasonal Anomalies of Ice-Cover Extent in the Barents and Kara Seas / A.P. Zhichkin // Bulletin of the Kola Scientific Center of the Russian Academy of Sciences. – 2015. – Vol. 20. – Iss. 1. – P. 55-64. (In Russian).
41. Zakharov, V.F. Sea Ice in the Climate System / V.F. Zakharov, ed. by A.F. Treshnikov. – St. Petersburg: Hydrometeoizdat, 1996. – 213 p. (In Russian).
42. Zubakin, G.K. Large-Scale Variability of the State of the Ice Cover of the Seas of the North European Basin / G.K. Zubakin. – Leningrad: Hydrometeoizdat, 1987a. – 160 p. (In Russian).
43. Zubakin, G.K. On the Ice Exchange of the Barents Sea / G.K. Zubakin // Proceedings of AARI. – 1987b. – Vol. 410. – P. 113-117. (In Russian).
44. Ivanov, V.V. Does Arctic Ocean Ice Cover Become Seasonal? / V.V. Ivanov, V.A. Alekseev, T.A. Alekseeva [et al.] // Earth Observation from Space. – 2013. – No. 4. – P. 50-65. (In Russian).
45. Ivanov, V.V. New Mechanisms of Polar Amplification Triggered by the Arctic Sea Ice Loss / V.V. Ivanov // RFBR Journal. – 2022. – Vol. 114. – No. 2. – P. 40-47. (In Russian).
46. Karakash, A.I. Ice Cover of the Greenland Sea and the Possibility of Predicting Ice Conditions in the Seas of the Western Sector of the Arctic / A.I. Karakash // Proceedings of the Central Institute of Polar Research. – 1950. – Iss. 17. (In Russian).

47. Karakash, A.I. Forecast of the Ice Edge Position in the Barents Sea / A.I. Karakash // Meteorology and Hydrology. – 1958. – No. 9. – P. 16-21. (In Russian).
48. Karsakov, A.L. Restoration of data on water temperature in the Kola Section for 2016–2017 / A.L. Karsakov, A.G. Trofimov, V.A. Ivshin [et al.] // Proceedings of VNIRO. – 2018. – Vol. 173. – P. 193-206. (In Russian).
49. Karsakov, A.L. 120 Years of Oceanographic Observations in the Kola Section / A.L. Karsakov, A.G. Trofimov, M.Yu. Antsiferov [et al.] – Murmansk: PINRO named after N.M. Knipovich, 2022. – 146 p. (In Russian).
50. Krasheninnikova, S.B. Causes and Features of Long-Term Variability of Ice Extent in the Barents Sea / S.B. Krasheninnikova, M.A. Krasheninnikova // Ice and Snow. – 2019. – Vol. 59. – No. 1. – P. 112-122. (In Russian).
51. Latonin, M.M. Arctic Amplification Phenomenon and Its Driving Mechanisms / M.M. Latonin, I.L. Bashmachnikov, L.P. Bobylev // Fundamental and Applied Hydrophysics. – 2020. – Vol. 13. – No. 3. – P. 3-19. (In Russian).
52. Lebedev, A.A. Method for Forecasting Ice Cover in the North Atlantic and Greenland Sea / A.A. Lebedev // Materials of Fisheries Research in the Northern Basin. – 1964. – Issue 2. – P. 108-118. (In Russian).
53. Lebedev, A.A. Long-term Anomalies of Ice-Thermal Inhomogeneities of the Ocean and the State of Atmospheric Processes in the North European Basin / A.A. Lebedev // Proceedings of AARI. – 1981. – Vol. 372. – P. 18-25. (In Russian).
54. Lebedev, A.A. Large Anomalies of Ice Cover in the North European Basin / A.A. Lebedev // Proceedings of AARI. – 1994. – Vol. 432. – P. 63-83. (In Russian).
55. Lebedev, A.A. Isobaric Coefficients of Ice Edge Displacement in Some Areas of the Barents Sea / A.A. Lebedev, N.S. Uralov // Proceedings of AARI. – 1973. – Vol. 307. – P. 52-62. (In Russian).
56. Lebedev, A.A. On the Features of the Thermal State of the North Atlantic and Atmospheric Circulation in the Formation of Anomalous Ice Cover in the Greenland Sea / A.A. Lebedev, N.S. Uralov // Proceedings of AARI. – 1976a. – Vol. 320. – P. 47-64. (In Russian).

57. Lebedev, A.A. Experience in Calculating Sea Ice Cover by Ice Balance Components (Using the Example of the East Greenland Sector) / A.A. Lebedev, N.S. Uralov // Proceedings of AARI. – 1976b. – Vol. 320. – P. 65-82. (In Russian).
58. Lebedev, A.A. On the Ice Balance of the Greenland Sea / A.A. Lebedev, N.S. Uralov // Proceedings of AARI. – 1977a. – Vol. 341. – P. 43-52. (In Russian).
59. Lebedev, A.A. Forecasting Ice Cover in the Greenland Sea in Connection with the Features of the Thermal State of the Atlantic Ocean and Atmospheric Circulation / A.A. Lebedev, N.S. Uralov // Problems of the Arctic and Antarctic. – 1977b. – Issue 50. – P. 36-39. (In Russian).
60. Lebedev, A.A. Results of Estimating the Annual Cycle of Ice Exchange between the Arctic Basin and the Seas of the North Atlantic / A.A. Lebedev, N.S. Uralov // Proceedings of AARI. – 1981. – Vol. 384. – P. 78-89. (In Russian).
61. Lis, N.A. Climate Variability of the Ice Extent in the Barents Sea and Its Individual Areas / N.A. Lis, E.S. Egorova // Arctic and Antarctic Research. – 2022. – Vol. 68. – No. 3. – P. 234-247. (In Russian).
62. Lis, N.A. Informativeness (Information-Bearing) of Factors Forming Interannual Variability of the Barents Sea and Its Individual Areas Ice Coveren / N.A. Lis, E.A. Cherniavskaia, Ye.U. Mironov, L.A. Timokhov, E.S. Egorova // Russian Arctic. – 2023. – Vol. 5. – No. 2. – P. 17-32. (In Russian).
63. Litvinova, O.S. Macrocirculation Conditions of the Winter Season in the South-East of Western Siberia / O.S. Litvinova // Geographical Bulletin. – 2018. – Vol. 47. – No. 4. – P. 67-77. (In Russian).
64. Malinin, V.N. Physico-Statistical Method for Forecasting Oceanographic Characteristics (Using the Example of the North European Basin) / V.N. Malinin, S.M. Gordeeva. – Murmansk: PINRO, 2003. – 129 p. (In Russian).
65. Malinin, V.N. Statistical Methods for Analysis of Hydrometeorological Information: Textbook. In 2 volumes: Volume 1. Primary Analysis and Construction of Empirical Dependencies / V.N. Malinin. – 2nd ed., revised and enlarged. – St. Petersburg: RSHU, 2020a. – 256 p. (In Russian).

66. Malinin, V.N. Statistical Methods for Analysis of Hydrometeorological Information: Textbook. In 2 volumes: Volume 2. Analysis of Time Series and Random Fields / V.N. Malinin. – 2nd ed., revised and enlarged. – St. Petersburg: RSHU, 2020b. – 196 p. (In Russian).
67. Climate Data Store of the European Earth Observation Program Copernicus [Electronic resource]. – Access mode: http://cds.climate.copernicus.eu, free.
68. Matishov, G.G. Climate of the West Arctic Seas at the Beginning of the XXI Century / G.G. Matishov, S.L. Dzhenyuk, A.P. Zhichkin [et al.] // Proceedings of the Russian Academy of Sciences. – 2011. – No. 3. – P. 17-32. (In Russian).
69. Matishov, G.G. Taking into Account of the Barents Sea Climate Secular Dynamics in Course of Marine Activity Planning / G.G. Matishov, S.L. Dzhenyuk, V.V. Denisov [et al.] // Proceedings of the Kola Science Center of the Russian Academy of Sciences. Series “Oceanology”. – 2013. – Vol. 14. – Issue 1. – P. 56-71. (In Russian).
70. Makhotin, M.S. Distribution of Atlantic Water Masses in the Barents Sea Based on Observations and Numerical Modeling / M.S. Makhotin, V.V. Ivanov // Proceedings of the Hydrometeorological Research Center of the Russian Federation. – 2016. – No. 361. – P. 169-191. (In Russian).
71. Mironov, Ye.U. Seasonal Changes in Ice Cover in the Fram Strait Based on Radar Surveys / Ye.U. Mironov // Proceedings of AARI. – 1997. – Vol. 437. – P. 108-114. (In Russian).
72. Mironov, Ye.U. Ice Conditions in the Greenland and Barents Seas and Their Long-Term Forecast / Ye.U. Mironov; Ed. by V.A. Spichkin. − St. Petersburg: AARI, 2004. − 319 p. (In Russian).
73. Mironov, Ye.U. Seasonal and Interannual Variations in the Greenland Sea Ice Age Composition in the Winter Period / Ye.U. Mironov, E.S. Egorova // Meteorology and Hydrology. – 2024. – No. 3. – P. 54-65. (In Russian).
74. Russian Arctic Seas in Modern Climate Conditions / Ed. by I.M. Ashika. – St. Petersburg: AARI, 2021. – 360 p. (In Russian).

75. Nesterov, E.S. North Atlantic Oscillation: Atmosphere and Ocean / E.S. Nesterov. – Moscow: Triada LTD, 2013. – 144 p. (In Russian).
76. Nikiforov, E.G., Regularities of Large-Scale Variability in the Hydrological Regime of the Arctic Ocean / E.G. Nikiforov, A.O. Shpaiher. – Leningrad: Gidrometeoizdat, 1980. – 269 p. (In Russian).
77. Official website of QGIS, a free and open-source geographic information system [Electronic resource]. – Access mode: https://qgis.org/ru/site/index.html, free.
78. Pishchalnik, V.M. Analysis of Dynamics for Anomalies of the Ice Cover in the Okhotsk Sea in the Period from 1882 to 2015 / V.M. Pishchalnik, V.A. Romanyuk, I.G. Minervin [et al.] // Izvestiya TINRO. – 2016. – Vol. 185. – P. 228-239. (In Russian).
79. Pishchalnik, V.M. Year-To-Year Dynamics of the Ice Cover Anomalies in the Tatar Strait for the Period from 1882 to 2018 / V.M. Pishchalnik, D.V. Dorofeeva, I.G. Minervin [et al.] // Izvestiya TINRO. – 2019. – Vol. 196. – P. 114-122. (In Russian).
80. Pishchalnik, V.M. Evaluation of the Ice Volume of the Sea of Okhotsk by the Ice Age Characteristics for the Period 2001–2019 / V.M. Pishchalnik, I.G. Minervin, P.A. Truskov // Izvestiya TINRO. – 2020. – Vol. 200. – No. 2. – P. 427-444. (In Russian).
81. Popova, V.V. Regional Features of Present Winter Snow Accumulation Variability in the North Eurasia from Data of Observations, Reanalysis and Satellites / V.V. Popova, A.B. Shmakin // Izvestiya RAS. Physics of the Atmosphere and Ocean. – 2010. – Vol. 46. – No. 2. – P. 161-175. (In Russian).
82. Repina, I.A. Remote Sensing in Ice Sea Dynamics and Modern Arctic Climate Investigation / I.A. Repina, V.V. Ivanov // Remote Sensing of the Earth from Space. – 2012. – Vol. 9. – No. 5. – P. 89-103. (In Russian).
83. Guideline Document 52.27.759 – 2011, Instruction on Forecasting Service. Section 3. Part III. Service of Marine Hydrological Forecasts. – Moscow: Triada LTD, 2011. – 194 p. (In Russian).

84. Manual on Ice Aviation Reconnaissance Production. – Leningrad: Hydrometeoizdat, 1981. – 240 p. (In Russian).
85. Observational Data Series on the Standard Oceanographic Section “Kola Meridian” of the Knipovich Polar Research Institute of Marine Fisheries and Oceanography [Electronic resource]. – Access mode: http://www.pinro.vniro.ru/ru/razrez-kolskij-meridian/ryady-nablyudenij, free.
86. Barents Sea System / Ed. by A.P. Lisitsyn. – Moscow: GEOS, 2021. – 672 p. (In Russian).
87. Smirnov, N.P. North Atlantic Oscillation and Climate / N.P. Smirnov, V.N. Vorobyov, S.Yu Kochanov. – St. Petersburg: Publishing House of RGGMU, 1998. – 121 p. (In Russian).
88. Smirnov, V.N. Features of the Dynamics and Deformation Mechanics of the Arctic Basin Ice / V.N. Smirnov // Arctic and Antarctic Research. – 2007. – No. 75. – P. 73-84. (In Russian).
89. Smirnov, V.G. Satellite Monitoring of the Sea Ice / V.G. Smirnov, A.V. Bushuev, I.A. Bychkova [et al.] // Arctic and Antarctic Research. – 2010. – Vol. 85. – No. 2. – P. 62-76. (In Russian).
90. Smirnov, V.G. Possibilities of Remote Sensing Methods as a Reliable Source of Operational Objective Information on the State of the Ice Cover of Polar Seas / V.G. Smirnov, I.E. Frolov, A.V. Bushuev [et al.] // In: Oceanography and Sea Ice; Ed. by I.E. Frolov. – Moscow – St. Petersburg: LLC Paulsen, 2011. – P. 50-69. (In Russian).
91. Sumkina, A.A. Seasonal Ice Removal in the Barents Sea and Its Dependence on Heat Advection by Atlantic Waters / A.A. Sumkina, K.K. Kivva, V.V. Ivanov [et al.] // Fundamental and Applied Hydrophysics. – 2022. – Vol. 15. – No. 1. – P. 82-97. (In Russian).
92. Timofeeva, A.B. Multi-Year Variability of the Fast Ice Thickness in the Laptev Sea According to Polar Stations Data // A.B. Timofeeva, M.V. Sharatunova // Russian Arctic. – 2021. – No. 12. – P. 62-76. (In Russian).

93. Timofeeva, A.B. Ice Cover of the Russian Arctic Seas Along the Northern Sea Route in the Current Climatic Period / A.B. Timofeeva, A.V. Yulin, V.V. Ivanov [et al.] // Arctic: Ecology and Economics. – 2024. – Vol. 14. – No. 1. – P. 135-146. (In Russian).

94. Timokhov, L.A. Seasonal and Inter-Annual Variability of the Ice Cover of the Greenland Sea / L.A. Timokhov, N.A. Vyazigina, Ye.U. Mironov [et al.] // Ice and Snow. – 2018. – Vol. 58. – No. 1. – P. 127-134. (In Russian).

95. Timokhov, L.A. Climatic Changes of Seasonal and Inter-Annual Variability of the Ice Cover of the Greenland and Barents Seas / L.A. Timokhov, N.A. Vyazigina, Ye.U. Mironov [et al.] // Arctic and Antarctic Research. – 2019. – Vol. 65. – No. 2. – P. 148-168. (In Russian).

96. Tregubova, M.V. Multi-Year Dynamics of the Ice Cover of the Greenland Sea under Conditions of Modern Climate Change / M.V. Tregubova, O.M. Prokofyev, A.V. Mukhina // Symbol of Science. – 2015. – No. 5. – P. 265-267. (In Russian).

97. Treshnikov, A.F. Geographical Names of the Main Parts of the Relief of the Arctic Basin / A.F. Treshnikov, L.L. Balakshin, N.A. Belov [et al.] // Arctic and Antarctic Research. – 1967. – Issue 27. – P. 5-15. (In Russian).

98. Tyuryakov, A.B. Hydrometeorological Conditions of the Appearance of Two-Year Ice in the South-eastern Part of the Barents Sea / A.B. Tyuryakov, I.A. Ilyushchenkova, E.S. Egorova // Comprehensive Studies of the Natural Environment of the Arctic and Antarctic: Abstracts of Reports of the International Scientific Conference. – St. Petersburg: SSC RF AARI, 2020. – P. 306-309. (In Russian).

99. Tyuryakov, A.B. Cases of Increased Complete Ice Clearing in the Barents Sea over the Past Decade as an Indicator of Climate Warming in the Western Arctic Region / A.B. Tyuryakov, E.S. Egorova // Hydrometeorology and Ecology: Achievements and Prospects of Development: Proceedings of the V Anniversary All-Russian Conference named after L.N. Karlin MGO-2021. – Moscow: Pero Publishing, 2021. – P. 125-134. (In Russian).

100. Uralov, N.S. On the Methodology for Forecasting the Overall Ice Conditions of the Barents Sea in the Spring-Summer Months / N.S. Uralov // Proceedings of the State Oceanographic Institute. – 1960. – Issue 55. (In Russian).
101. Frolov, I.E. Scientific Researches in the Arctic. Vol. 2. Climate Change in the Ice Conditions of the Seas of the Eurasian Shelf / I.E. Frolov, Z.M. Gudkovich, V.P. Karklin [et al.] – St. Petersburg: Nauka, 2007a. – 136 p. (In Russian).
102. Frolov, I.E. Climatic Changes of Ice Conditions in the Arctic Seas of the Eurasian Shelf / I.E. Frolov, Z.M. Gudkovich, V.P. Karklin [et al.] // Arctic and Antarctic Research. – 2007b. – No. 75. – P. 149-160. (In Russian).
103. Yulin, A.V. Interannual and Seasonal Variability of Arctic Sea Ice Extent According to Satellite Observations / A.V. Yulin, N.A. Vyazigina, E.S. Egorova // Russian Arctic. – 2019. – No. 7. – P. 28-40. (In Russian).
104. Aagaard, K. The East Greenland Current North of Denmark Strait: Part 1 // K. Aagaard, L. K. Coachman // Arctic. – 1968. – Vol. 21. – P. 181-200.
105. Årthun, M. The Seasonal and Regional Transition to an Ice-Free Arctic / M. Årthun, I. H. Onarheim, J. Dörr [et al.] // Geophysical Research Letters. – 2021. – Vol. 48. – e2020GL090825.
106. Barry, R.G. The Arctic Sea Ice-Climate System: Observations and Modeling / R.G. Barry, M.C. Serreze, J.A. Maslanik [et al.] // Reviews of Geophysics. – 1993. – Vol. 31. – No. 4. – P. 397-422.
107. Beszczynska-Möller, A. Synthesis of Exchanges through the Main Oceanic Gateways to the Arctic Ocean / A. Beszczynska-Möller, R.A. Woodgate, C.M. Lee [et al.] // Oceanography. – 2011. – Vol. 24. – P. 82-99.
108. Beszczynska-Möller, A. Variability in Atlantic Water Temperature and Transport at the Entrance to the Arctic Ocean, 1997–2010 / A. Beszczynska-Möller, E. Fahrbach, U. Schauer [et al.] // ICES Journal of Marine Science. – 2012. – Vol. 69. – No. 5. – P. 852-863.
109. Bi, H. Arctic Sea Ice Area Export through the Fram Strait Estimated from Satellite-Based Data: 1988–2012 // H. Bi, K. Sun, X. Zhou [et al.] // IEEE Journal of

Selected Topics in Applied Earth Observations and Remote Sensing. – 2016. – Vol. 9. – No. 7. – P. 3144-3157.

110. Bi, H. Recent Satellite-Derived Sea Ice Volume Flux through the Fram Strait: 2011–2015 / H. Bi, Y. Wang, W. Zhang [et al.] // Acta Oceanologica Sinica. – 2018. – Vol. 37. – No. 7. – P. 107-115.
111. Bliss, A.C. Regional Variability of Arctic Sea Ice Seasonal Change Climate Indicators from a Passive Microwave Climate Data Record / A.C. Bliss, M. Steele, G. Peng [et al.] // Environmental Research Letters. – 2019. – Vol. 14. – No. 4. – 045003.
112. Bonan, D.B. Constraining the date of a seasonally ice-free Arctic Using a Simple Model / D.B. Bonan, T. Schneider, I. Eisenman [et al.] // Geophysical Research Letters. – 2021. – No. 48. – e2021GL094309.
113. Buzin, I.V. Estimations of Some Components of Ice Conditions in Northeastern Barents Sea / I.V. Buzin // International Journal of Offshore and Polar Engineering. – 2006. – Vol. 16. – No. 4. – P. 274-282.
114. Cai, Q. Accelerated Decline of Summer Arctic Sea Ice During 1850–2017 and the Amplified Arctic Warming During the Recent Decades / Q. Cai, J. Wang, D. Beletsky [et al.] // Environmental Research Letters. – 2021. – Vol. 16. – 034015.
115. Chatterjee, S. Combined Influence of Oceanic and Atmospheric Circulations on Greenland Sea Ice Concentration / S. Chatterjee, R.P. Raj, L. Bertino [et al.] // Cryosphere. – 2021. – Vol. 15. – No. 3. – P. 1307-1319.
116. Chylek, P. Annual Mean Arctic Amplification 1970–2020: Observed and Simulated by CMIP6 Climate Models / P. Chylek, C. Folland, J. D. Klett [et al.] // Geophysical Research Letters. – 2022. – Vol. 49. – e2022GL099371.
117. Comiso, J.C. Accelerated Decline in the Arctic Sea Ice Cover / J.C. Comiso C.L. Parkinson, R. Gersten [et al.] // Geophysical Research Letters. – 2008. – Vol. 35. – L01703.
118. Cox, K. A. Interannual Variability of Arctic Sea Ice Export into the East Greenland Current / K.A. Cox, J.D. Stanford, A.J. McVicar [et al.] // Journal of Geophysical Research. – 2010. – Vol. 115. – C12063.

119. Divine, D.V. Historical Variability of Sea Ice Edge Position in the Nordic Seas / D.V. Divine, C. Dick // Journal of Geophysical Research. – 2006. – Vol. 111. – C01001.

120. Egorova, E.S. Assessment of the Seasonal and Multiyear Variability in the Sea Ice Volume Export via the Fram Strait / E.S. Egorova, Ye.U. Mironov // International Journal of Offshore and Polar Engineering. – 2023b. – Vol. 33. – P. 18-26.

121. Esau, I. The Arctic amplification and its impact: A synthesis through Satellite Observations / I. Esau, L.H. Pettersson, M. Cancet [et al.] // Remote Sensing. – 2023. – Vol. 15. – No. 5. – 1354.

122. Furevik, T. The Flow of Atlantic Water to the Nordic Seas and Arctic Ocean / T. Furevik, C. Mauritzen, R. Ingvaldsen // Arctic Alpine Ecosystems and People in a Changing Environment // ed. by J. B. Ørbæk, R. Kallenborn, I. Tombre [et al.]. – Springer, Berlin, Heidelberg, 2007. – P. 123-146.

123. Goldenberg, S.B. The Recent Increase in Atlantic Hurricane Activity: Causes and Implications / S.B. Goldenberg, C.W. Landsea, A.M. Mestas-Nunez [et al.] // Science. – 2001. – Vol. 293. – No. 5529. – P. 474-479.

124. Graff, L. S., Arctic Amplification Under Global Warming of 1.5 and 2 °C in NorESM1-Happi / L.S. Graff, T. Iversen, I. Bethke [et al.] // Earth System Dynamics. – 2019. – Vol. 10. – P. 569-598.

125. Haine, T. Arctic Freshwater Export: Status, Mechanisms, and Prospects / T. Haine, B. Curry, R. Gerdes [et al.] // Global and Planetary Change. – 2015. – Vol. 125. – P. 13-35.

126. Hakkinen, S. Shifting Surface Currents in the Northern North Atlantic Ocean / S. Hakkinen, P.B. Rhines // Journal of Geophysical Research. – 2009. – Vol. 114. – C04005.

127. Hansen, B. North Atlantic–Nordic Seas Exchanges // B. Hansen, S. Østerhus // Progress in Oceanography. – 2000. – Vol. 45. – No. 2. – P. 109-208.

128. Håvik, L. Evolution of the East Greenland Current from Fram Strait to Denmark Strait: Synoptic Measurements from Summer 2012 / L. Håvik, R.S. Pickart, K.

Våge [et al.] // Journal of Geophysical Research: Oceans. – 2017. – Vol. 122. – No. 3. – P. 1974-1994.

129. Hersbach, H. The ERA5 Global Reanalysis / H. Hersbach, B. Bell, P. Berrisford [et al.] // Quarterly Journal of the Royal Meteorological Society. – 2020. – Vol. 146. – No. 730. – P. 1999-2049.
130. Hordon, R.M. Icelandic Low / R.M. Hordon // Encyclopedia of World Climatology. Encyclopedia of Earth Sciences Series / ed. by J.E. Oliver. – Springer, Dordrecht, 2005. – P. 428-429.
131. IPCC Special Report on the Ocean and Cryosphere in a Changing Climate. – Cambridge, United Kingdom and New York, NY, USA: Cambridge University Press, 2019. – In press.
132. Ivanov, V.V. Transformation of Atlantic Water in the North-Eastern Barents Sea in Winter / V.V. Ivanov, I.E. Frolov, K.V. Filchuk // Arctic and Antarctic Research. – 2020. – Vol. 66. – No. 3. – P. 246-266.
133. Jakobsson, M. The International Bathymetric Chart of the Arctic Ocean (IBCAO) Version 3.0 / M. Jakobsson, L. Mayer, B. Coakley [et al.] // Geophysical Research Letters. – 2012. – Vol. 39. – L12609.
134. Jahn, A. How Predictable is the Timing of a Summer Ice-Free Arctic? / A. Jahn, J.E. Kay, M. M. Holland [et al.] // Geophysical Research Letters. – 2016. – No. 43. – P. 9113-9120.
135. JCOMM Expert Team on Sea Ice. Sea-Ice Nomenclature: Snapshot of the WMO Sea Ice Nomenclature No. 259. – Geneva, Switzerland: WMO-JCOMM, 2014. – 121 p.
136. Koenig, Z. The Yermak Pass Branch: a Major Pathway for the Atlantic Water Morth of Svalbard? / Koenig, Z., Provost, C., Sennéchael, N. [et al.] // Journal of Geophysical Research: Oceans. – 2017. – Vol. 122. – No. 12. – P. 9332-9349.
137. Krumpen, T. Recent Summer Sea Ice Thickness Surveys in Fram Strait and Associated Ice Volume Fluxes / T. Krumpen, R. Gerdes, C. Haas [et al.] // Cryosphere. – 2016. – Vol. 10. – No. 2. – P. 523-534.

138. Kwok, R. Variability of Fram Strait Ice Flux and North Atlantic Oscillation / R. Kwok, D.A. Rothrock // Journal of Geophysical Research Atmospheres. – 1999. – Vol. 104. – C3. – P. 5177-5189.
139. Kwok, R., Fram Strait Sea Ice Outflow / R. Kwok, G.F. Cunningham, S.S. Pang // Journal of Geophysical Research. – 2004. – Vol. 109. – C01009.
140. Kwok, R. Outflow of Arctic Ocean Sea Ice into the Greenland and Barents Seas / R. Kwok // Journal of Climate. – 2009. – Vol. 22. – No. 9. – P. 2438-2457.
141. Kwok, R. Arctic Sea Ice Thickness, Volume and Multiyear Ice Coverage: Losses and Coupled Variability (1958–2018) / R. Kwok // Environmental Research Letters. – 2018. – Vol. 13. – No. 10. – 105005.
142. Lind, S. Variability and Impacts of Atlantic Water Entering the Barents Sea from the North / S. Lind, R.B. Ingvaldsen // Deep Sea Research Part I: Oceanographic Research Papers. – 2012. – Vol. 62. – P. 70-88.
143. Liu, Y. Spatio-Temporal Analysis of East Greenland Polar Front / Y. Liu, J. Wang, G. Han [et al.] // Frontiers in Marine Science. – 2022. – 9:943457.
144. Loeng, H. Features of the Physical Oceanographic Conditions of the Barents Sea / H. Loeng // Polar Research. – 1991. – Vol. 10. – No. 1. – P. 5-18.
145. Loeng, H. Water Fluxes through the Barents Sea / H. Loeng, V. Ozhigin, B. Ådlandsvik // ICES Journal of Marine Science. – 1997. – Vol. 54. – No. 3. – P. 310-317.
146. Lundesgaard, Ø. Import of Atlantic Water and Sea Ice Controls the Ocean Environment in the Northern Barents Sea / Ø. Lundesgaard, A. Sundfjord, S. Lind [et al.] // Ocean Science. – 2022. – Vol. 18. – P. 1389-1418.
147. Martin, T., P. Wadhams, Sea-Ice Flux in the East Greenland Current / T. Martin, P. Wadhams // Deep Sea Research Part II: Topical Studies in Oceanography. – 1999. – Vol. 46. – No. 6-7. – P.1063-1082.
148. Min, C. Sea Ice Export through the Fram Strait Derived from a Combined Model and Satellite Data Set / C. Min, L. Mu, Q. Yang [et al.] // The Cryosphere. – 2019. – Vol. 13. – P. 3209-3224.

149. Müller, M. Decline of Sea-Ice in the Greenland Sea Intensifies Extreme Precipitation over Svalbard / M. Müller, T. Kelder, C. Palerme // Weather and Climate Extremes. – 2022. – Vol. 36. – 100437.
150. Onarheim, I.H. Toward an Ice-Free Barents Sea / I.H. Onarheim, M. Årthun // Geophysical Research Letters. – 2017. – No. 44. – P. 8387-8395.
151. Onarheim, I.H. Seasonal and Regional Manifestation of Arctic Sea Ice Loss / I.H. Onarheim, T. Eldevik, L.H. Smedsrud [et al.] // Journal of Climate. – 2018. – Vol. 31. – P. 4917-4932.
152. Overland, J.E., The Recent Arctic Warm Period / J.E. Overland, M. Wang, S. Salo // Tellus A: Dynamic Meteorology and Oceanography. – 2008. – Vol. 60. – P. 589-597.
153. Ozhigin, V.K. The Eastern Basin Water and Currents in the Barents Sea / V.K. Ozhigin, A.G. Trofimov, V.A. Ivshin // ICES Annual Science Conference, 2000. – ICES CM. 2000/L: 14. 19 pp.
154. Polyakov, I.V. Variability of the Intermediate Atlantic Water of the Arctic Ocean over the Last 100 years / I.V. Polyakov, G.V. Alekseev, L.A. Timokhov [et al.] // Journal of Climate. – 2004. – Vol. 17. – No. 23. – P. 4485-4497.
155. Previdi, M. Arctic Amplification of Climate Change: a Review of Underlying Mechanisms / M. Previdi, K.L. Smith, L.M. Polvani // Environmental Research Letters. – 2021. – V. 16. – 093003.
156. Rieke, O. Rapid Sea Ice Changes in the Future Barents Sea / O. Rieke, M. Årthun, J. S. Dörr // The Cryosphere. – 2023. – Vol. 17. – P. 1445-1456.
157. Ricker, R. Satellite-Derived Sea Ice Export and its Impact on Arctic Ice Mass Balance / R. Ricker, F. Girard-Ardhuin, T. Krumpen [et al.] // Cryosphere. – 2018. – Vol. – 12. No. – 9. P. – 3017-3032.
158. Rikiishi, K. The role of Atmospheric Circulation in the Growth Of Sea-Ice Extent in Marginal Seas Around the Arctic Ocean / K. Rikiishi, H Ohtak, Y. Katagiri // Annals of Glaciology. – 2005. – Vol. 42. – P. 352-360.
159. Rudels, B. On the Mass Balance of the Polar Ocean, with Special Emphasis on the Fram Strait / B. Rudels. – Norsk Polarinstitutt Skrifter 188, Oslo, 1987. – 53 pp.

160. Rudels, B. On the Intermediate Depth Waters of the Arctic Ocean / B. Rudels, E.P. Jones, L.G. Anderson [et al.] // The Role of the Polar Oceans in Shaping the Global Climate: The Nansen Centennial Volume / ed. by O.M. Johannessen, R.D. Muench, J.E. Overland. – American Geophysical Union, Washington, DC. 1994. – P. 33-46.
161. Rudels, B. The Thermohaline Circulation of the Arctic Ocean and the Greenland Sea / B. Rudels // Philosophical Transactions: Physical Sciences and Engineering. – 1995. – Vol. 352. – No. 1699. – P. 287-299.
162. Schauer, U. Atlantic Water Flow through the Barents and Kara Seas / U. Schauer, H. Loeng, B. Rudels [et al.] // Deep Sea Research Part I: Oceanographic Research Papers. – 2002. – Vol. 49. – No. 12. – P. 2281-2298.
163. Serreze, M.C. Icelandic Low Cyclone Activity: Climatological Features, Linkages with the NAO, and Relationships with Recent Changes in the Northern Hemisphere Circulation / M.C. Serreze, F. Cars, R.G. Barry [et al.] // Journal of Climate. – 1997. – Vol. 10. – No. 3. – P. 453-464.
164. Serreze, M.C. Processes and Impacts of Arctic Amplification: A Research Synthesis / M.C. Serreze, R.G. Barry // Global and Planetary Change. – 2011. – Vol. 77. – No. 1. – P. 85-96.
165. Serreze, M.C. Arctic Sea Ice Trends, Variability and Implications for Seasonal Ice Forecasting / M.C. Serreze, J. Stroeve // Philosophical Transactions of the Royal Society A: Mathematical, Physical and Engineering Sciences. – 2015. – Vol. 373. – No. 2045. – 20140159.
166. Shapiro, I. April Sea Ice Extent in the Barents Sea, 1850–2001 / I. Shapiro, R. Colony, T. Vinje // Polar Research. – 2006. – Vol. 22. – No. 1. – P. 5-10.
167. Smedsrud, L.H. Recent Wind Driven High Sea Ice Area Export in the Fram Strait Contributes to Arctic Sea Ice Decline / L.H. Smedsrud, A. Sirevaag, K. Kloster [et al.] // Cryosphere. – 2011. – Vol. 5. – No. 4. – P. 821-829.
168. Smedsrud, L.H. The Role of the Barents Sea in the Arctic Climate System / L.H. Smedsrud, I. Esau, R.B. Ingvaldsen [et al.] // Reviews of Geophysics. – 2013. – Vol. 51. – No. 3. – P. 415-449.

169. Smedsrud, L.H. Fram Strait sea ice export variability and September Arctic Sea Ice Extent over the Last 80 Years / L.H. Smedsrud, M. H. Halvorsen, J.C. Stroeve [et al.] // Cryosphere. – 2017. – Vol. 11. – No. 1. – P. 65-79.

170. Spreen, G. Fram Strait Sea Ice Volume Export Estimated Between 2003 and 2008 from Satellite Data // G. Spreen, S. Kern, D. Stammer [et al.] // Geophysical Research Letters. – 2009. – Vol. 36. – No. 19. – L19502.

171. Spreen, G. Arctic Sea Ice Volume Export through Fram Strait from 1992 to 2014 / G. Spreen, L. de Steur, D. Divine [et al.] // Journal of Geophysical Research. Oceans. – 2020. – Vol. 125. – No. 6. – e2019JC016039.

172. Stroeve, J., Changing State of Arctic Sea Ice Across All Seasons / J. Stroeve, D. Notz // Environmental Research Letters. – 2018. – Vol. 13. – No. 10. – 103001.

173. Thompson, D.W.J. The Arctic Oscillation Signature in the Wintertime Geopotential Height and Temperature Fields / D.W.J. Thompson, J.M. Wallace // Geophysical Research Letters. – 1998. – Vol. 25. – No. 9. – P. 1297-1300.

174. Thompson, D.W.J. Annular modes in the extratropical circulation. Part I. Month to month variability / D.W.J. Thompson, J.M. Wallace // Journal of Climate. – 2000. – Vol. 13. – P. 1000-1016.

175. Trewartha, G.T. An Introduction to Climate / G.T. Trewartha, L.H. Horne. – 5th edn. New York: McGraw-Hill, 1980. – 416 pp.

176. Tschudi, M.A. An Enhancement to Sea Ice Motion and Age Products at the National Snow and Ice Data Center (NSIDC) / M.A. Tschudi, W.N. Meier, J.S. Stewart // The Cryosphere. – 2020. – Vol. 14. – P. 1519-1536.

177. Tsukernik, M. Atmospheric Forcing of Fram Strait Sea Ice Export: a Closer Look / M. Tsukernik, C. Deser, M. Alexander R. Tomas // Climate Dynamics. – 2010. – Vol. 35. – P. 1349-1360.

178. Vinje, T. Sea Ice Conditions in European Sector of the Marginal Seas of the Arctic, 1966–1975 / T. Vinje // Arbok Norsk Polarinstitutt, Oslo, 1975. – P. 163-174.

179. Vinje, T. Drift, Composition, Morphology and Distribution of the Sea Ice Fields in the Barents Sea / T. Vinje // Norsk Polarinstitutt, Skr. Nr. 179 C. – Oslo, 1985. – 26 p.

180. Vinje, T., Monitoring Ice Thickness in Fram Strait / T. Vinje, N. Nordlund, A. Kvambekk // Journal of Geophysical Research. – 1998. – Vol. 103. – No. C5. – P. 10437-10449.

181. Vinje, T. Anomalies and Trends of Sea-Ice Extent and Atmospheric Circulation in the Nordic Seas During the Period 1864–1998 / T. Vinje // Journal of Climate. – 2001a. – Vol. 14. – No. 3. – P. 255-267.

182. Vinje, T. Fram Strait Ice Fluxes and Atmospheric Circulation: 1950–2000 / T. Vinje // Journal of Climate. – 2001б. – Vol. 4. – No. 16. – P. 3508-3517.

183. von Appen, W.-J. Exchange of Warming Deep Waters across Fram Strait / W.-J. von Appen, U. Schauer, R. Somavilla [et al.] // Deep Sea Research Part I: Oceanographic Research Papers. – 2015. – Vol. 103. – P. 86-100.

184. Watanabe, E. Arctic Dipole Anomaly and its Contribution to Sea Ice Export from the Arctic Ocean in the 20th Century / E. Watanabe, J. Wang, A. Sumi [et al.] // Geophysical Research Letters. – 2006. – V. 33. – No. 23. – L23703.

185. Wang, J. Is the Dipole Anomaly a Major Driver to Record Lows in Arctic Summer Sea Ice Extent? / J. Wang, J. Zhang, E. Watanabe [et al.] // Geophysical Research Letters. – 2009. – Vol. 36. – L05706.

186. Wittmann, W.I. Comments on the Mass Budget of Arctic Pack Ice / W.I. Wittmann, J. J. Schule jr. // Proceedings of the Symposium on the Arctic Heat Budget and Atmospheric Circulation, ed. by J. O. Fletcher. – Santa Monica, California, Rand Corporation, 1966. – P. 215-246.

187. Wu, B.Y. Dipole Anomaly in the Winter Arctic Atmosphere and its Association with Sea Ice Motion / B.Y. Wu, J. Wang, J.E. Walsh // Journal of Climate. – 2006. – Vol. 19. – P. 210-225.

188. Xia, W. Assessing Trend and Variation of Arctic Sea-Ice Extent during 1979–2012 from a Latitude Perspective of Ice Edge / W. Xia, H. Xie, C. Ke // Polar Research. – 2014. – Vol. 33. – 21249.

189. Zamani, B. Fram Strait Sea Ice Export Affected by Thinning: Comparing High-Resolution Simulations and Observations / B. Zamani, T. Krumpen, L. Smedsrud [et al.] // Climate Dynamics. – 2019. – Vol. 53. – No. 5-6. – P. 3257-3270.

190. Zhang, Z. Arctic Sea Ice Volume Export through the Fram Strait from Combined Satellite and Model Data: 1979–2012 / Z. Zhang, H. Bi, K. Sun [et al.] // Acta Oceanologica Sinica. – 2017. – Vol. 36. – No. 1. – P. 44-55.

191. Zhou, S. Trends of NAO and AO and Their Associations with Stratospheric Processes / S. Zhou, A.J. Miller, J. Wang [et al.] // Geophysical Research Letters. – 2001. – Vol. 28. – No. 21. – P. 4107-4110.